University of Alberta

DIRECT SHEAR FAILURE OF A SYNTHETIC ROCK CONTAINING DISCONTINUOUS JOINTS

by

Yifei Cui

A thesis submitted to the Faculty of Graduate Studies and Research
in partial fulfillment of the requirements for the degree of

Master of Science

in

Geotechnical Engineering

Department of Civil and Environmental Engineering

©Yifei Cui

Spring 2012

Edmonton, Alberta

Abstract

Direct shear tests were used to establish the shear behaviour of continuous planar-joints, discontinuous stepped-joints and discontinuous open-joints. The joints were cast in a Synthetic rock made of plaster, sand and water and tested under normal stresses that ranged from 50 kPa to 3.5 MPa. A total of 88 direct shear tests were carried out. The shear behaviour of both the continuous and discontinuous joints was found to be dependent on the normal stress. At normal stresses below the magnitude of tensile strength, approximately 1.8 MPa, the joint behaviour of the continuous planar joints was essentially elastic-perfectly plastic. Implying that the peak strength of the planar joint was essentially the same as the residual strength. At normal stresses above the magnitude of the tensile strength, continuous and discontinuous joints displayed either strain weakening or brittle behaviour. Hence at these normal stresses the peak strength exceeds the residual strength. No single failure envelope could be used to describe the shear of the joints, even the continuous planar joints. A primary reason for this non-unique failure envelope was the large dilation that occurred at high normal stresses. This dilation was attributed to grain crushing, and the roughness resulting from this crushing and gouge formation as shearing occurred.

The *Phase²* elasto-plastic finite element software was used to simulate a number of the direct shear tests. The properties for the synthetic rock were established from uniaxial compressive strength and Brazilian tensile strength tests. The *Phase²* simulations were in reasonable agreement with the laboratory direct shear tests for the continuous planar-joints and the

discontinuous stepped-joints when the normal stress was less than the magnitude of the tensile strength. However, at normal stresses above the magnitude of the tensile strength, the agreement between *Phase²* and the laboratory tests was reduced. There was essentially no agreement between the *Phase²* results and the discontinuous open-joint laboratory results. These findings suggest that the material properties for a continuum model may have to be calibrated to the laboratory results that were determined following the stress path simulated in the continuum model.

Acknowledgements

I would like to express my heartfelt gratitude to my supervisor, Dr. C. Derek Martin. His scientific literacy, constructive criticisms and continuous encouragement made me learn further than I had learned in the past.

I also like to thank Dr. Dave Chan, Dr. Dave C. Sego, Dr. Ward Wilson and Dr. Rick Chalaturnyk and the other Professors who are in charge of the graduate students' basic lectures in the field of Geology and Geotechnical material and design.

Thank you to the graduate students in the geotechnical group in the Department of Civil and Environmental Engineering, University of Alberta, who held discussions together and provided me with great ideas when I met problems in my research study.

Finally, I wish to thank Steve Gamble and Christine Hereygers for their consistent assistance and advice with the laboratory test.

Table of Contents

List of Tables

List of Figures

List of Figures in Appendix

1 Introduction

Civil and mining engineering projects require rock slope excavations. The failure of such slopes usually involves sliding along continuous weak planes. In rock masses where these planes are not continuous, sliding may also involve the creation of new slip surfaces. Jennings [1] pointed out that during sliding, the high stress concentrations in the vicinity of the tip of the discontinuous joint might lead to brittle fracture of the intact rock. The total failure process is composed of sliding along the existing joints and interaction with the new joints induced by tensile stresses. Lajtai [2] examined synthetic rocks containing discontinuous shears using the laboratory direct shear test. He concluded that the rupture stress in a direct shear resulted in a discontinuous yield envelope. Eberhardt [3] performed numerical analysis of the 1991 Randa rockslide in the southern Swiss Alps that contained both continuous and discontinuous joints as shown in Figure 1.1. Eberhardt concluded that the failure of the rock slope required the progressive degradation and destruction of cohesive intact rock bridges. Despite the recognition that failure of rock slopes may involve the failure of discontinuous joints, there is no accepted method for establishing the failure criteria of such a failure process.
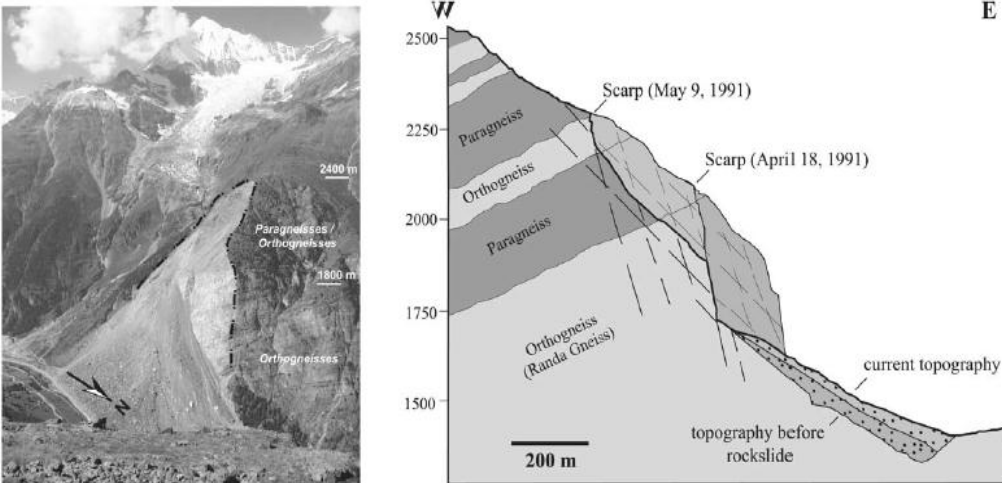
Figure 1.1 Photo of the 1991 Randa rockslide and cross-sectional illustration showing the sliding events with respect to time (From Eberhardt [3])

1.1 Need for calibration studies

In recent years, rapid development in computing technology has established numerical analyses as an important component of geotechnical practice (Rocscience [4]), particularly

when analyzing complex problems such as the Randa Slope shown in Figure 1.1. As with all forms of analyses input parameters are required. In general, continuum numerical analyses require fewer input parameters than discrete element analyses. However, with continuum analyses the failure process must be described beforehand using appropriate constitutive models. The discrete element analyses do not rely on prescriptive constitutive models, but instead require detailed calibration of micro properties to represent the macro-scale response. Regardless of which method is used for the analyses, there is a need to ensure that the proposed approach is valid. In order to evaluate the various modeling options available, the starting point is comparison with well-documented measured results. For the case of discontinuous joints in rock slopes, a starting point is the direct shear laboratory test.

1.2   Objective and Scope of Work

The objectives of research of this thesis can be summarized as follows:

(1) Create a synthetic rock and conduct a laboratory test to establish the material properties and strength criteria for various loading paths.

(2) Conduct direct shear tests of the synthetic rock containing a thorough going planar joint and various configurations of a discontinuous joint.

(3) Conduct numerical analysis of the laboratory tests using continuum mechanics and compare the laboratory results with the numerical results.

1.3   Outline of Thesis

This thesis is subdivided into six chapters. A short description of the contents in each chapter is given as below.

Chapter 1 introduces the background, research objectives and outlines of the thesis.

Chapter 2 gives a literature review of the rock mass description, the formation of a shear zone on both intact rock and jointed rock cases under direct shear conditions, the previous models and laboratory tests carried, and discussion on the advantage and disadvantage of each model.

Chapter 3 provides the laboratory test carried by the student on the properties of discontinuous rock, including a basic strength test on synthetic rock and direct shear tests on samples of different shapes of joints.

In Chapter 4, the figure-based analysis from the laboratory test is provided. The strength behaviour of discontinuous rock under the direct shear condition is studied further.

Chapter 5 describes the numerical analysis contained in both the continuum mechanics approach and the discrete fracture network approach by using *Phase^2* 8.0 in order to compare laboratory results. The test results are compared to previous investigations on the direct shear test and the differences are explained.

Chapter 6 presents the conclusion from the conducted research and recommendations for future research on the properties of discontinuous rock are presented.

Appendix A includes additional figures showing details of the sample preparation procedure, laboratory equipment, shape of samples before the tests, and crushed samples after the tests, illustrating crack propagation, shear zone formation and shape of the failure.

1.4   Extent and limitations

This thesis is limited to the strength behavior of synthetic weak rock containing discontinuous joints. Synthetic weak rock has brittle behavior and it will be present in most nature rock for construction projects in mountain areas of British Columbia and Alberta.

The study is focused on continuous loading conditions; no attention has been given to kinematic loading such as seismic loading.

1.5 References

[1]   Jennings, J. E. 1970. Mathematical Theory for the Calculation of the Stability of Slopes in Open Cast Mines. *Proceedings of the Theoretical Background to the Planning of Open Pit Mines with Special Reference to Slope Stability Johannesburg, Republic of South Africa.* 87-102.

[2]   Lajtai, E. Z. 1969. Shear strength of weakness planes in rock. *International Journal of Rock Mechanics and Mining Sciences Geomech Abstr*, Vol. 6, No. 7: 499 -515.

[3]   Eberhardt, E., Stead, D., Coggan, J. S. 2004. Numerical analysis of initiation and progressive failure in natural 1991 Randa Slide. *International Journal of Rock Mechanics and Mining Sciences*. Vol. 41, 69-87.

[4]   Rocscience Inc. 2008. Two-dimensional finite element slope stability analysis. Phase2 v 7.0

2 Review of rock strength with discontinuous joints

Many engineering structures, such as mines, underground excavations, and bridges are constructed in or on rock formations. Such formations commonly contain continuous and discontinuous joints. Evaluating the shear strength of continuous joints and the stability of engineered structures on such joints is relatively straightforward. However, when the rock mass is composed of both discontinuous joints and intact rock bridges estimating the shear strength is more challenging.

2.1 Rock mass with continuous joint

Hoek and Bray [1] identified 4 types of rock slope failure recorded by the International Society for Rock Mechanics (ISRM) [2], three of which were dominated by continuous throughgoing joints (Figure 2.1):

(1) Heavily jointed rock with no identifiable structural pattern will lead to circular failure.

(2) Highly ordered joint structures will lead to plane failure.

(3) The intersection of sets of joints will lead to wedge failure.

(4) Steeply dipping joints will lead to toppling failure.

(a)   (b)

| (c) | (d) |
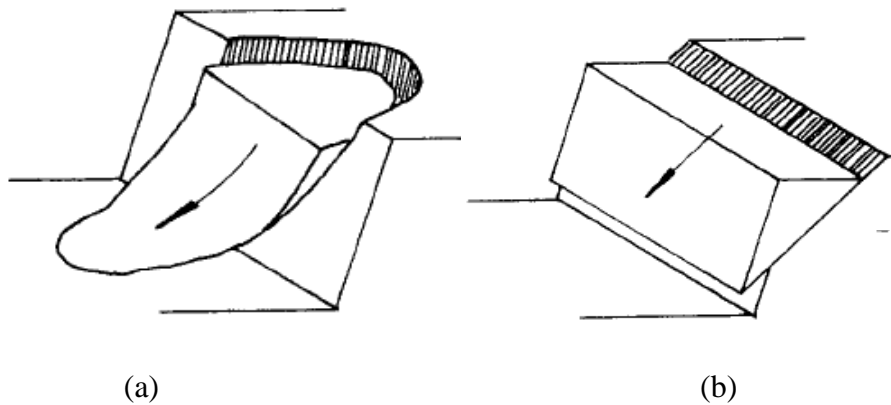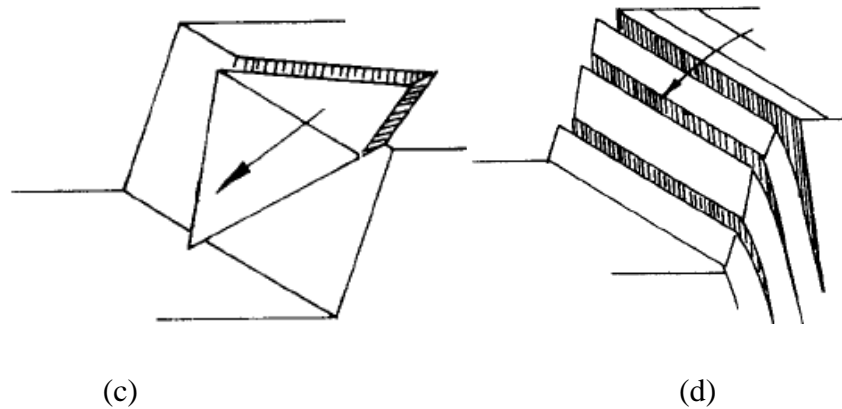
Figure 2.1. Four types of rock slope failure induced by orientation of joint (from Hoek and Bray [1]): (a) Circular Failure, (b) Plane failure, (c) Wedge failure, (d) Toppling failure.

The rock mass description and the estimation of rock mass strength by ISRM standard [2] assumes joints are continuous. However, many rock masses contain joints which do not form continuous surfaces. When a slope contains jointed mass combines of solid bridge and fissure, how the rupture surface forms is needs to be discussed.

2.2   Development of a shear zone

2.2.1   Development of a shear zone in intact rock

Cloos [3] used simple shear loading to examine the development of a shear zone in clay. They found that the fracture patterns observed in those experiments were similar to those found in rock. Tchalenko [4] reproduced the simple shear experiments of Riedel and his observations are reproduced in Figure 2.2. In Figure 2.2, at Stage A, where the resistance to shear is maximum, Riedel Shears form at an inclined angle with a half value of the internal friction angle of clay to the direction of shearing. Despite the name "Reidel Shears", these are extensional fractures caused by compressive stresses in the direction of the crack and by tensile stresses perpendicular to the crack. As the resistance to shear decreases from A through D in Figure 2.3 (b), the Riedel fractures grow in a complex manner that ultimately leads to a formation of a thorough going principal shear plane. Skempton [5] concluded, based on detailed field mapping of shear zones in clays and sandstones, that the principle shear plane links the Riedel Shears. The residual shear strength is reached only after large displacements beyond point D in Figure 2.2.

6
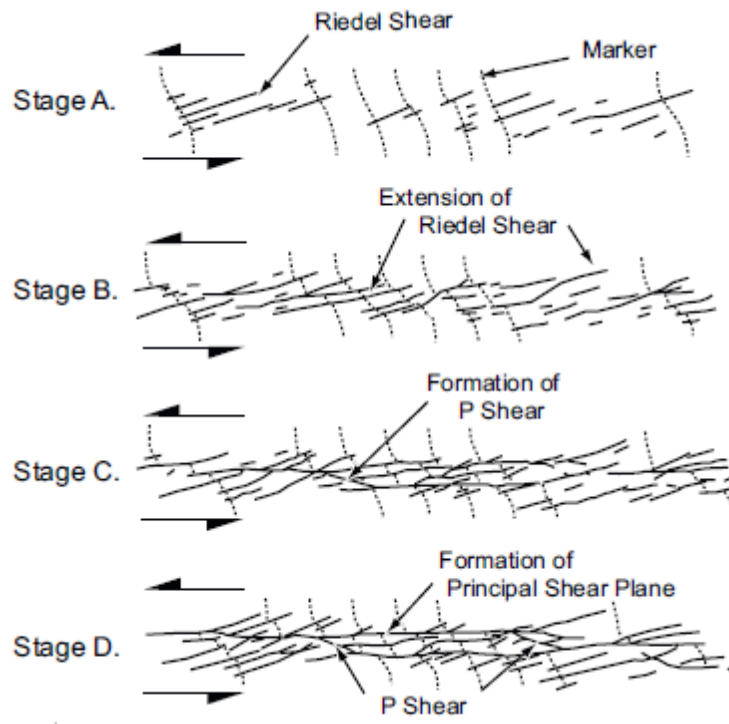
(a)
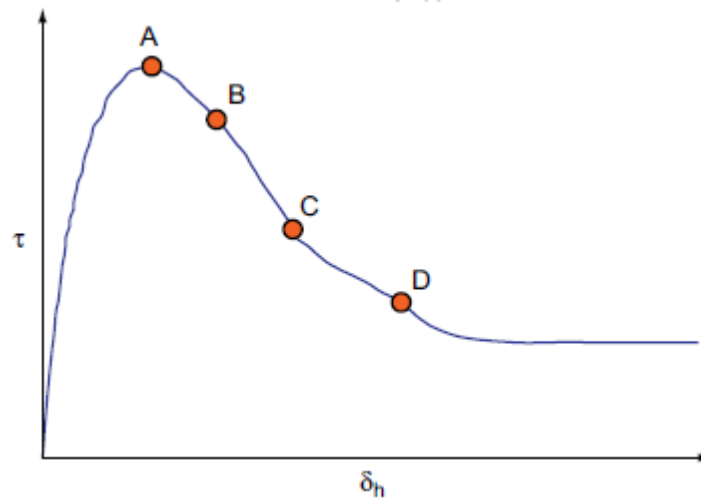
(b)

Figure 2.2. Development of shear zones under different shear stages of a direct shear test on Kaolin (from Tchalenko[5], modified by Cho[6]).

Cho et al. [6] used discrete element modeling to track the developments of a rupture surface in weak intact synthetic rock at low (1 kPa) and high (1.85 MPa) normal stress. The development of the shear zone observed by Cho et al under low (1 kPa) normal stress is shown in Figure 2.3. The development of the fracturing in the discrete element simulations was divided by four stages. The initial fracturing that developed in Stage **A** during the pre-peak loading was concentrated near the edge of the shear box. The fractures that developed at peak loading (Stage **B**) are similar to those observed by Tchalenko [4] at peak strength. Cho et al. [6] were able to examine the fracturing mechanisms as the rupture surface developed. They concluded that despite the direct shear loading, the majority of the fractures that made up the rupture surface formed in tension, regardless of the magnitude of the normal stress. The residual stage **C** and **D** in Figure 2.3 shows the development of the principal displacement plane. Cho et al. [6] noted that the shear zone under low normal stress remained relatively narrow while as the normal stress increased, so did the thickness of the rupture surface.
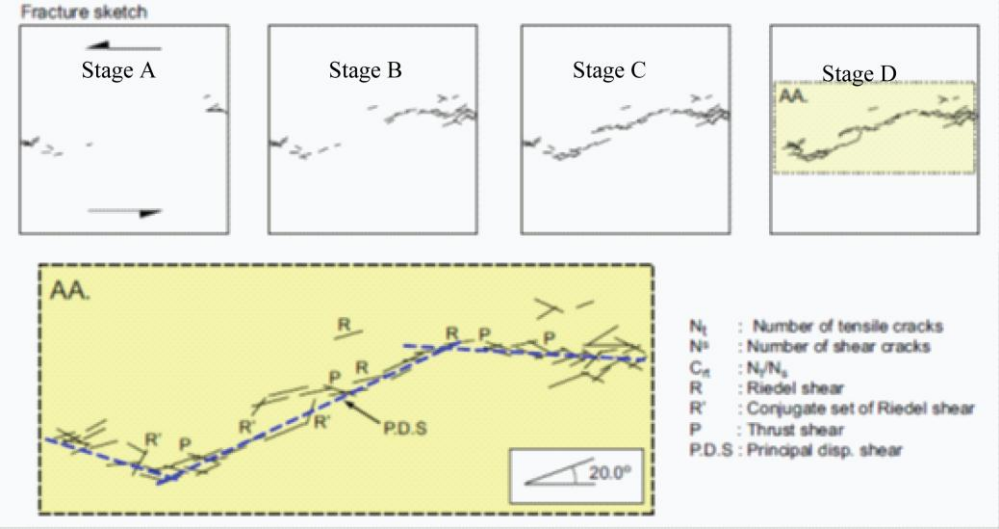
Figure 2.3. Development of shear zones under different shear stages of a direct shear test on Kaolin with 1 kPa normal stress (from Cho [6]).

2.2.2   Development of a shear zone in rough fractures

Ladanyi and Archambault [7] carried out a series of direct shear test on synthetic rock (concrete brick) containing interlocked rock surfaces inclined at 30 degrees. The three phases of a typical test performed in the direct shear are shown in Figure 2.4. They found that during testing, the intact rock blocks were first fissured and subsequently shearing occurred through the already partially damaged rock.
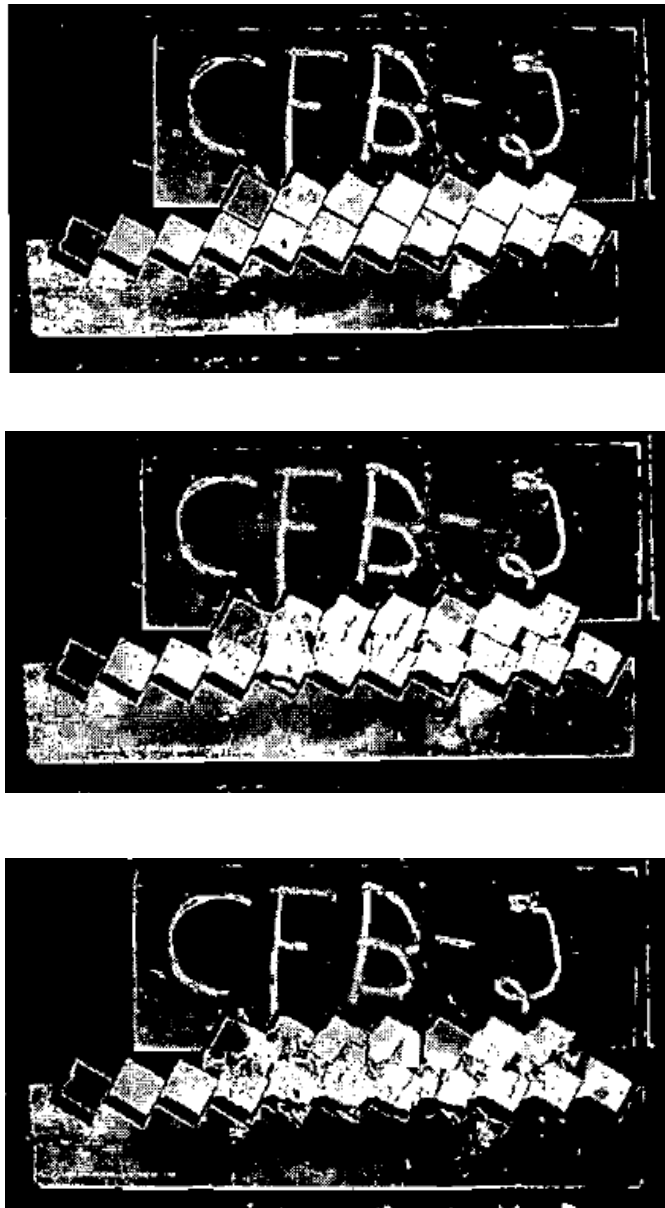
Figure 2.4. Three phases of uniform rough joint in direct shear (from Ladanyi and Archambault [7]).

2.2.3 Development of a shear zone with infilled fractures

Ladanyi and Archambault [8] also carried out a series of direct shear test on synthetic rock joint made with concrete bricks and filled with soil-like material. The schematic diagram of their direct shear apparatus for testing filled joints is illustrated in Figure 2.5. Clay and sandy silt were selected as the infilling material. The shear stress to normal stress ratio versus shear displacements from their direct shear test results for clay filling joint are shown in Figure 2.6. It was observed that at the first stage of shearing the joints displayed a locking characteristic, i.e., the clay was sheared and extruded until the shear stress was transferred to the rock to rock contacts. During the second stage when shear displacement reached 2.5 mm or more, these rock contacts fractured. It was during this stage that the peak strength was reached. During the last stage of shearing the residual strength is reached after a shear displacement exceeding 12.7 mm.

Ladanyi and Archambault concluded that the strength of the clay filled joints was much weaker than the unfilled joints, and it would decrease steadily with an increase of filling thickness. The majority of observations made for clay filling joint were also found to be valid for sandy silt filled joints.
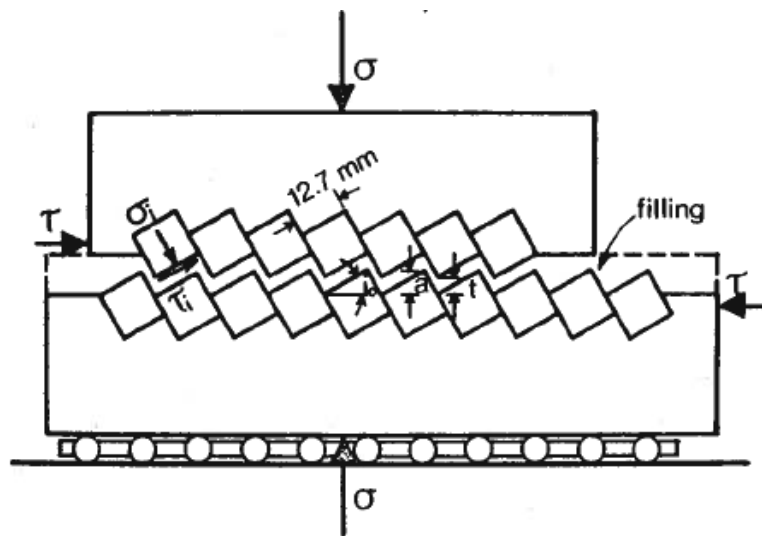
Figure 2.5. Schematic diagram of the direct shear apparatus for testing filled joints, where σ and τ are normal and shear stress applied on the sample, σ_i and τ_i are normal and shear stress calculated along inclined joint, i_o is the angel of inclined joint, and t is the thickness of infilled joint (from Ladanyi and Archambault [8]).
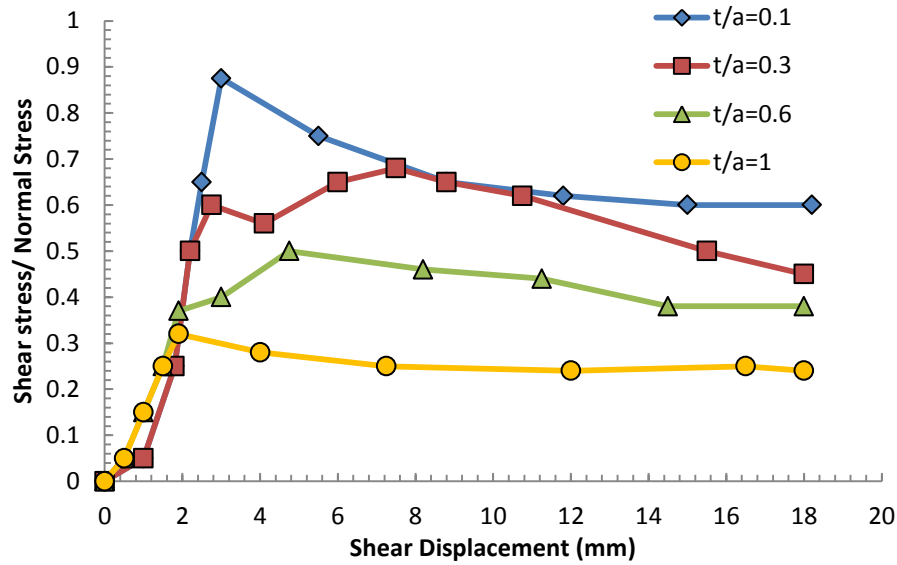
Figure 2.6. Shear deformability of clay-filled joints with joint inclined angle $i_o = 30^o$, normal stress $\sigma_n = 8.69$ MPa, and increasing filling thickness (t/a ratio), modified from Ladanyi and Archambault [8].

2.2.4   Development of a shear zone in rock with discontinuous fractures

The direct shear strength of rock containing discontinuous fractures is derived from two sources: strength of the intact rock and shear strength of the fractures. Lajtai [9] and Xia [10] investigated the development of a shear zone in synthetic rock containing discontinuous fractures. Lajtai [9] carried out a series of direct shear tests using solid plaster specimens containing different artificial voids and planes to represent discontinuous joints (Figure 2.7). From Figure 2.7 (a), the oblique primary tension fracture in the middle of block is observed with secondary shear fractures on the edges of the sample. Figure 2.7 (b) shows a shear zone that developed along a smooth fracture under ultimate strength conditions. Lajtai concluded that at low normal stress, the tensile strength of the intact rock bridges controlled the shear strength, while at high normal stress, the fracture frictional resistances controlled the shear strength.
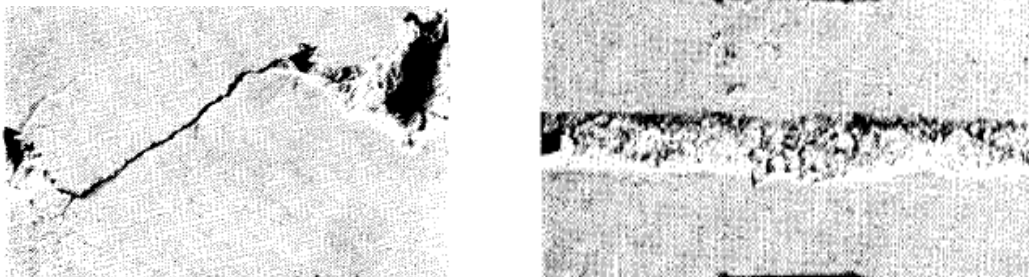
(a)   (b)

Figure 2.7. Fracture patterns in blocs after the direct shear test (from Lajtai [9]).

Xia [10] carried out a series of direct shear tests on synthetic rock samples made with cement and sand containing discontinuous joints at both ends of the sample (Figure 2.8). Xia [10] proposed that the crack propagation during the tests had a microscopic explanation. He noted that with an increase in shear stress, the initial crack grew feather-like at the tip of the joints in a direction that was not parallel to the direction of the shear. A tensile crack then appeared near the tip of the fissure in the direction of the horizontal shear stress. The dilation process associated with the roughened fractures and accompanying strength decrease during the initial shear, which caused the shear resistance to be concentrated in the solid bridge between the two fractures. With increasing shear, the fracture propagated through the intact rock bridge until a complete rupture occurred. The process is shown in Figure 2.9.
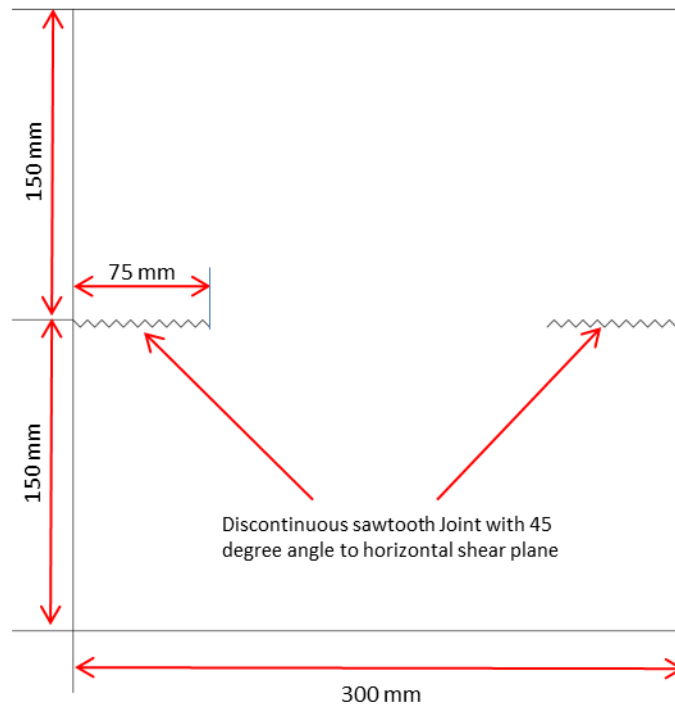
Figure 2.8. Synthetic rock containing two joints at the edge (from Xia [8] with length unit in mm).

12
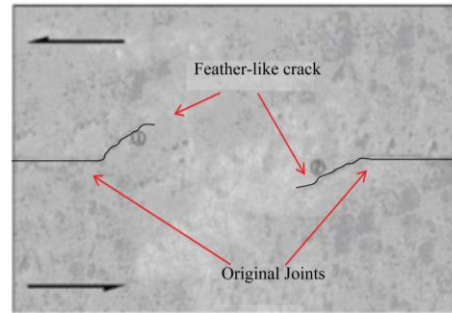
(a)
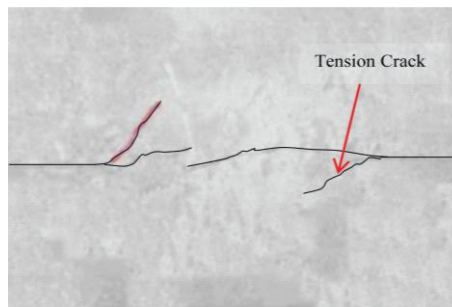
(b)
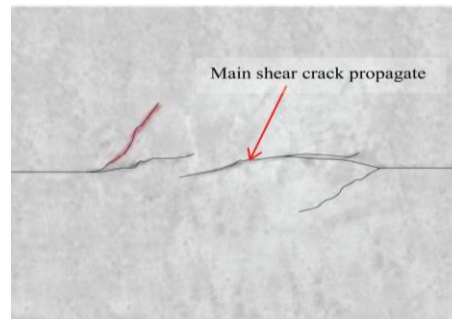
(c)

Figure 2.9. Development of a shear zone under different shear stages of the direct shear test on synthetic rock (from Xia [10]): (a) Feather-like crack growth on the tip of the original joints with the direction of growth not parallel to the shear plane. (b) Tensile crack appearing on the tip of the fissure in the direction of the horizontal shear stress. (c) Shear crack propagated until the failure of the whole rock sample.

Gehle and Kutter [11] carried out a total of 131 direct shear tests on synthetic rock samples made with pure gypsum containing discontinuous joints at both ends of the sample (Figure 2.10). From the shear stress - displacement curve (Figure 2.11) they concluded that three phases of shearing could be identified. The first phase of the shearing was initiated by the

formation of wing cracks (at SR1a), which started from the tip of the original joints and grew into the intact bridges (Figure 2.12(a)). The first phase ended with the generation of additional new fractures (at SR1b) connecting two wing cracks generated from the original joint (Figure 2.12 (b)). The second phase of shearing is characterized by a friction process and volume increase in the shear zone. SR2 was the peak stress measured in this phase. The final phase of shearing was reached after a large shear displacement and crashing of the solid bridge with SR3 as the measured resistance.
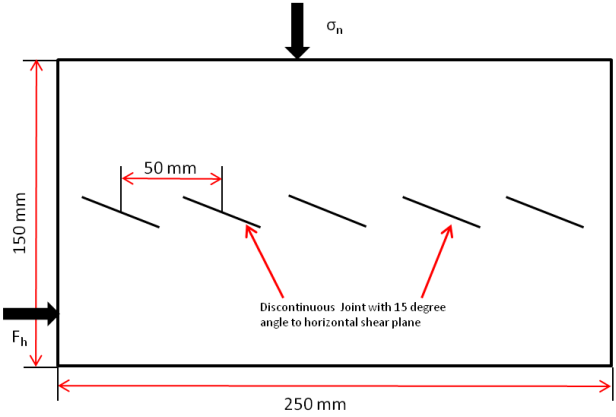
Figure 2.10. Geometrical parameters of shear specimen with discontinuous joint, from Gehle and Kutter [11].
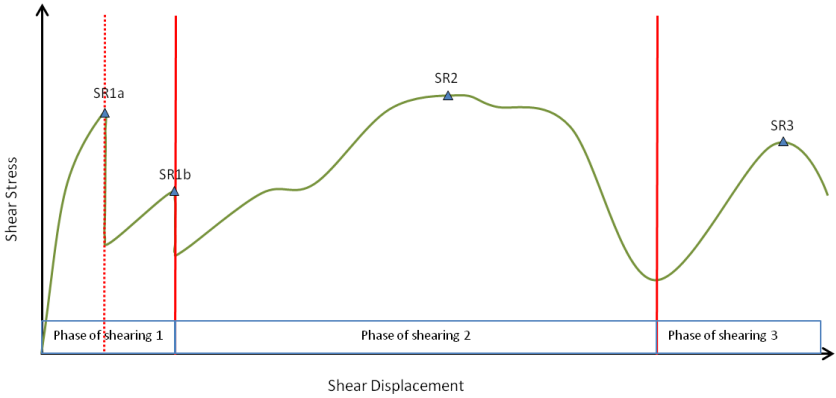
Figure 2.11. Idealized shear test laboratory result modified from Gehle and Kutter [11].

14
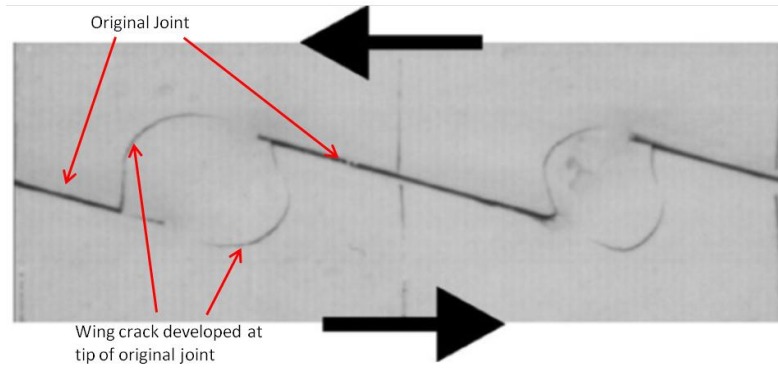
(a)
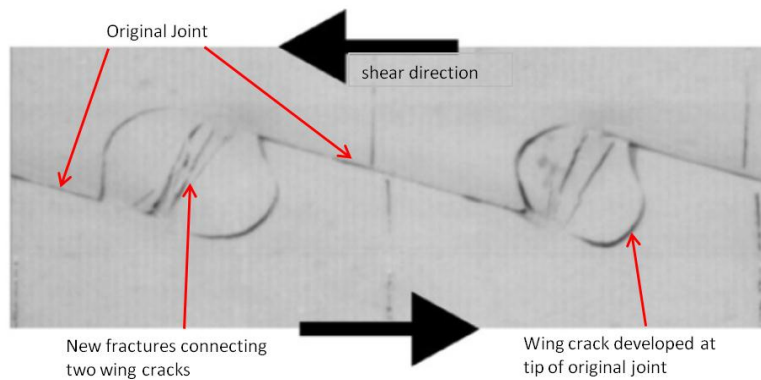
(b)

Figure 2.12. Crack development during the first phase of shearing, modified from Gehle and Kutter [11].

2.2.5   Strength criterion for direct shear

It is clear from the preceding description of the observations made during the development of a rupture surface in a direct shear that the failure process is complex. In this section, the failure criteria that have been used to establish the shear strength associated with this complex process is reviewed.

2.2.6   Early Approach

The early approach of strength criteria of discontinuities is mainly based on work done by Coulomb (1776) and Mohr (1882). According to Jaegar and Cook [12] the shear strength (τ) along a smooth plane in two dimensions is given by:

$$\tau = c + \sigma_n \tan \phi, \tag{2.1}$$

where c is the cohesive strength of the surface, σ_n is the normal stress and ϕ is the angle of internal friction.

Patton [13] conducted several direct shear tests on regular "saw-tooth" specimens and demonstrated that the strength could be approximated by a bilinear failure envelope (Figure 2.13). When the normal stress is low, the strength is dominated by the geometric dilation imposed by the saw-tooth pattern:

$$\tau = \sigma_n \tan(\phi_b + i), \tag{2.2}$$

where ϕ_b is the friction angle of the joint surface and i is the inclined angle of the saw-tooth to the horizontal plane. When normal stress is increased above some critical value, the shear along the joint plane will take place:

$$\tau = c_x + \sigma_n \tan(\phi_r), \tag{2.3}$$

where ϕ_r is the residual friction angle of joint surface and c_x is the apparent cohesion of the rock.
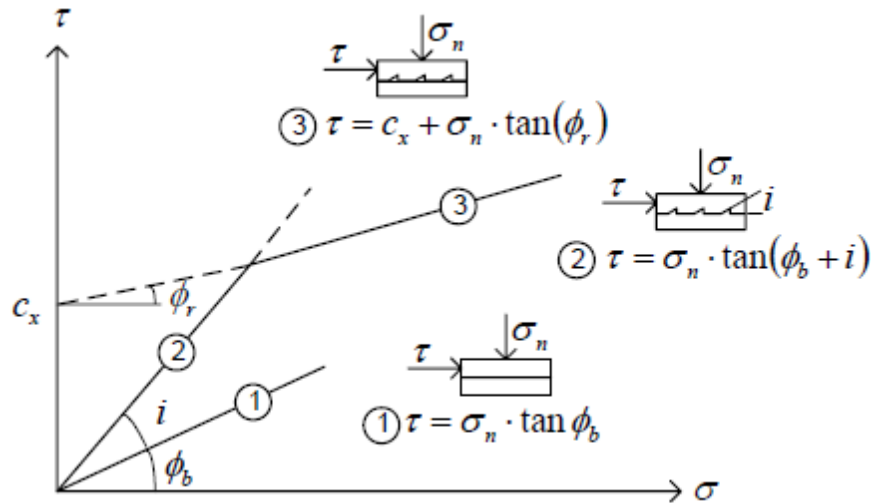
Figure 2.13. Bilinear failure envelope proposed by Patton [13] (Modified by Johansson [14]).

Barton [15] modified Partton's criteria with a parabola defined through Figure 2.14:

$$\tau = \sigma_n \tan\left[(\text{JRC}) \log\left(\frac{\text{JCS}}{\sigma_n}\right) + \phi_b\right], \tag{2.4}$$

16

Where σ_n is normal stress, JRC is the joint roughness coefficient, JCS is the joint wall compressive strength, and ϕ_b is the basic friction angle.
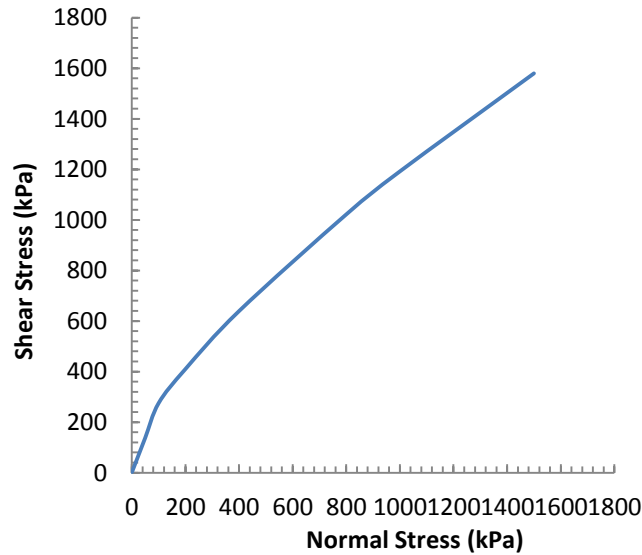
Figure 2.14 Failure criteria modified after Barton's equation [15] by assuming JRC $= 20$, JCS $= 10$ MPa, and $\phi_b = 30°$.

The previous criteria were developed for continuous throughgoing joints. In the next section, the criteria used for discontinuous joints are examined.

2.2.7   Muller's model

In the case of a completely continuous smooth joint in a rock mass, the shear strength τ is only a function of the normal stress σ_n and the angle of residual friction ϕ_r (see case 1 in Figure 2.13):

$$\tau = \sigma_n \tan \phi_r, \tag{2.5}$$

If a joint is discontinuous, the fracture plane contains both solid rock bridge and fissure. The total shear strength is determined by the internal friction in the case of solid bridges and by joint friction. For such situations Muller [16] proposed that the total shear strength could be estimated by:

$$\tau = c + (1 - k)\sigma_n \tan \phi + k\sigma_n \tan \phi_j, \tag{2.6}$$

17

Where $k = \frac{\text{area of open joint}}{\text{total area}} = \frac{2a}{b}$ states the degree of separation show in Figure 2.15 below, c is the cohesion of the intact rock, ϕ is the friction angle of the intact rock and ϕ_j is the friction angle of the joint.
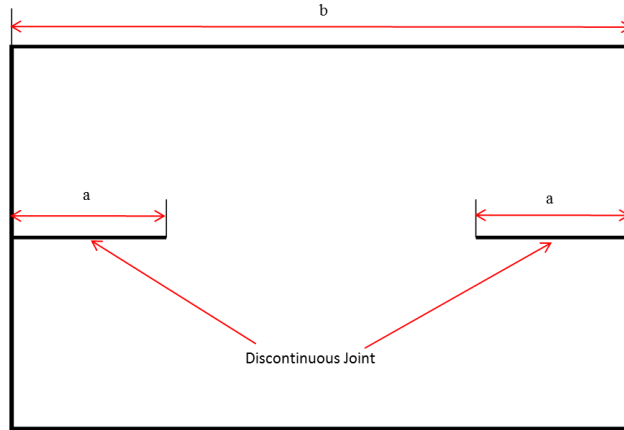
Figure 2.15. The calculation of the degree of separation in a simple rock sample contains a discontinuous joint at end.

Muller's criterion focused on the rock sample under shear stress before failure; it did not consider the high concentration of stress at the tip of the fissure. Meanwhile, Muller did not consider the cohesion provided by the joint surface even it was relatively small compared with the cohesion of the intact rock. More importantly, Muller assumed that the normal stress applied to the shear was box was the same as that acting along the intact rock and open joint at the peak strength. In other words, cohesion and frictional strength, regardless of whether it developed in the intact rock or an open joint was simultaneously mobilized.

2.2.8   Jennings's model

Similar to Muller's model, Jennings [17] made an assumption that the failure of rock bridges and joints follows Mohr-Coulomb failure criterion when the facing slope contains jointed mass combines of solid bridge and fissure, shown in Figure 2.16.

Jennings averaged the degree of separation and the cohesion of rock bridges and joints and suggested the shear strength (τ) could be given by:

$$\tau = \overline{c} + \sigma_n \tan\overline{\phi} = kc_j + (1-k)c_b + \sigma_n[k\tan\phi_j + (1-k)\tan\phi_b], \tag{2.7}$$

Where $\bar{c}$ is the average cohesion expressed by the cohesion of joint c_j and rock bridge c_b, and $\bar{\phi}$ is the average friction angle expressed by the friction angle of joint ϕ_j and the friction angle of rock bridge ϕ_b, k is the degree of separation and $k = 6a/(6a + 5b)$ from Figure 2.16.

The comparison of Muller's and Jenning's failure criterion to Xia's [10] direct shear test results is plotted in Figure 2.17. The basic properties of synthetic rock used in Xia's laboratory test are shown in Table 2.1. The result in Figure 2.17 suggests that Jenning's failure criterion given by Equation 2.7 is close to Xia's results, but does overestimates the shear strength.
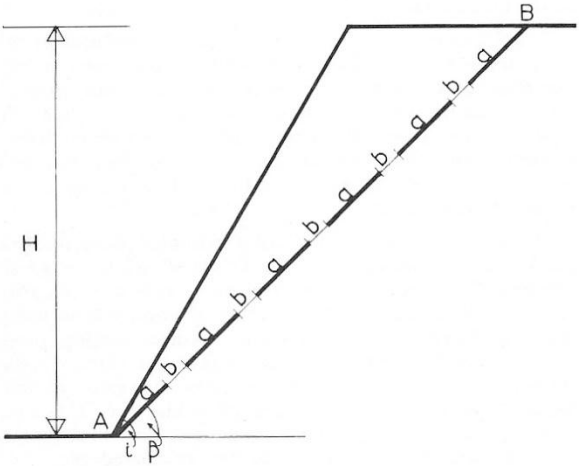
Figure 2.16. Rock mass contains discontinuous joints in the slope stability problem, "a" is the stated length of the joint, and "b" represents the intact rock length in between the joints (from Jennings [17]).
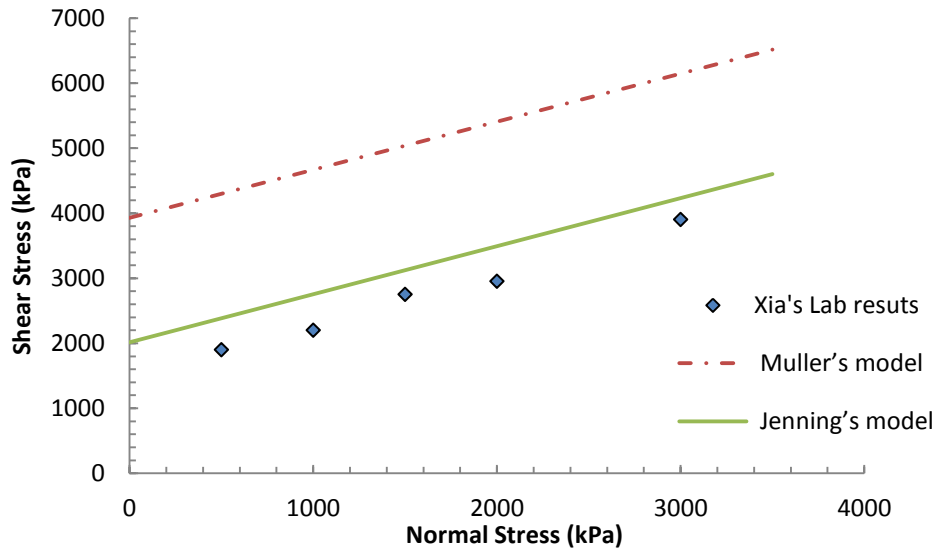
Figure 2.17. Comparison of Muller's [16] and Jennings's [17] failure criterion to Xia's [10] direct shear test results.

Cohesion of rock c_b (kPa)	Friction Angle ϕ_b (deg)	Poisson's ratio ν	Uniaxial Compressive Strength (MPa)	Young's modulus E (GPa)
3930	39.5	0.16	18	3.7
Cohesion of Joint c_j (kPa)	Residual Friction Angle ϕ_j (deg)	Degree of separation k	Tensile Strength (MPa)	
100	33.2	0.5	1.71	

Table 2.1 Basic properties of synthetic rock used in Xia's laboratory test [10]

Jennings assumed that failure surface was in the same direction as the applied shear. As shown by Cho et al. [6], during direct shear testing the development of the surface is progressive and not always parallel to the direction of the applied shear, particularly at low normal stresses. Such a criterion may tend to overestimate shear strength.

2.2.9 Lajtai's model

Lajtai [9] used a series of direct shear test on continuous and discontinuous joint surface oriented in the same direction of the applied shear force to develop his failure criterion. He first showed that the shear strength of a through-going was only a function of the normal stress and

friction angle, i.e., cohesion could be neglected (see Figure 2.18). The results from Lajtai's tests for the discontinuous joints are summarized in Figure 2.19 and Figure 2.20.
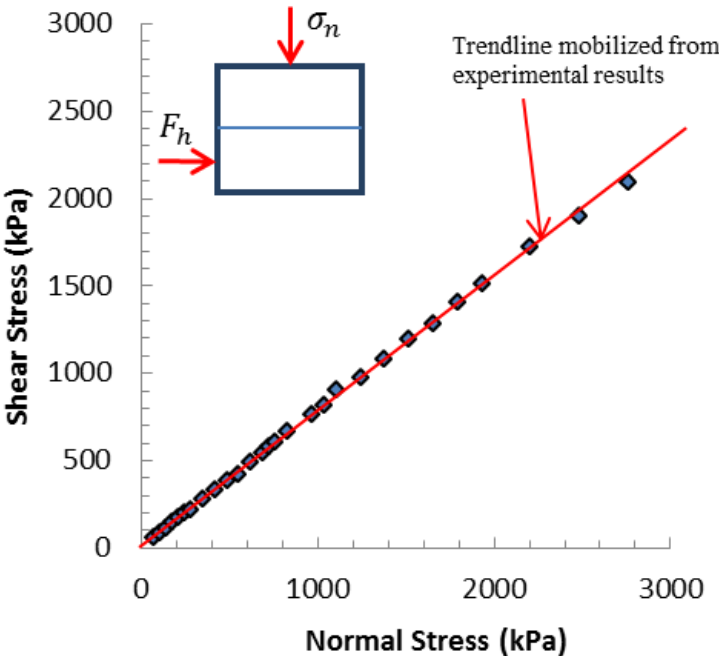
Figure 2.18. Experimental results modified from direct shear tests on continuous joint shear blocks modified from Lajtai [9].

21
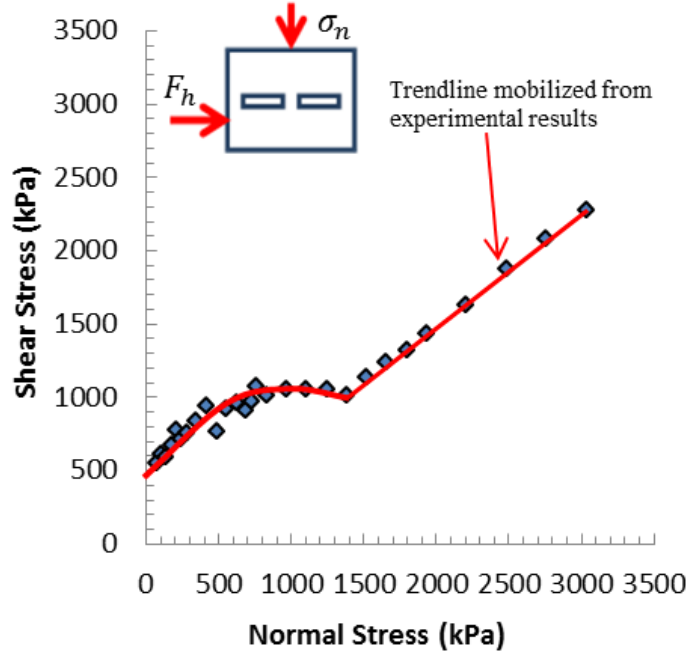
Figure 2.19. Experimental results modified from direct shear tests on open discontinuous joint shear blocks modified from Lajtai [9].
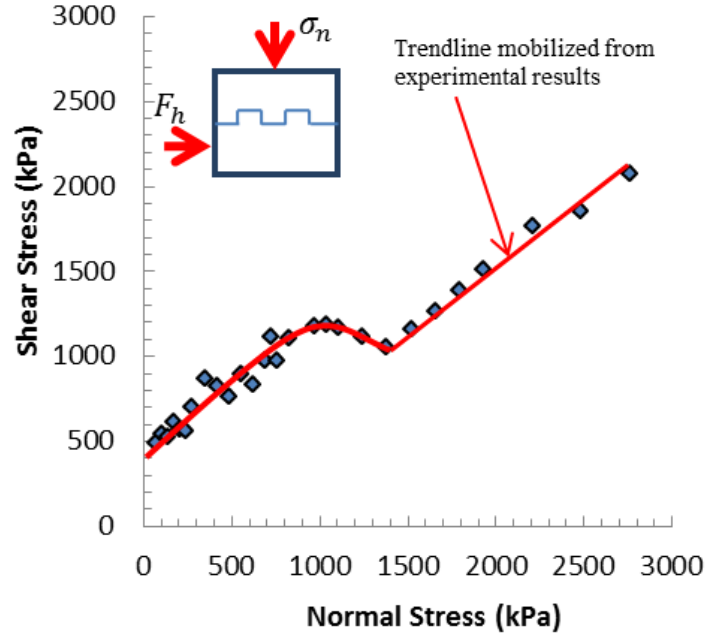
Figure 2.20. Experimental results modified from direct shear tests on closed discontinuous joint shear blocks modified form Lajtai [9].

Based on these test results, Lajtai [18] concluded that the fracture process could be divided into three distinct stages: (1) primary tension fracturing, (2) secondary shear fracturing, and (3) development of the shear zone in the applied shear direction. Consequently, the failure envelope for such conditions was neither linear nor nonlinear and could not be captured by a single failure criterion. Lajtai [18] suggested that the maximum and minimum resistance force to shear of the solid rock bridges could be expressed as:

$$\tau_{\min} = (1 - k)[T(T - \frac{\sigma_n}{1-k})]^{0.5},$$ (2.8)

$$\tau_{\max} = 1 - T(1 - k) + Ck\sigma_n \tan \phi_r,$$ (2.9)

where C is the mobilization factor for joint friction and T is the uniaxial tension strength of synthetic rock.

Lajtai [18] then suggested the direct shear strength was controlled separately by tensile failure, shear failure and by failure at conditions of ultimate strength for both open joint and closed

joint conditions. For the open joint case, the rock bridges have to resist all stresses and the direct shear stress τ is expressed differently by conditions of failure.

Tensile failure gives:

$$\tau = [T(T - \sigma_n)]^{0.5}, \tag{2.10}$$

Where σ_n is normal stress applied on a rock sample.

Shear failure gives:

$$\tau = 0.5[\frac{(2c+\sigma_n \tan \phi)^2}{1+(\tan \phi)^2} - \sigma_n^2]^{0.5}, \tag{2.11}$$

Where c is the cohesion of rock samples and ϕ is the angle of internal friction

Failure at ultimate strength gives:

$$\tau = \sigma_n \tan \phi_r, \tag{2.12}$$

where ϕ_r is the angle of friction at residual strength. Lajtai [18] then combined three types of failure in the open joint case into one figure, shown below.
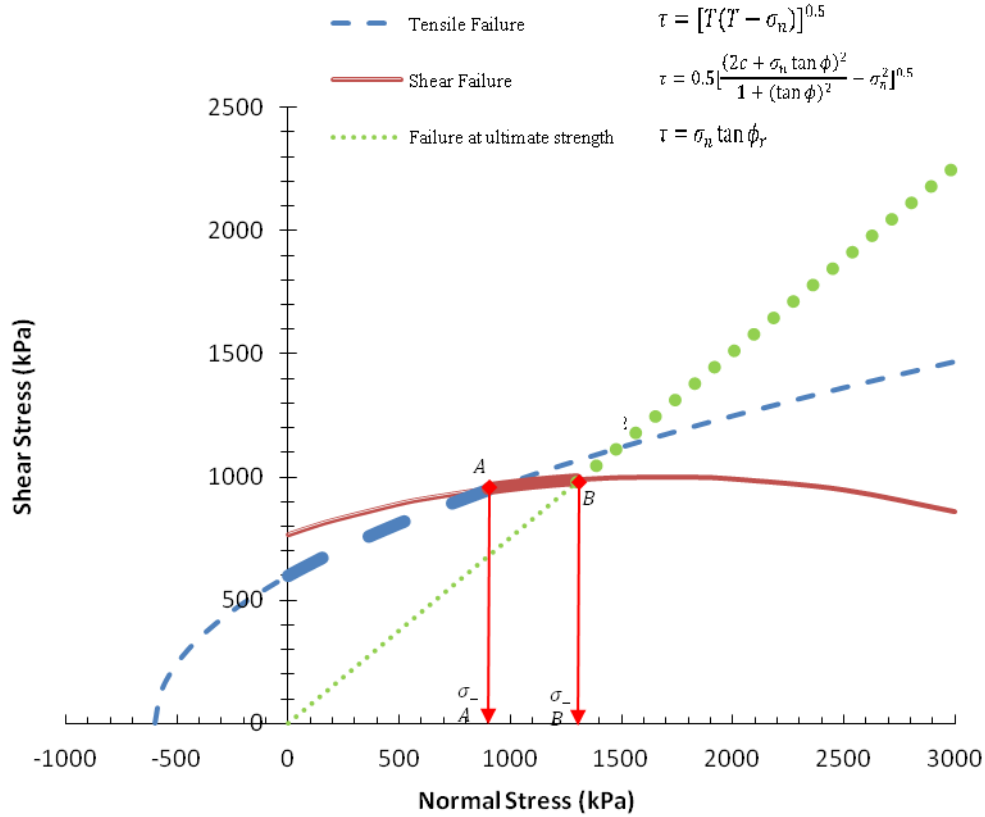
Figure 2.21. Failure criteria for direct shear on rock samples contains discontinuous open joint modified from Lajtai [18], the combined failure envelope for results given in Figure 2.19 is illustrated by the "thick lines".

It was observed that the intersection between tensile failure and shear failure curve is point **A**, and the intersection between shear failure and failure at ultimate strength is point **B**. When normal stress is low, expressed as $\sigma_n < \sigma_A$, the tensile failure will dominate the yielding; when normal stress is high, expressed as $\sigma_n > \sigma_A$, shear failure will dominate the yielding. However, when normal stress is larger than σ_B, the failure condition will turn to ultimate strength and only the basic friction angle of the joint will control the failure criterion. A transparent line marked on the figure showing that the combination failure criterion was consistent with the experimental results shown in Figure 2.21.

Lajtai [18] then used the same method to conclude the failure criterion in the case of a closed discontinuous joint; he stated that the friction may or may not provide an additional source of strength depending on the scale of the mobilization factor C, where $0 < C < 1$.

$$\tau = Ck\sigma_n \tan\phi_j + (1-k)\left[T(T-\sigma_n)\right]^{0.5} \quad \text{for tensile failure,} \tag{2.13}$$

$$\tau = Ck\sigma_n \tan \phi_j + \frac{(1-k)}{2} \left[\frac{(2c+\sigma_n \tan \phi)^2}{1+(\tan \phi)^2} - \sigma_n^2 \right]^{0.5} \text{ for shear failure,} \tag{2.14}$$

$$\tau = \sigma_n \tan \phi_p \text{ for failure at ultimate strength,} \tag{2.15}$$

where ϕ_j is the angle of joint friction and k is the degree of separation.

Lajtai [18] concluded that cohesion dominates the yielding of material under low normal stress while friction dominates the yielding of material under high normal stress. Lajtai's shear strength criterion overcame the disadvantages of the average method proposed by Muller and Jennings. However, Lajtai considered the three types of failure separately in his model, which makes it difficult to apply in practice.

2.2.10 Liu and Xia's model

Liu and Xia [19-21] proposed a new model in direct shear tests focused on the combined action of shear and tension. The model contained two original joints at two ends of a shear plane and two proposed new joints after the start of the test as shown in Figure 2.22.
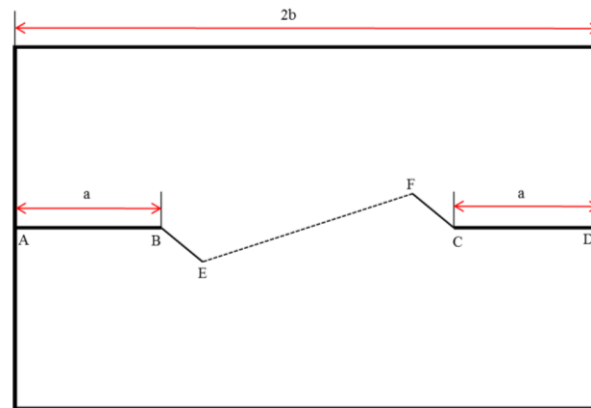
Figure 2.22. Rock Model prepared for direct shear test by Liu and Xia [19]. Original joint **AB** and **CD**, with new joint **BE** and **CF** assumed after the start of the test.

The failure mode is assumed to be the same as Xia's [10] laboratory observation. With the increase of shear stress, the new crack **BE** and **CF** propagated at the tip of the original joint **AB** and **CD** under tensile stress. The final shear plane **EF** was caused by shear failure. The direction of the maximum principle stress was assumed as the same direction as the new crack propagation direction **BE**; the direction of the minimum principle was assumed to be perpendicular to **BE**. The shear strength criterion under the combined action of shear and

tension was proposed by Liu and Xia, and is solved by the finite differential method shown below:

$$\tau = \left[\frac{b-ac_n}{b}\tan\left(0.5\tan^{-1}\left(\frac{2\tau}{\sigma_n}\right)+\frac{\phi_0}{2}-\frac{\pi}{4}\right)+\frac{a}{b}c_n\tan\phi_j\right]+\frac{(b-a)c_0\cos\phi_0\sin\left(\left(\frac{\pi}{2}\right)-0.5\tan^{-1}\left(\frac{2\tau}{\sigma_n}\right)\right)}{b\cos\left(\frac{1}{2}\tan^{-1}\left(\frac{2\tau}{\sigma_n}\right)+\frac{\phi_0}{2}-\frac{\pi}{4}\right)\sin\left(\frac{\pi}{4}-\frac{\phi_0}{2}\right)}+$$

$$\frac{a}{b}c_j \qquad\qquad\qquad\qquad\qquad\qquad\qquad\qquad\qquad\qquad\qquad\qquad (2.16)$$

where c_n is the coefficient of pressure transmission on the joint surface ($0 < c_n < 1$)

c_0, ϕ_0 are the cohesive strength and angle of internal friction of the rock bridge,

ϕ_j is the angel of joint friction of the fissure,

c_j is the cohesive strength of the joint, which will be relatively small.

In Equation 2.16 τ appears on both sides of the equation and hence must be solved numerically.

Liu and Xia compared the results from Equation 2.16 using the properties in Table 2.2 with the laboratory results from Ren and Bai [22-24] for direct shear tests of synthetic rock containing a discontinuous joint. The calculated shear strength using Equation 2.16 is in good agreement with the laboratory results (Table 2.3). In these tests, the normal stress range is limited to 1 to 3 MPa and hence it is not known if the methodology is applicable to a wider range of normal stress. More rock samples for laboratory tests are needed to establish a clear relationship between the shear strength and applied normal stress in fracture rock mechanics.

Table 2.2 Physical and mechanical parameters of model materials

Unit Weight (kN/m^3)	Uniaxial Compression Strength (MPa)	Tensile Strength (MPa)	Poisson's Ratio	Elastic Modulus (Gpa)
15	14.3	2.78	0.1	4.68
Cohesion of internal friction (MPa)	Internal friction Angle ($^\circ$)	Cohesion of joint friction (MPa)	Joint Friction Angle ($^\circ$)	
4.23	26.5	0	35.2	

Table 2.3 Direct shear test result under different fissure distribution

Test No.	Left Joint length (cm)	Solid bridge length (cm)	Right Joint length (cm)	σ_n (MPa)	τ_{lab} (Mpa)	$c_{calculated}$ (Mpa)
1	13.5	3	13.5	2	1.49	1.42
2	12	6	12	2	1.67	1.72
3	9	12	9	1	1.75	1.88
4	9	12	9	2	2.29	2.36
5	9	12	9	3	2.87	2.78

2.3   Summary

Early approaches for estimating the shear strength of discontinuous joints estimated the total shear strength by considering the shear strength contribution from a joint and that from the intact rock bridge. Muller's [16] and Jennings's [17] criteria used this approach assuming that the failure surface forms in the same direction as the applied shear stress. However, laboratory direct shear experiments showed that the development of a shear zone containing a discontinuous joint requires the initiation of new fractures. These new fractures develop as tensile fractures but do not develop in the direction of the applied shear. Liu and Xia's [19-21] recognized the need to account for these tensile fractures and proposed a shear strength criterion that attempted to account for the strength contribution from both of the rock bridges, the open joint and the newly developed fractures. Their proposed solution required numerical iteration and was supported by limited laboratory test results.

Lajtai [9] observed during direct shear testing of rock containing a discontinuous joint, that it was not possible to describe the development of the rupture surface with a single equation. In order for the throughgoing rupture surface to form the existing joints must interact with the newly initiated tensile fractures and this interaction leads to the development of a principal slip plane. To capture this complex process Lajtai [18] proposed that the shear strength of the Principal slip plane (ultimate or residual strength after large displacements) could be predicted using the traditional linear form of the Mohr-Coulomb equation given by Equation 2.5. For the shear strength that includes the initiation of the tensile fractures, Lajtai proposed a strength criterion based on the early work of Griffith. Lajtai proposed that the boundary between the two equations could be defined by the normal stress equal to the tensile strength of the material. In other words once the normal stress exceeded the value of the tensile strength, the traditional linear form of the Mohr-Coulomb equation was applicable. The importance of Lajtai's work was that it drew attention to the difficulty of establishing the shear strength of discontinuous joints at low normal stresses, such as encountered in small rock slopes. In the following chapters laboratory tests and numerical analysis are used to evaluate Lajtai's suggestions.

2.4   References

[1]   Hoek, E., Bray, J. 1974. Rock Slope Engineering. The Institution of Mining and Metallurgy. London. p.309.

[2]   ISRM. Suggested Methods for the Quantitative Description of Discontinuities in Rock Mass. *Int. J. Rock Mech. Min. sci. & Geomech. Abstr*. Vol. 15. pp. 319-368.

[3]   Cloos, E. 1955. Experimental Analysis of Fracture Patterns. *Bull. Of Geol. Soc. Of America.* 66: 241-256.

[4]   Tchalenko, J. S. 1970. Similarities between Shear Zones of Different Magnitudes. *Geological Society of America Bulletin*, Vol. 81: 1625-1640.

[5]   Skempton, A.W. 1967. Some Observations on Tectonic Shear zones. *In: Proceedings of the first International congress on Rock Mechanics*, Lisbon. V1: pp. 329-335.

[6]   Cho, N., Martin, C. D., Sego, D. C. 2008. Development of a shear zone in brittle rock subjected to direct shear. *International Journal of Rock Mechanics & Mining Sciences*. Vol. 45: 1335-1346.

[7]   Ladanyi, B., Archambault, G. 1970. Simulation of Shear Behavior of a Jointed Rock Mass. *In Proceedings 11th US Symposium on Rock Mechanics (AIME)*, 105–125.

[8]   Ladanyi, B., Archambault, G. 1977. Shear Strength and Deformability of Filled Indented Joints. In International Symposium, the Geotechnics of Structurally Complex Formations, Capri, 2: 317–326.

[9]   Lajtai, E. Z. 1969. Shear strength of weakness planes in rock. *Int J Rock Mech Min Sci Geomech Abstr*, Vol. 6, No. 7: 499-515.

[10]   Xia, Cai-chu., Xiao, Wei-min., Ding, Zeng-zhi. 2010. Modification of Jennings Strength Criterion for Intermittent Joints Considering Rock Bridge Weakening and Joint Surface Undulating Angle. *Chinese Journal of Geotechnical Engineering.* Vol. 29, No.3: 485-492.

[11]   Gehle, C., Kutter, H. K. 2003. Breakage and shear behaviour of intermittent rock joints. *International journal of Rock Mechanics & Mining Sciences*. Vol. 40: 687-700.

[12]   Jeager, J. C., Cook, N. G. W., Zimmerman, R.W. 2007. Fundamentals of Rock Mechanics. 4th edition. John Wiley & Sons: 65-78

[13]   Patton, F. D. 1966. Multiple modes of shear failure in rock. Proc. 1st. *Congr. Int. Soc. Rock Mech.* 1, pp. 509-513.

[14] Johansson, F. 2009. Shear Strength of Unfilled and Rough Rock Joints in Sliding Stability Analyses of Concrete Dams. Ph.D. thesis. Department of Civil and Architectural Engineering, Royal Institute of Technology.

[15] Barton, N. 1973. Review of a New Shear Strength Criterion for Rock Joints. *Engineering Geology*. 7:287-332.

[16] Müller L. 1963. *Der Felsbau*, Enke, Stuttgart.

[17] Jennings, J.E. 1970. Mathematical Theory for the Calculation of the Stability of Slopes in Open Cast Mines. *Proceedings of the Theoretical Background to the Planning of Open Pit Mines with Special Reference to Slope Stability Johannesburg, Republic of South Africa.* 87-102.

[18] Lajtai, E. Z. 1969. Strength of discontinuous rocks in direct shear. *Geotechnique*, Vol.19, No. 2: 218-233.

[19] Liu, Yuan-ming., Xia, Cai-chu. 2006. Study on models and strength behavior of rock mass containing discontinuous joints in direct shear. *Chinese Journal of Geotechnical Engineering*, Vol. 28, No.10: 1242-1247.

[20] Liu, Yuan-ming., Xia, Cai-chu. 2007. Advances in research of rock masses containing discontinuous joints in direct shear test. *Rock and Soil Mechanics*, Vol. 28, No. 8: 1719-1724.

[21] Liu, Yuan-ming., Xia, Cai-chu., Li, Hong-zhe. 2007. Development in Joints Research and its Application to Rock Mass containing Discontinuous Joint. *Chinese Journal of Underground Space and Engineering*, Vol. 3, No. 4: 682-693.

[22] Ren, Wei-zhong., Bai, Shi-wei., Feng Ding-xiang., Chen, Jin-qing., Jia, Zhong-he. 2000. Strength behavior of rock mass containing coplanar close intermittent joints under direct shear condition. *Proceeding of 6ᵗʰ Congress of Chinese Rock Mechanics and Engineering*. *Beijing, Science Pres*: pp. 147-151.

[23] Ren, Wei-zhong., Wang, Geng-sun., Bai, Shi-wei., Feng, Ding-xiang., Chen Jin-qing., Chia, Johnho. 2003. Strength behavior of rock mass containing coplanar close intermittent joints under direct shear condition. *Chinese Journal of Rock Mechanics and Engineering*, Vol. 22, No. 10: 1167-1672.

[24] Bai, Shi-wei., Ren, Wei-zhong., Feng, Ding-xiang., Zhou, Shao-huai. 1999. Study of Strength behavior of rock containing close intermittent joints under direct shear condition. *Rock and Soil Mechanics*, Vol.20, No. 2: 10-15.

3 Selection and characterizing the synthetic rock

An extensive laboratory testing program was carried out to establish the material parameters for the following loading paths:

(1) Uniaxial Compression test

(2) Brazilian test

(3) Direct shear test

The Uniaxial Compression and Brazilian tests were performed to determine the basic parameters of synthetic rock behaviour. The intact properties from these tests were then inserted into the finite element analysis software for numerical simulation.

The focus of this research is the strength of discontinuous joints. The strength of a joint is typically established using the direct shear-loading path. A series of direct shear tests were performed with various joint configurations. The results from those tests are described in the following chapter. In this chapter the basic properties of the synthetic rock are provided.

3.1 Selection of synthetic rock material

Brittleness and heterogeneity are two important behaviour characteristics of natural rock. The selection of a synthetic material that represents a natural rock must display these characteristics. Three materials were considered as potential candidates for our synthetic rock: concrete, sulfaset, and plaster.

Concrete has been widely studied. It exhibits both brittle and heterogeneous behaviour of synthetic rock because aggregates can be mixed with cement to simulate the behaviours of natural rock. The main disadvantage of concrete is the 28 days of curing time required for full strength. For this reason, concrete was not selected.

Sulfaset and plaster have similar properties and characteristics. The major difference is that sulfaset starts as a liquid while plaster starts as a cohesive plastic material. For our purposes we needed to create discontinuous joints and it was more practical to create the discontinuous joint using plaster rather than sulfaset. In addition, Lajtai [1] used plaster for his laboratory tests and hence this provided a more direct comparison with published results. For these reasons, plaster was selected as the candidate synthetic rock and the characteristics of our plaster synthetic rock are outlined below.

The mix design for the synthetic rock must provide a heterogeneous brittle material with a high uniaxial compressive strength to tensile strength ratio. Sand with a mean grain size of approximately 0.3 mm was used to create heterogeneity within the synthetic rock. The size distribution of the sand is shown in Figure 3.1. After a series of initial tests the final mix design selected was sand, plaster and water, by weight, 3:3:2. Figure A. 6 of Appendix A illustrates the procedure used to develop a uniform sample using of sand and plaster.
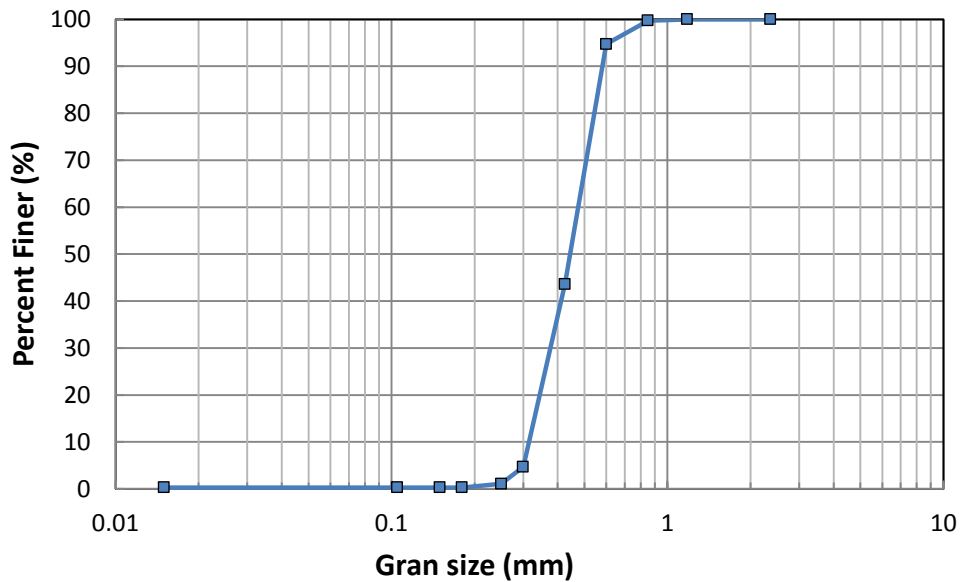
Figure 3.1 Grain size distribution of play sand added in synthetic rock

3.2 Uniaxial Compression Test

Uniaxial compression tests were carried out on cylinder specimens of 50 mm diameter by 100 mm length following the International Society of Rock Mechanics (ISRM) [2] procedure. Axial strain was measured by a vertical LVDT and applied loading was measured automatically by using the rock mechanics testing system shown in Figure A. 1 of Appendix A. All data were recorded in the data acquisition system shown in Figure A. 2.

Figure 3.2 shows the typical failure shape of a synthetic rock specimen in uniaxial compression. Figure 3.2 (a) shows the crack starting from the top of the sample and propagating to the middle. Figure 3.2(b) shows a typical cone shaped fracture formed at the top of the specimen. Both failed specimens have some high angled fractures. Figure 3.3 shows six samples of the uniaxial compression axial stress versus the axial strain response. The result shows consistency of pre-peak stiffness among the samples. Sample 2 and 6 show significantly brittle behaviour after peak stage.

<center>(a)   (b)</center>
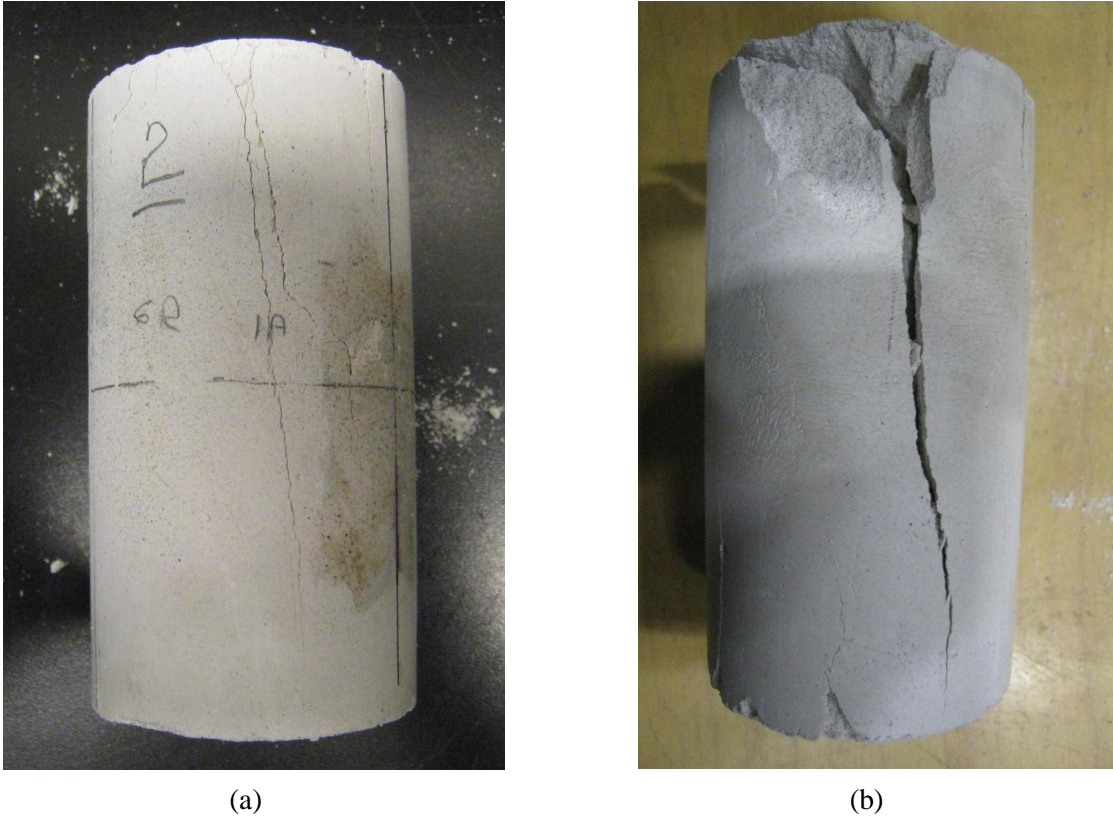
Figure 3.2. Typical failure shape of a synthetic rock specimen under uniaxial compressive load.
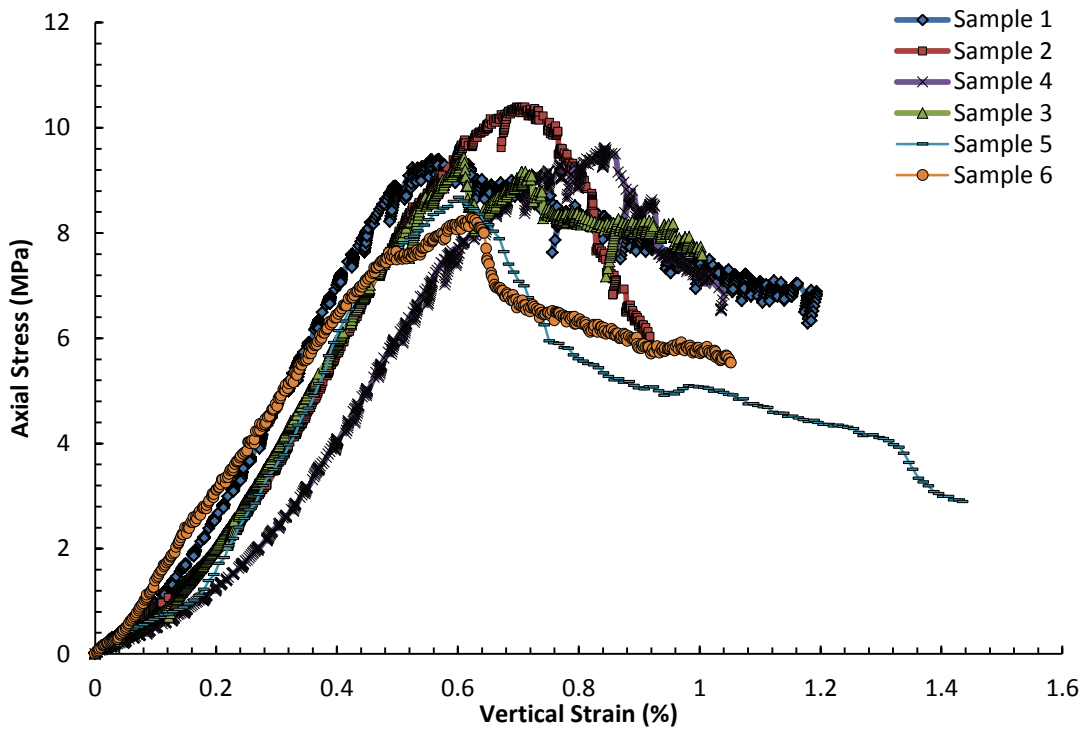
Figure 3.3. Uniaxial compressive test result of intact synthetic rock.

3.3 Brazilian Test

The indirect tensile strength of brittle synthetic rock was investigated using the eight conventional Brazilian Tests following the ISRM standard [3]. Goodman [4] proposed that the Brazilian test provides a higher tensile strength than that of the direct tension test because of the effect of fissures. Short fissures weaken a direct tension specimen more severely than they weaken a Brazilian specimen. The Brazilian test was also selected because of the simple testing procedure. The sample diameter was 50 mm and the height to diameter ratio was 0.75 with a loading rate of 0.005 mm/s, as suggested in ISRM standards [3]. The loading plate and test machine is shown in Figure A. 3. The failure shape is mainly a straight tensile fracture through the diameter of the sample shown in Figure 3.4.

Seven results out of eight tests are shown in Figure 3.5 because one test result was far from the specification by the ISRM standard. This illustrates that the initial normal stiffness is not consistent. The reason for this behaviour may be due to the existence of internal pores. Because the Brazilian disk shape was not perfectly circular but a little elliptical this resulted in different contact conditions and made the final failure strength different. The average failure tensile strength is determined as 1.84 MPa.

Figure 3.4. Tensile fracture of the sample after the Brazilian Test.
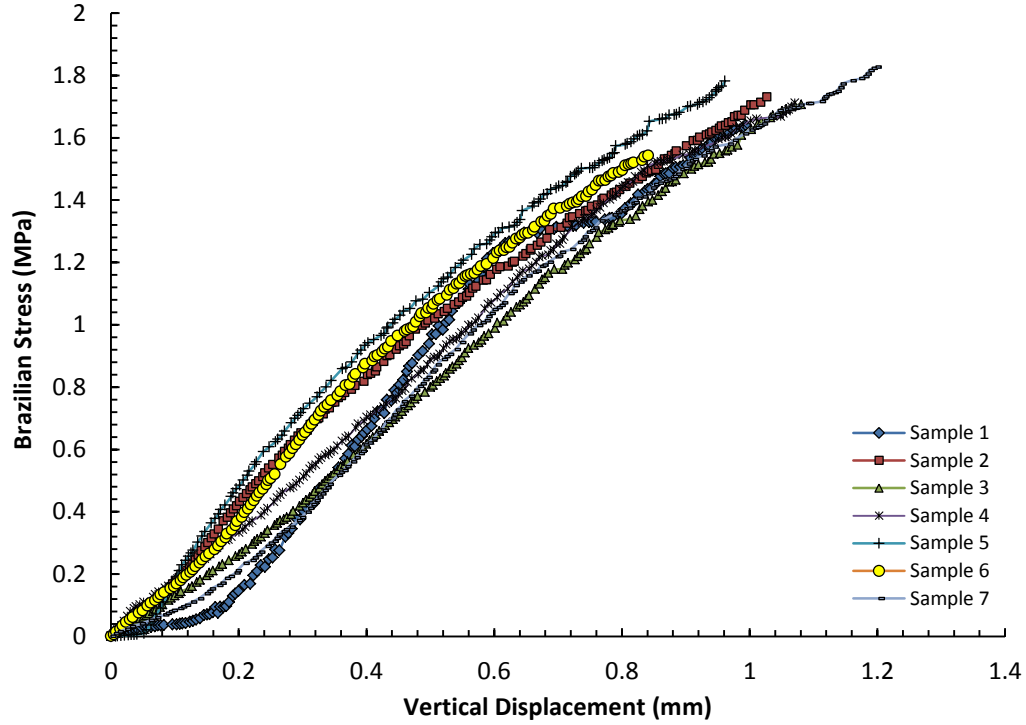
Figure 3.5. Brazilian test results for intact synthetic rock.

3.4 Deformation Modulus and Poisson's Ratio

The axial and radial displacements measured during the uniaxial compressive tests were used to establish the Young's modulus and Poison's ratio. The axial displacements of rock samples were recorded by a vertical LVDT on the test machine. The four strain gauges were bounded laterally at equal radial distance on the middle height of the rock specimen surface in order to measure the radial displacement during the test. There are another two LVDT controlled gauges pointed at the center of the circle at the surface of the rock along the diameter line in order to measure the lateral displacement of rock during compression. The surface strain gauge and test system are shown in Figure A. 4.

The calculation procedure was followed by the ISRM standards [2]. The average Young's modulus was calculated from the linear portion of the axial strain versus the axial stress curve shown in Figure 3.6 (a) using the formula:

$$E = \frac{\Delta\sigma}{\Delta\varepsilon_a} \ ,$$ (3.1)

where $\Delta\sigma$ is the difference in axial stress, and $\Delta\varepsilon_a$ is the difference in axial strain.

The lateral strain was determined by a change in two LVDT's readings from the equation:

34

$$\epsilon_d = \frac{\Delta d}{d_0} \ , \tag{3.2}$$

Where d_0 is the original diameter of the sample, and Δd is the total change of lateral displacement along the diameter line.

Poisson's ratio was calculated from both axial strain and lateral strain versus an axial stress curve by the equation:

$$\upsilon = -\frac{\text{slope of axial stress–strain curve}}{\text{slope of lateral stress–strain curve}} \ , \tag{3.3}$$

The measured axial stress versus lateral strain response is shown in Figure 3.6. As illustrated in Figure 3.6 the lateral strain response appears unrealistic, giving Poisson ratios of 0.05. This may be due to the reaction of moisture with the plaster surface, causing the strain gauge not to bond. It was discovered that consistent results using glue to bond the radial strain gauges to the sample could not be achieved. Previous published results (Liu and Xia [5] - [7]) suggested that Poisson's ratio varied from 0.15 to 0.3. Poisson's ratio of synthetic rock was finally estimated as 0.2. The intact synthetic rock properties from our laboratory testing are shown in Table 3.1.
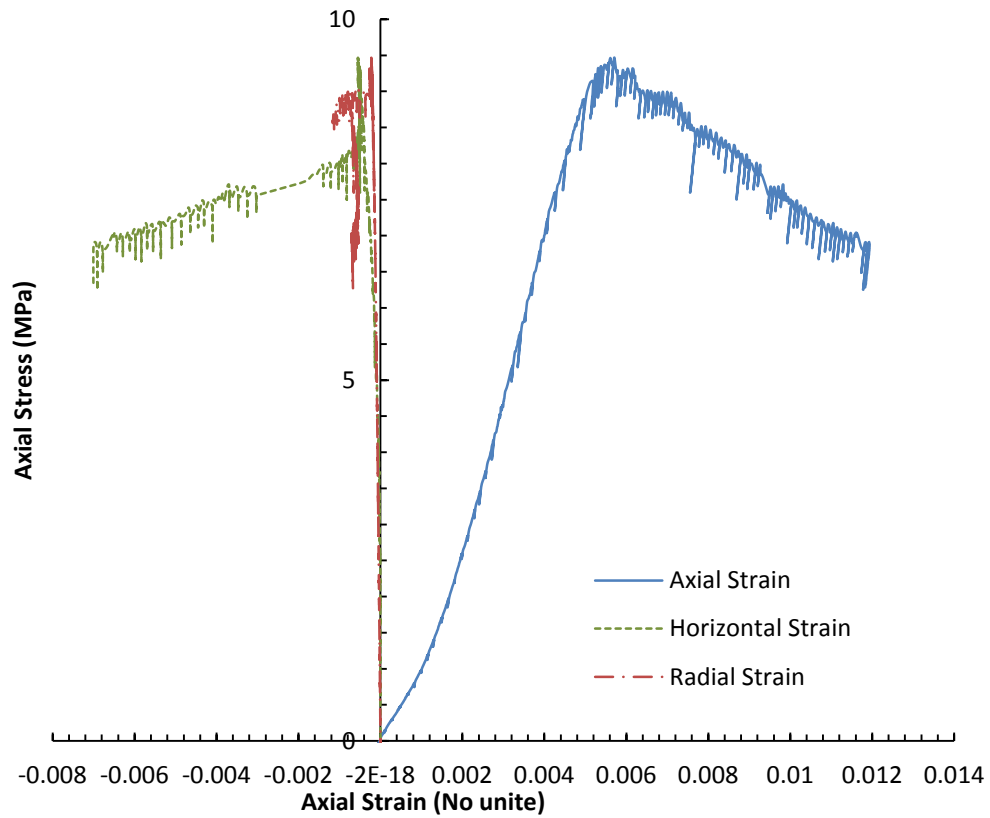
Figure 3.6. Uniaxial compressive test results of a synthetic rock cylinder sample with comparison of axial strain and radial strain.

	Number of Tests	Average Value	Maximum Value	Minimum Value	Standard Deviation
Uniaxial Compressive Strength (MPa)	6	9.74	10.6	9.16	0.6
Brazilian Tension Strength (MPa)	7	1.84	2	1.6	0.15
Young's Modulus (GPa)	6	2.13	2.23	2.06	0.06
Poisson's Ratio	6	0.05	0.08	0.01	0.03

Table 3.1. Basic Parameters of Rock obtained from a Uniaxail Compressive Test.

The Mohr-Coulomb strength parameters cohesion c and friction angle ϕ of intact rock were calculated from Coulomb's shear strength criterion mentioned by Brady and Brown [8]. The intrinsic strength of intact rock in compression is given as:

$$\sigma_1 = \text{UCS} + \sigma_3 \tan\psi, \tag{3.4}$$

$$\tan\psi = \frac{1+\sin\phi}{1-\sin\phi}, \tag{3.5}$$

and

$$\text{UCS} = \frac{2c\cos\phi}{1-\sin\phi}, \tag{3.6}$$

where ψ is the angle of slope in a principal stress coulomb strength envelope shown in Figure 3.7, and UCS is the uniaxial compressive strength.

The calculated c-ϕ strength parameters are shown in Table 3.2 with the strength envelope provided in Figure 3.7.

(a)   (b)
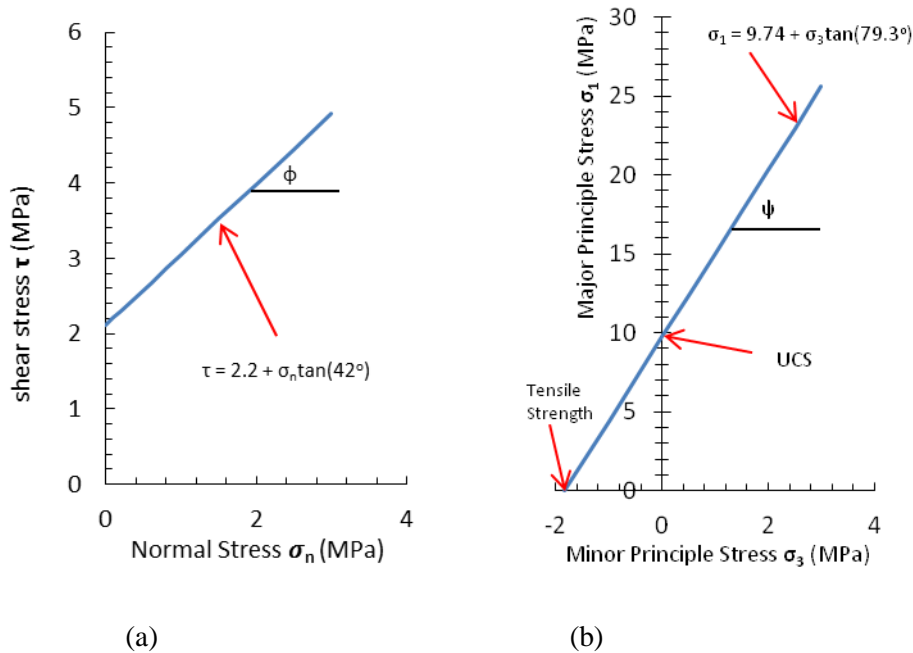
Figure 3.7. Coulomb strength envelopes of intact synthetic rock in terms of (a) shear and normal stresses, and (b) principal stresses.

Table 3.2 The intrinsic cohesion (c) and frictional (ϕ) properties calculated from the intact uniaxial compressive strength.

	Number of samples	Average	Maximum	Minimum	Standard Deviation
Cohesion (Mpa)	6	2.2	2.6	1.8	0.283
Friction Angle (degree)	6	42	46	38	2.858

3.5   Summary

This chapter describes the selection and laboratory testing of synthetic rock to establish the intact rock properties. The selected synthetic rock consisted of plaster, sand, and water. The mixture set quickly and developed a consistent uniaxial compressive strength after seven days of curing at room temperature. The mean uniaxial compressive strength of the synthetic rock was 9.74 MPa, and ranged from 9.16 to 10.6 MPa, while the mean Brazilian tensile strength was 1.84 MPa, ranging from 1.6 to 2 MPa. The ratio of the mean uniaxial compressive strength to mean Brazilian tensile strength was 5.3, which is similar to that reported for natural rock such as shale and phyllite found in mountain area in British Columbia (Cai [9]).

Poisson's ratio of the synthetic rock was the most difficult intact rock property to measure. This was caused by the inability of the glued strain gauges to develop a good bond with the plaster. Based on published information, Poisson's ratio was estimated as 0.2.

3.6   References

[1]   Lajtai, E. Z. 1969. Shear strength of weakness planes in rock. *Int. J. Rock. Mech. Min. Sci. Geomech. Abstr.* Vol. 6, No. 7: 499 -515.

[2]   ISRM. 1978. Suggested Methods for Determining the Uniaxial Compressive Strength and Deformability of Rock Materials. *Int. J. Rock Mech. Min. Sci. Abstr* 137-140

[3]   ISRM. 1978. Suggested Methods for Determining Tensile Strength of Rock Materials. *Int. J. Rock Mech. Min. Sci. Abstr.* 15:99-103

[4]   Goodman, R. E. 1989. Introduction to Rock Mechanics, 2nd edition, *John Wiley &* Sons. 64-66

[5]   Liu, Yuan-ming., Xia, Cai-chu. 2006. Study on models and strength behavior of rock mass containing discontinuous joints in direct shear. *Chinese Journal of Geotechnical Engineering*, Vol. 28, No.10: 1242-1247.

[6]   Liu, Yuan-ming., Xia, Cai-chu. 2007. Advances in research of rock masses containing discontinuous joints in direct shear test. *Rock and Soil Mechanics*, Vol. 28, No. 8: 1719-1724.

[7]   Liu, Yuan-ming., Xia, Cai-chu., Li, Hong-zhe. 2007. Development in Joints Research and its Application to Rock Mass containing Discontinuous Joint. *Chinese Journal of Underground Space and Engineering*, Vol. 3, No. 4: 682-693.

[8]   Brady, B. H. G., Brown, E. T. 1985. Rock Mechanics for Underground Mining. Allen & Unwin, London, pp.86-126.

[9]   Cai, M. 2009. A simple method to estimate tensile strength and Hoek-rown strength parameter *mi* of brittle rocks. *Proceedings of the 3rd CANUS Rock Mechanics Symposium, Toronto, Canada,* 1: 1-12.

4 Behaviour of discontinuous joint subjected to direct shear

A series of direct shear tests were carried out to establish the behaviour of discontinuous joints in shear. The rupture surface varied from planar and continuous to discontinuous. A total of 88 samples were tested.

4.1 Direct shear testing

4.1.1 Sample Preparation

The synthetic rock material used for the direct shear test was the same as in the uniaxial compressive test. The sample was prepared with the top and bottom part separately by using two 50 mm by 50 mm (top and bottom area) molds to make different crack shapes. The cross sectional crack shapes of 15 degrees, 45 degrees and 90 degrees were chosen from the mold. The sample was first mixed with sand, plaster and water in a container and then pulled into the mold while still in a liquid state. The mixing process is shown in Figure A. 5. After 24 hours for curing, the mold was taken off and the samples were cured at normal room temperature and humidity conditions for longer than seven days before testing. The sample containing a joint shape of 15, 45, 90 degrees and a planar smooth joint are shown in Figure A. 6.

The preparation procedure of a sample containing an open joint was different compared with a sample containing a closed joint. The sample was prepared in a mold with two pre-made gaps on the opposing surface with a 1 mm wide inserted steel sheet as shown in Figure A. 9. The sample was first mixed with sand, plaster and water in a container and then pulled into the mold while still in a liquid state. The mixing process was the same as with the closed joint sample shown in Figure A. 5. The steel sheet was pulled out from the mold two hours after the initial set of the sample in order to leave a 1 mm open gap in the sample. After 24 hours of curing, the mold was removed and the samples were cured at normal room temperature and humidity conditions for longer than seven days before testing. The samples A, B, and C containing different shapes of the open joint are shown in Figure A. 10.

4.1.2 Direct Shear Device

The direct shear test machine is shown in Figure A. 7. The direct shear test machine incorporated a load cell and LVDT in both shear and normal direction in order to measure shear force and displacements. The data were recorded by using a data logger linked to a computer shown in Figure A. 8. The time interval of the data recording system was chosen as one second in order to catch peak the stress variation.

The tests were performed with different shapes of joints under different normal stresses ranging from 25 kPa to 3500 kPa. The normal load was directly applied manually to the top of the sample by loading weights when the normal stress was less than 500 kPa. Under high normal stress larger than 800 kPa, a cantilever arm was set up at the bottom of the top loading cap in order to produce a bending moment inducing a large loading to the top of the sample, as shown in Figure A. 8. An air level was placed on the cantilever arm in order to confirm the loading as vertically downward. The maximum shear displacement was less than 8.5 mm because of the short distance of movement of the lower shear box restricted by the machine. The data were analyzed after test following the ISRM standard [1].

4.2 Continuous planar-joint

4.2.1 Sample Dimension

The cross-sectional joint shape of 0 degrees (smooth planar joint) samples are shown in Figure 4.1.
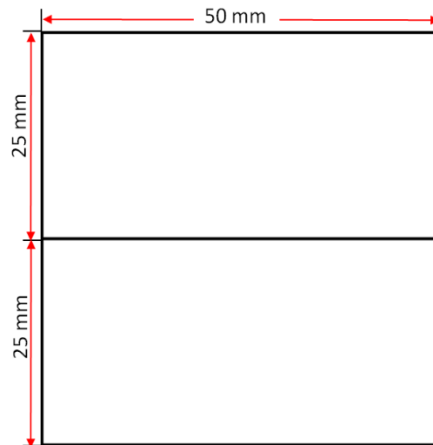
Figure 4.1:   Direct shear sample containing a planar continuous joint

4.2.2 Residual shear strength of planar continuous joint

Direct shear tests on the planar continuous joint were carried out over normal stresses ranging from 50 kPa to 3.5 MPa. The shear stress versus shear displacement results from those tests are given in Figure 4.2. At normal stresses ranging from 50 kPa to 2 MPa the shear stress – displacement curves showing typical elastic-plastic behaviour, i.e., the peak stress and the residual stress is essentially the same. At 400 kPa normal stress there is a slight strain weakening behaviour.

When the normal stress is 2.5 MPa or larger the planar joint show a noticeable strain weakening behaviour (Figure 4.2 (c)). At a shear displacement of 8 mm the samples had not reached its residual strength. Inspection of the joint surface indicated that at these high normal stresses the joint surface was very rough while the joint surface at low normal stress remained planar and smooth to touch. Photos of these joint surfaces are shown in Figure A. 11 in Appendix A. It is likely that under high normal stress (≥2.5 MPa), granular gouge particles develop during shearing leading to the roughened surface shown in the photo. The evidence for the development of this gouge can be observed in the dilation of the samples during shearing.

(a)

(b)

(c)

43
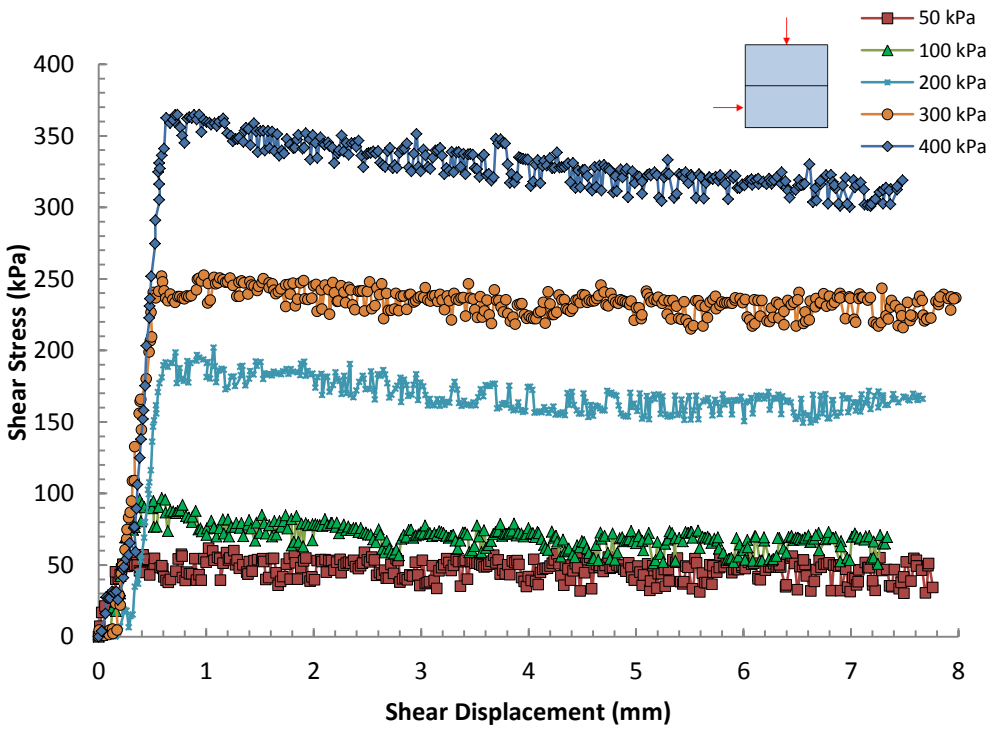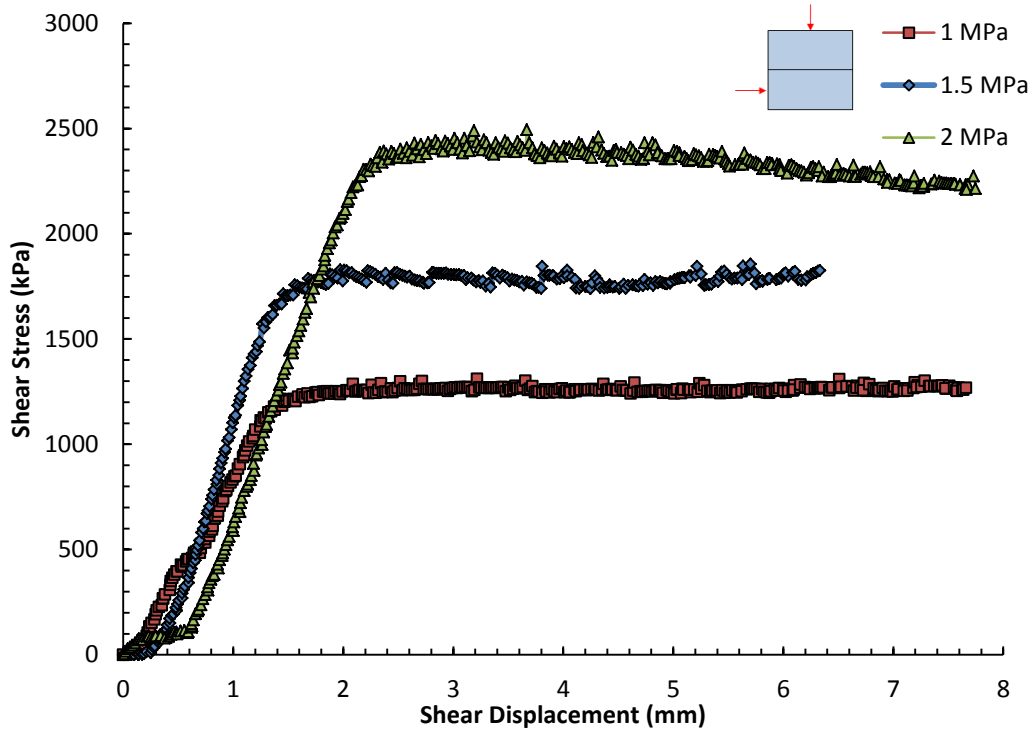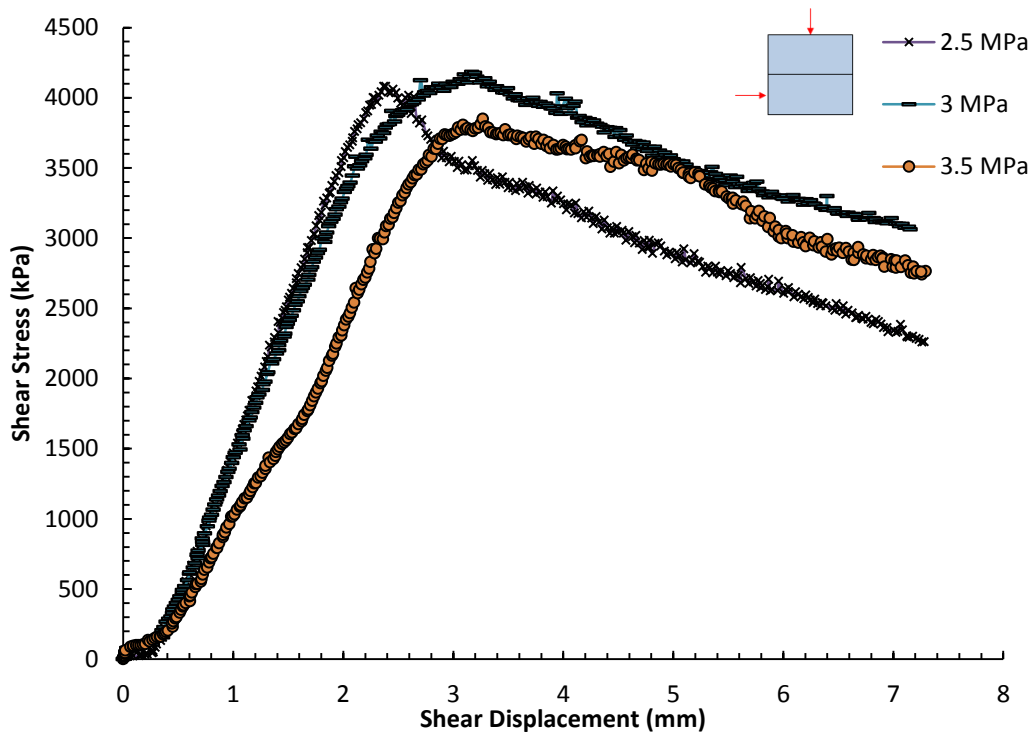
Figure 4.2: (a) Shear stress – displacement curve under normal stress smaller than 400 kPa, (b) Shear stress – displacement curve behaviour under normal stress between 1 MPa and 2 MPa, and (c) Shear stress – displacement curve behaviour under normal stress larger than 2.5 MPa.

The vertical displacement (dilation) during shearing of planar joint surface samples under different normal stress is plotted in Figure 4.3. Inspection of Figure 4.2 reveals that peak shear stress was reached between 1mm at low normal stress and approximately 2 mm at high normal stress. Figure 4.3 show that when the normal stress was greater than 2 MPa, unusual dilation took place after the peak shear stress was reached. This is further evidence of the development of a roughened fracture surface during shearing. These results suggest that particle crush during shearing when the normal stress is greater than the tensile strength (1.8 MPa).
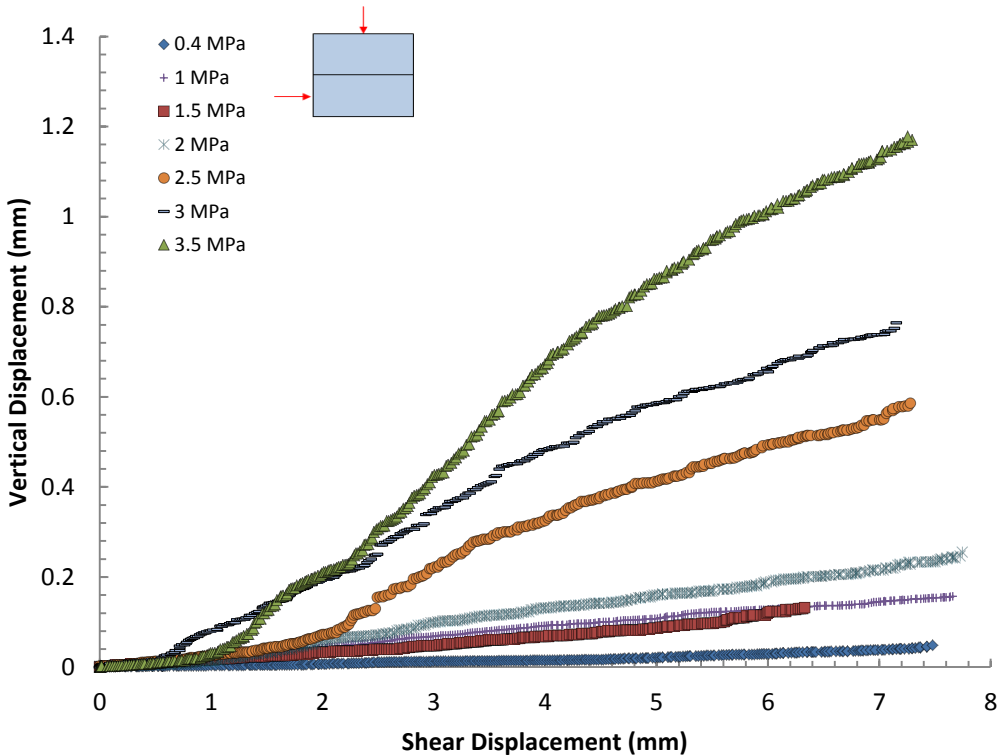
Figure 4.3. Dilation versus shear displacement of planar joint surface samples under different normal stress.

The residual shear strength results obtained from the direct shear tests on the smooth planar joint are shown in Figure 4.4 in shear stress versus normal stress space. The frictional angle of

the planar joint was estimated using linear least squares at approximately 38 degrees with zero cohesion under low (≤400 kPa) normal stresses. When the normal stress ranged from 1 MPa to 2 MPa, the residual strength envelope is given by a friction angle of 46 degrees with an apparent cohesion of 200 kPa. This apparent cohesion does not exist at low normal stress and likely reflects the initiation of the development of a roughened joint surface, observed at higher normal stresses. All three samples that were tested with a normal stress of 2.5, 3 and 3.5 MPa, showed essentially the same peak shear strength of approximately 4 MPa.
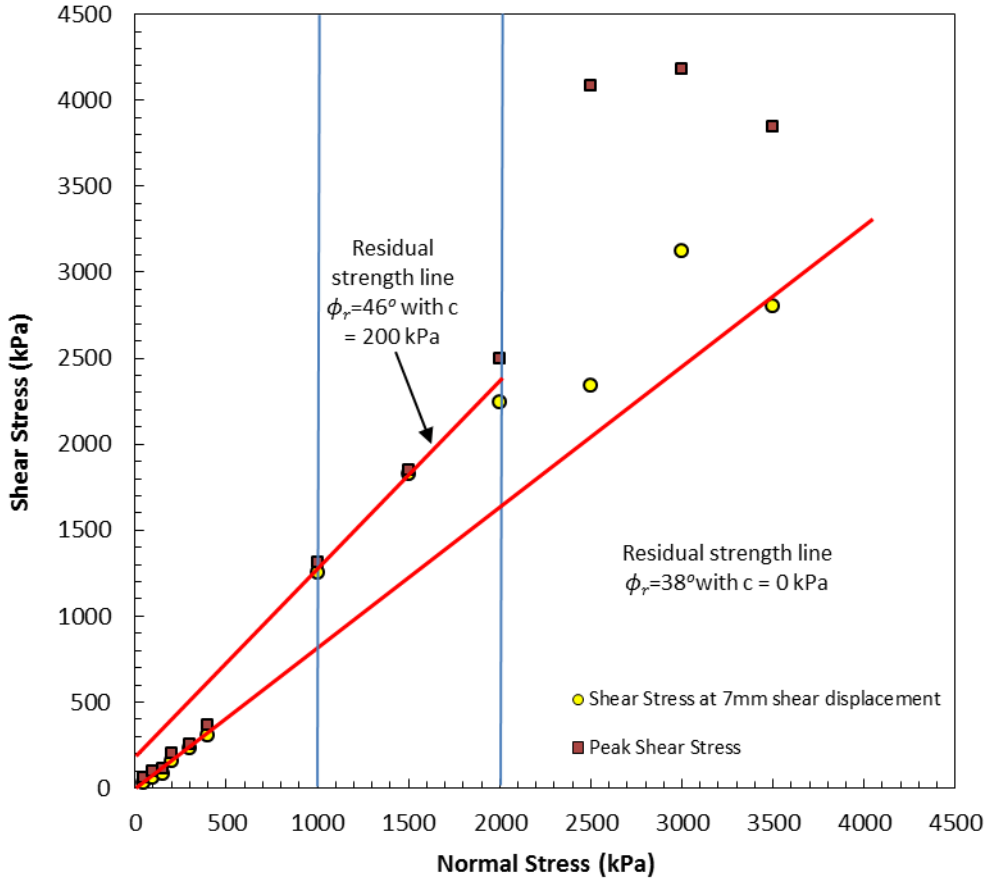
Figure 4.4. Residual shear strength envelope with an increase of normal stress obtained from direct shear test on a planar surface sample.

4.2.3 Shear and normal stiffness of planar continuous joint

The average shear stiffnesses at the pre-peak stage were obtained from the direct shear tests on the continuous planar joint sample. The shear stiffness at the pre-peak stage as a function of normal stress is plotted in Figure 4.5. It can be observed in in Figure 4.5 that the shear stiffness increases with increasing normal stress. At a normal stress of 2 MPa, the shear stress appears to

45

plateau off at a value of approximately 2000 kPa/mm. Below the normal stress of 1000 kPa, the increase in shear stiffness as a function of normal stress is much greater than increase that occurs at normal stress values above 1000 kPa. The average shear stiffness values at the pre-peak stage were separated into two groups, below and above a normal stress of 1000 kPa and summarized in Table 4.1.
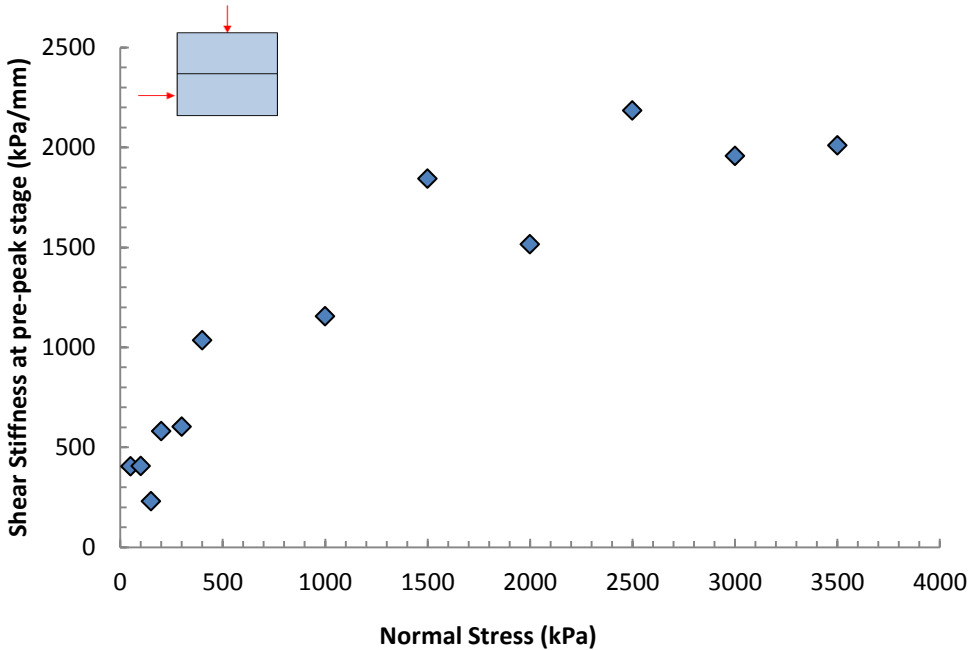
Figure 4.5. Shear stiffness behaviour at a pre-peak stage obtained from the direct shear test on a planar joint for various normal stresses.

Table 4.1 Shear stiffness at a pre-peak stage obtained from the direct shear test on a planar joint under different normal stress.

Normal Stress (kPa)	Shear Stiffness (kPa/mm)	Shear Stiffness (kPa/m)	Shear Stiffness
50	403	403000	Averaged from σ_n= 50 to 400 kPa 444 kPa/mm
100	405	404579	
150	229	229000	
200	580	580110	
300	602	602020	
400	1034	1033865	
1000	1154	1153642	Averaged from σ_n= 1000 to 3500 kPa 1671 kPa/mm
1500	1843	1842458	
2000	1514	1514249	
2500	2184	2183879	
3000	1957	1956855	
3500	2008	2008403	

The normal stiffness of a planar joint sample was obtained before the direct shear test by adding a normal load continuously and recording the vertical displacement of the sample by using the Rock Mechanics Testing System (See Figure A. 1). The maximum normal stress was controlled as 3 MPa in order to prevent crack initiation in the intact rock section. The test results are shown in Figure 4.6 and the normal stiffness was calculated by formula:

$$K_n = \frac{\Delta\sigma_n}{\Delta\delta_{n(\text{record})}} \quad , \tag{4.1}$$

where $\Delta\sigma_n$ is the normal stress difference during the loading process, and $\Delta\delta_{n(record)}$ is the normal displacement difference recorded during the loading process. When the elastic deformation of rock mass samples and the steel cap on top of the sample were taken into consideration (Jacobsson and Flansbjer [2]), the displacement difference was replaced by:

$$\Delta\delta_{n(\text{system})} = \Delta\delta_{n(\text{record})} - \frac{L\Delta\sigma_n}{E} - \frac{L_{\text{steel}}\Delta\sigma_n}{E_{\text{steel}}} \quad , \tag{4.2}$$

$$K_n = \frac{\Delta\sigma_n}{\Delta\delta_{n(\text{system})}} \quad , \tag{4.3}$$

where E is Young's modulus of the rock sample obtained from a uniaxial compressive test as 2.134 GPa, E_{steel} is the Young' modulus of the steel cap as 210GPa, and L and L_{steel} are the height of the sample measured as 50 mm. Because of the high Young's modulus of steel, it was considered as an incompatible material. However, the small movement of the steel cap was still taken into consideration in order to make the results more precise.

The normal stiffness was found to different under different normal stress, as shown in Figure 4.6 (a) and increased with the increase of normal stress shown in Figure 4.6 (b). However, the normal stiffness can be averaged into two values when under low or high normal stress. When normal stress is less than 1500 kPa, the normal stiffness was calculated as 3700 kPa/mm; when normal stress is more than 1500 kPa but less than 3000 kPa, the normal stress was calculated as 12000 kPa/mm.
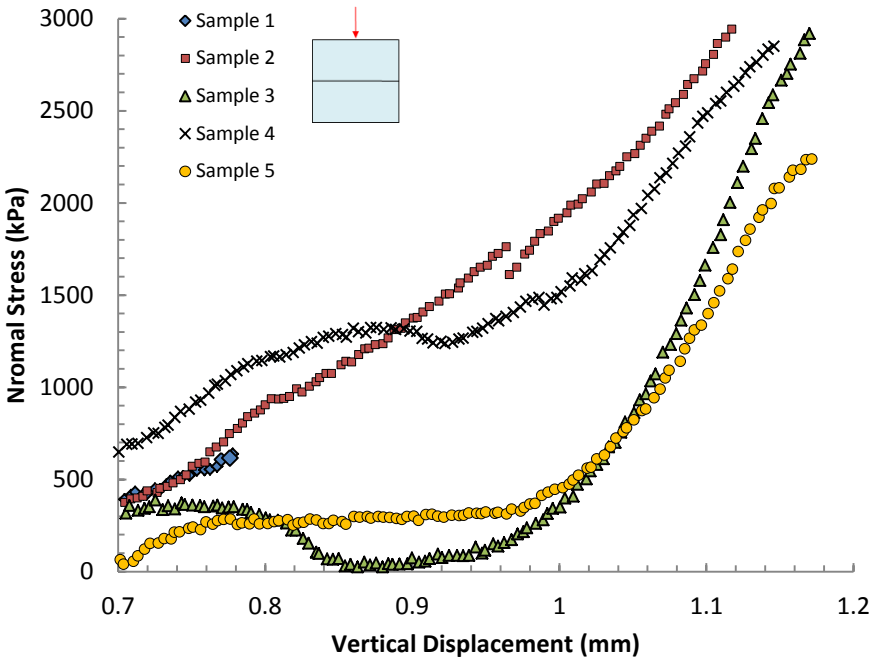
(a)
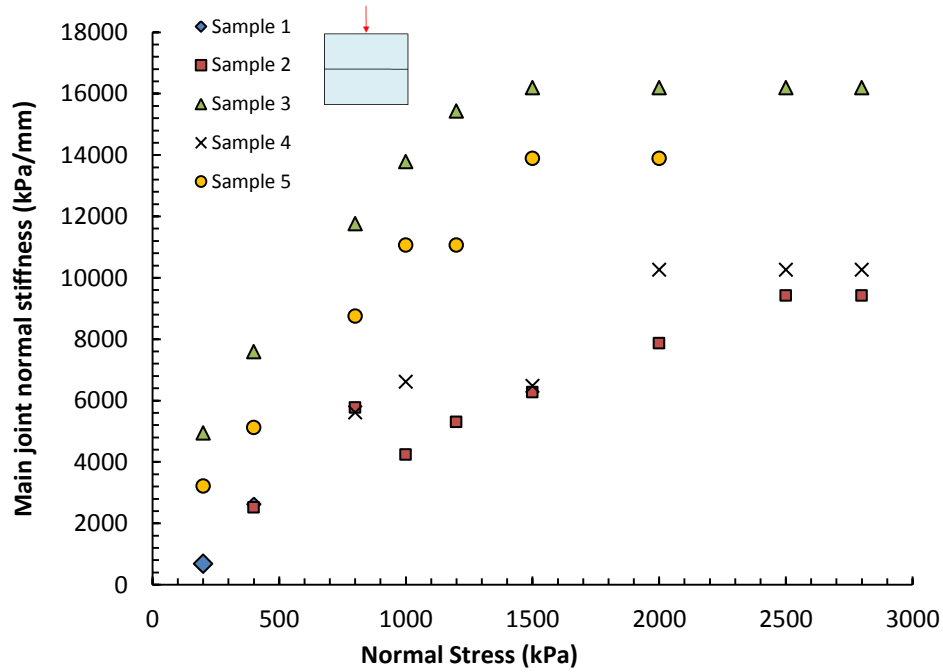
(b)

Figure 4.6: (a) Normal stiffness behaviour of the sample before the direct shear test, (b) Normal stiffness behaviour obtained from a uniaxial compressive test on a planar joint with the increase of normal stress.

4.3 Discontinuous stepped-joints

4.3.1 Sample Dimension

The cross-sectional joint shape of 15 degrees, 45 degrees, and 90 degrees samples are shown in Figure 4.1.
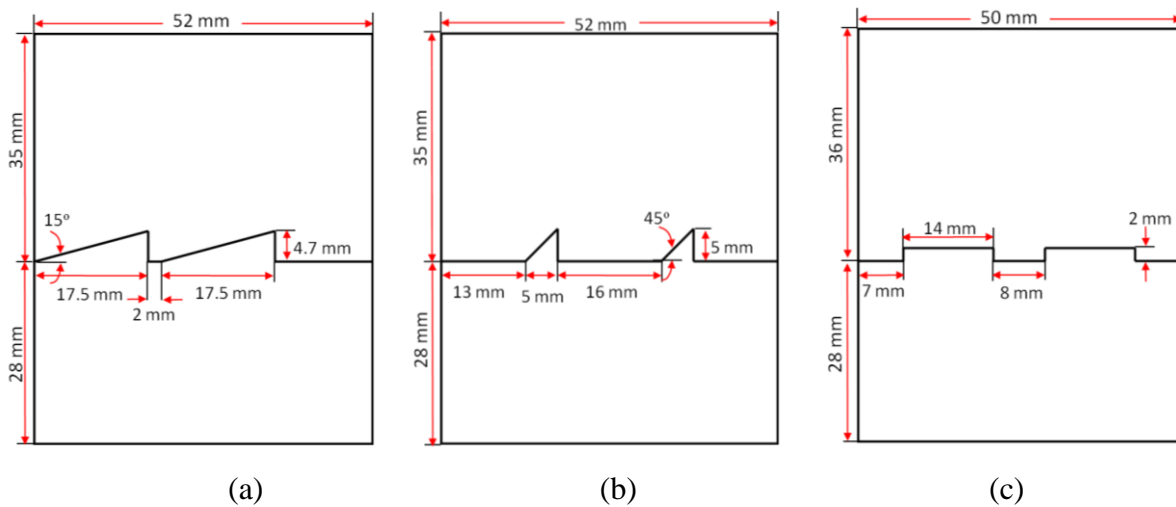
Figure 4.7: (a) Sample with 15 degree inclined joint shape, (b) Sample with 45 degree inclined joint shape, (c) Sample with 90 degree stepped joint shape.

4.3.2 *Shear stress-shear displacement*

The shear stress and horizontal displacement measurements of 15 degree, 45 degree and 90 degree joint shape samples are illustrated from Figure 4.8 to Figure 4.10, which significantly shown that the samples have a brittle behavior after the peak stage. The initial non-linearity of some stress-displacement curves shown in Figure 4.8 is attributed to seating of the sample during the initial loading. There is no indication that this nonlinear behaviour is related to crushing of pores created during sample preparation by non-uniformly mixing in the intact rock. The horizontal shear displacements at each peak stage are different under different normal stresses. The higher the normal stress, the higher the residual strength will be found, which coincides with the results of the residual shear strength envelope shown in Figure 4.4.
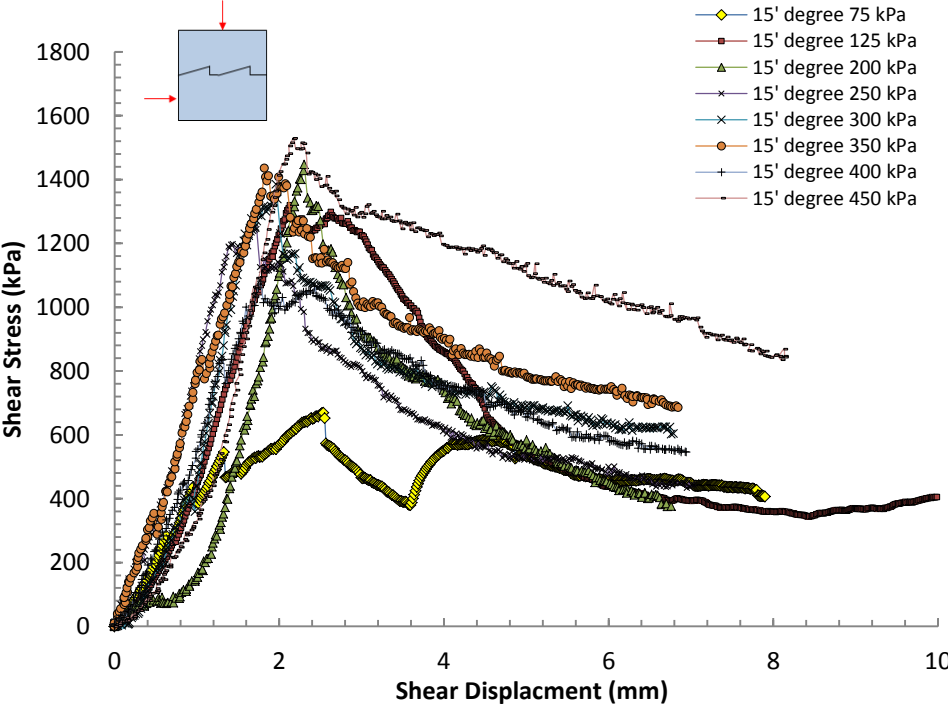
Figure 4.8. Shear stress and displacement for each normal stress applied on synthetic rock in the 15 degree joint shape sample.
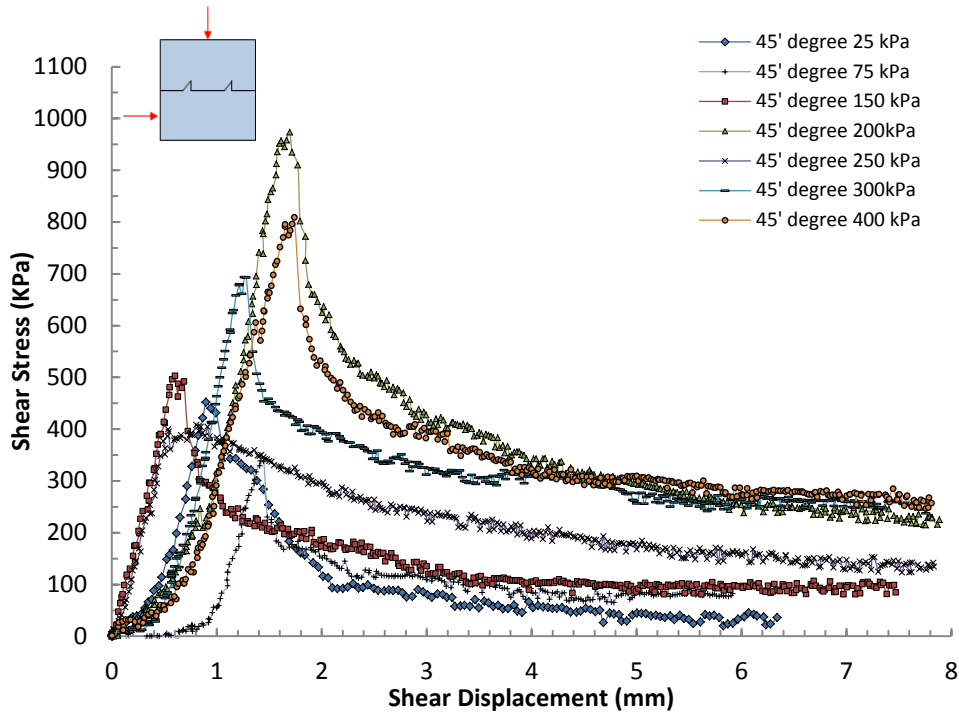
Figure 4.9. Shear stress and displacement for each normal stress applied on synthetic rock in the 45 degree joint shape sample.
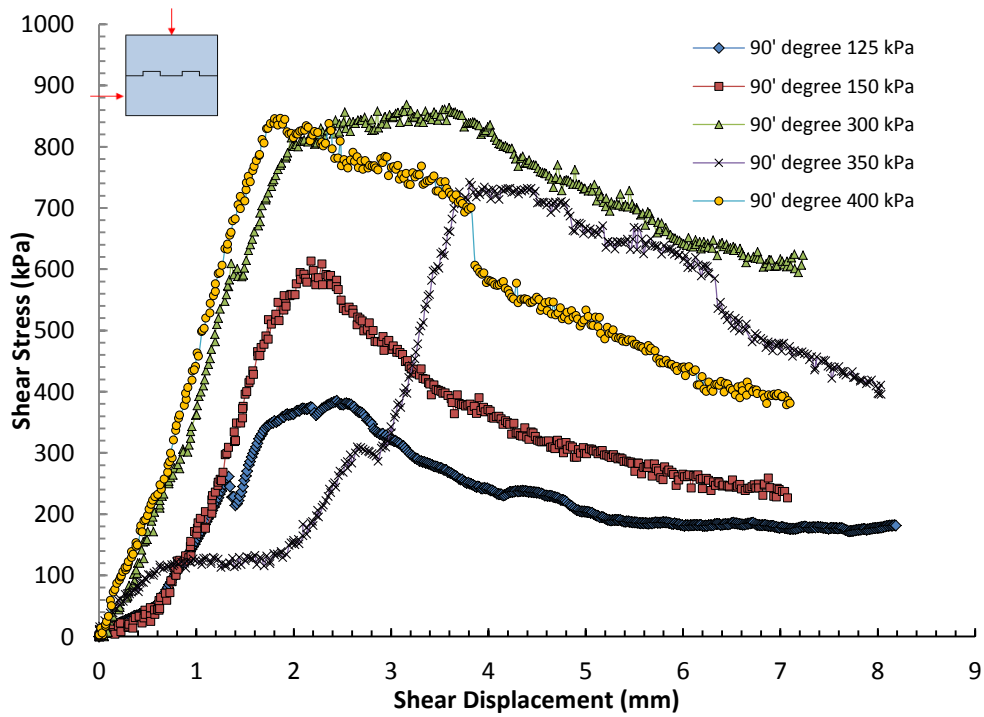
Figure 4.10. Shear stress and displacement for each normal stress applied on synthetic rock in the 90 degree joint shape sample.

4.3.3   Shear strength of discontinuous joints

The peak shear strength and shear stress at different stages of shear displacement obtained from the direct shear tests under low normal stress (less than 500 kPa) conditions are plotted in Figure 4.11 to Figure 4.13. The results show that the shear stress at each stage of shear displacement will increase with the increase of normal stress. Samples containing different shapes of joints will results in different failure criterion. When the joint shape is 90 degrees, it behaves tooth like; the peak shear stress is not consistent with the fit curve because of the geometric shape influenced bending moment at the peak stage.
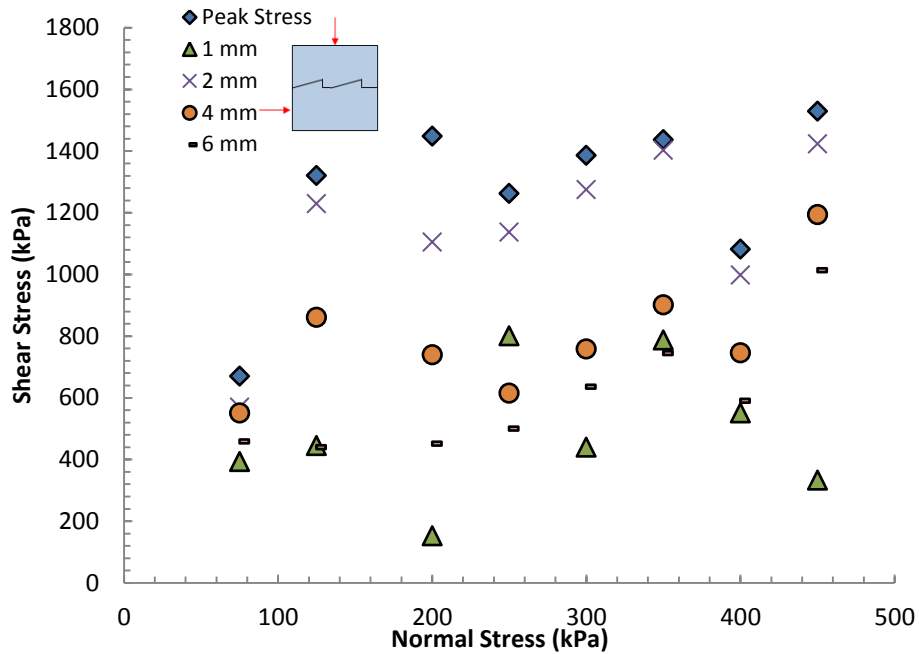
Figure 4.11. Shear stress versus normal stress envelope at different stages of shearing on a 15 degree stepped joint sample.
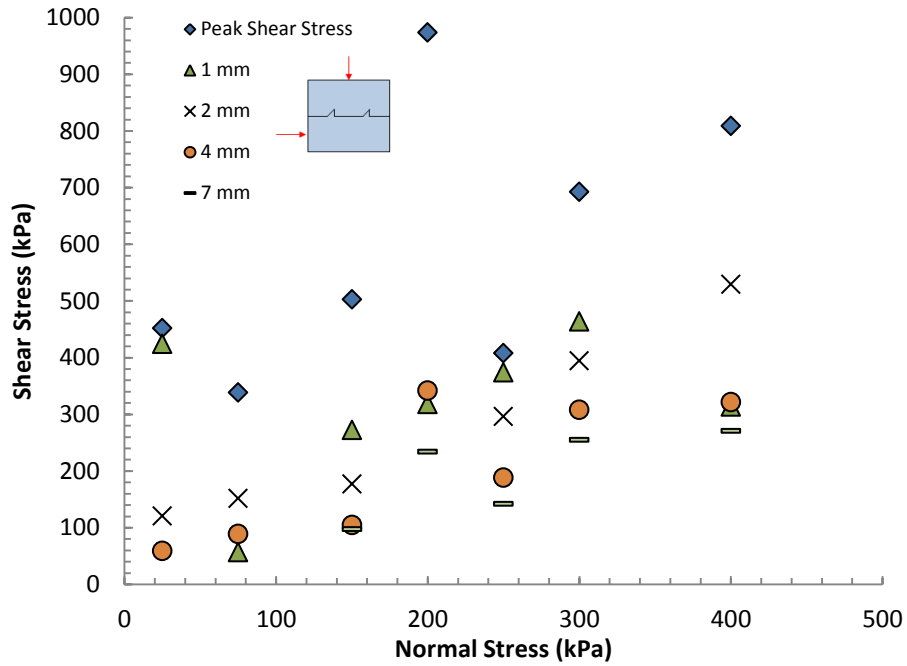
Figure 4.12. Shear stress versus normal stress envelope at different stages of shearing on a 45 degree stepped joint sample.
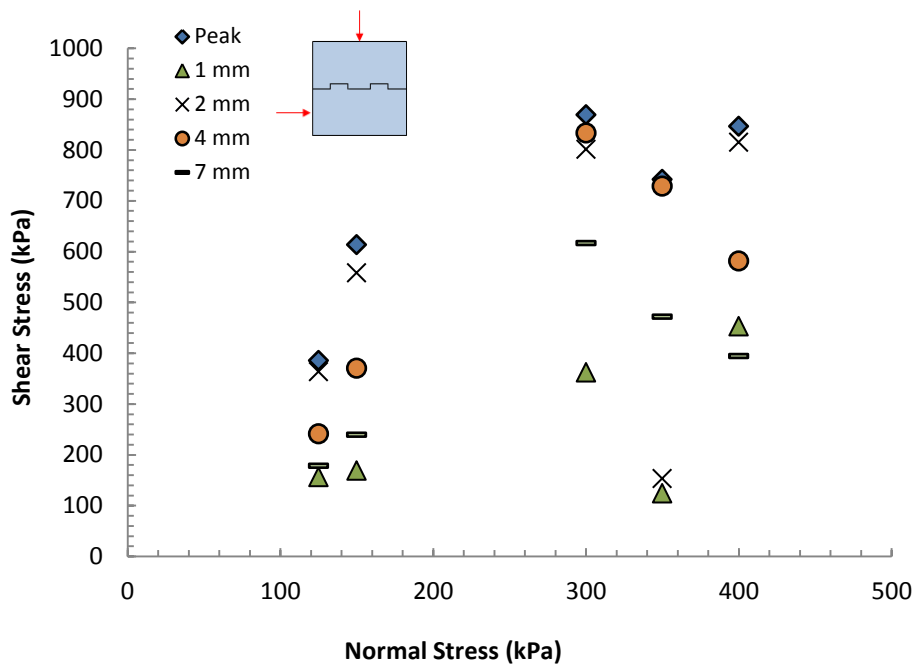
Figure 4.13. Shear stress versus normal stress at different stages of shearing on a 90 degree stepped joint sample.

4.4 Discontinuous open-joint

4.4.1 Sample Dimension

The cross-sectional joint shapes of sample A, B, and C are shown in Figure 5.8 with the degree of separation k measured.

(a) $k = 0.48$ (b) $k = 0.48$ (c) $k = 0.56$
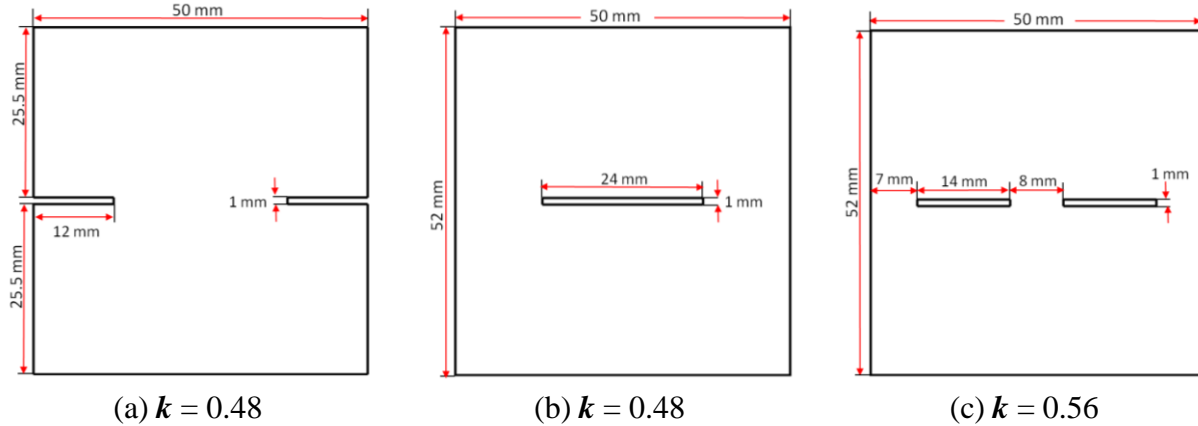
Figure 4.14 (a) Sample A with two 12 mm open joint on the side, (b) Sample B with one 24 mm open joint in the middle, and (c) Sample C with two 14 mm open joints.

4.4.2 Shear stress - shear displacement

An issue with the open joint is the normal stress and shear stress acting on the undeveloped rupture surface. In the previous tests the rupture surface was fully developed. In these open joint samples the application of the normal stress is magnified at the plane of the open joint due to the voids in joint plane. If the shear stress and normal stress is adjusted for the voids the magnitudes simply increase, and hence the strength would increase. To maintain consistency in the presentation and interpretation, the increase in the shear stress and normal stress magnitudes due to the open voids is ignored.

The shear stress versus horizontal displacement measurements of open joint shape samples A, B, and C are illustrated from Figure 4.15 to Figure 4.18. These joints display brittle behavior after the peak stress is reach when the normal stress is less than 3MPa. However, the brittle behaviour is essentially suppressed when the normal stress is larger than 3 MPa, regardless of the open joint configuration.
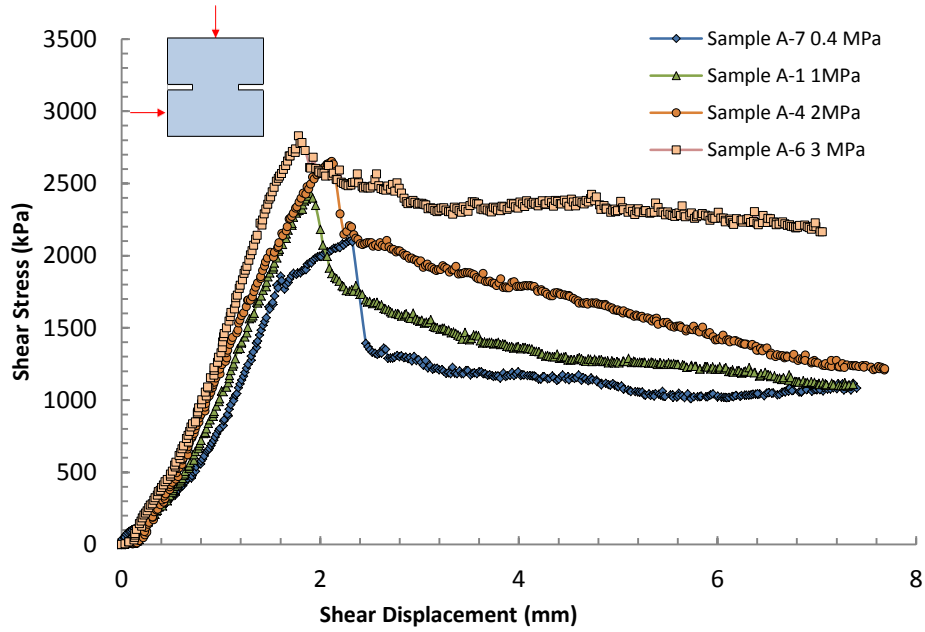
Figure 4.15. Shear stress versus shear displacement of Sample A under different normal stresses, (note the brittle behavior at $\sigma_n < 2MPa$).
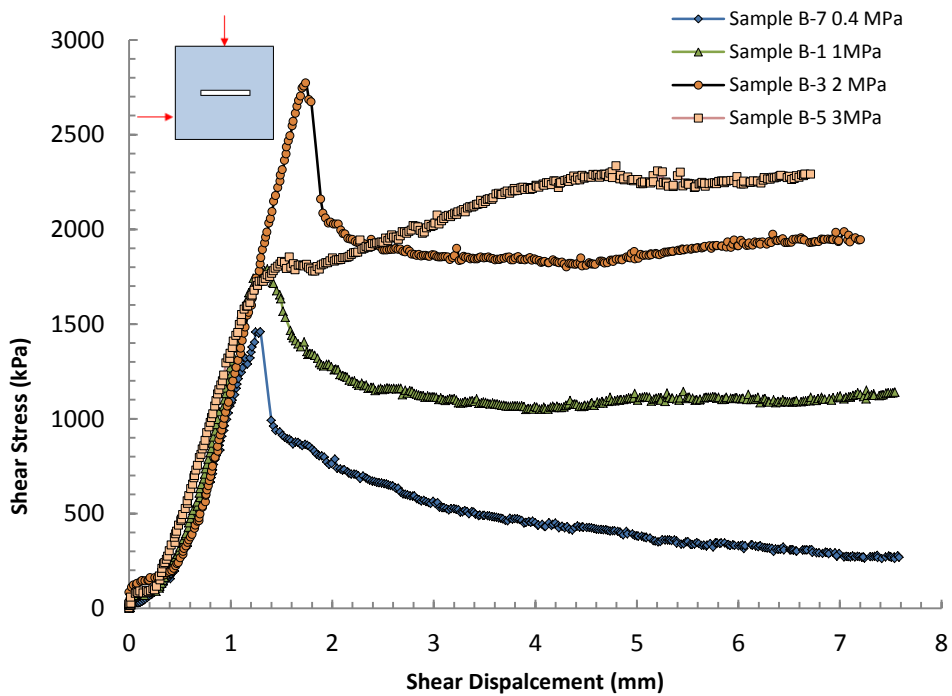
Figure 4.16. Shear stress behaviors versus shear displacement of Sample B under different normal stresses.
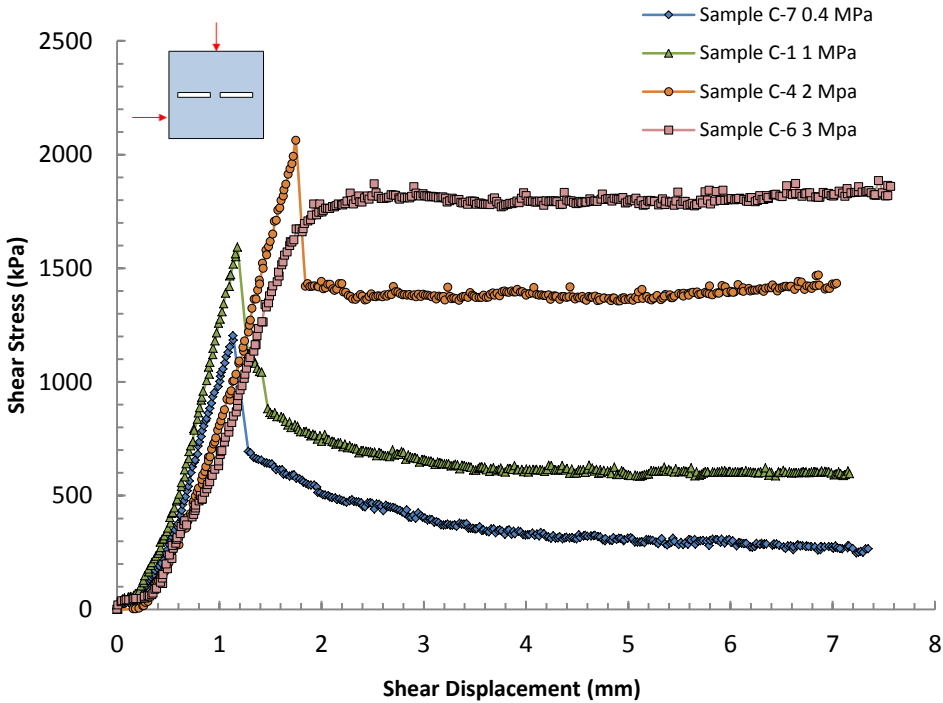
Figure 4.17. Shear stress versus shear displacement of Sample C under different normal stresses

The vertical displacement versus shear displacement measured from Sample A, B, and C open joint shape samples are illustrated from Figure 4.18 to Figure 4.20. The results illustrates that the dilation accelerates at approximately 1.5 to 2 mm of horizontal displacements.   In general the higher the normal stress the greater the dilation. However, the joint in Figure 4.18 also displayed large dilation at low normal stress (400 kPa). This may have been caused by slight rotation of the sample during seating of the initial normal stress.
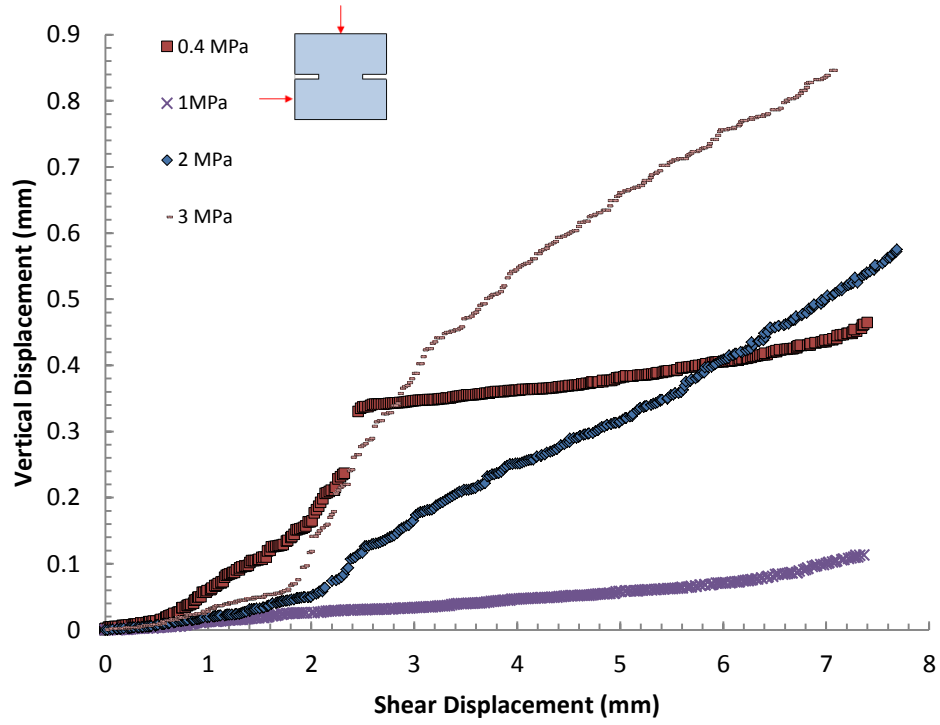
Figure 4.18. Dilation behaviors along the shear displacement of Sample A under different normal stresses.
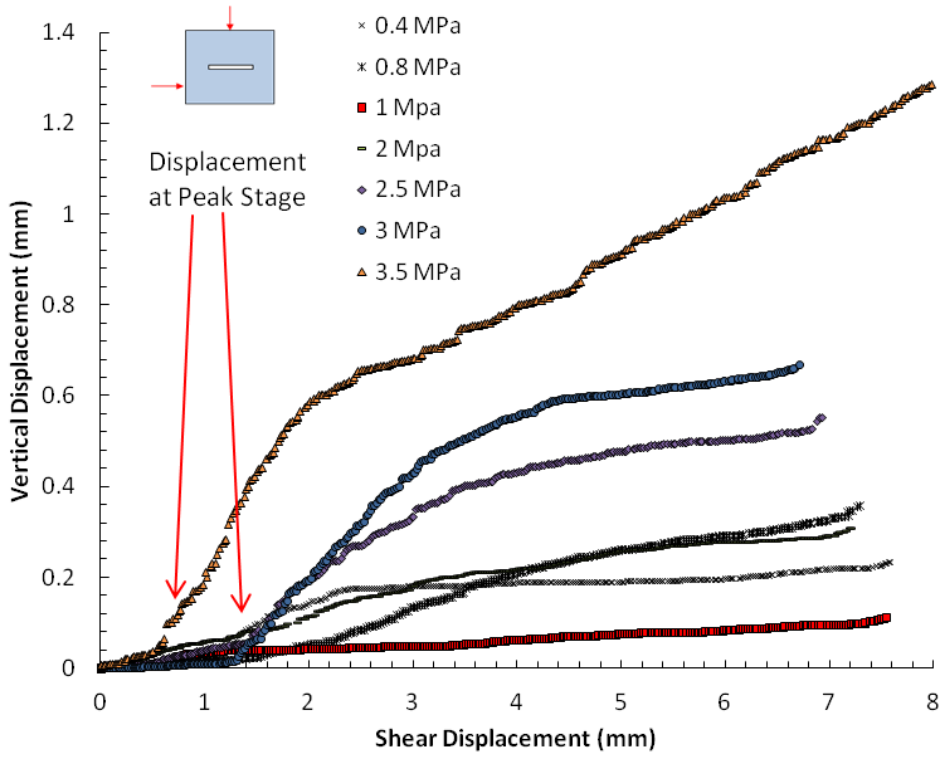
Figure 4.19. Dilation behaviors along the shear displacement of Sample B under different normal stresses.
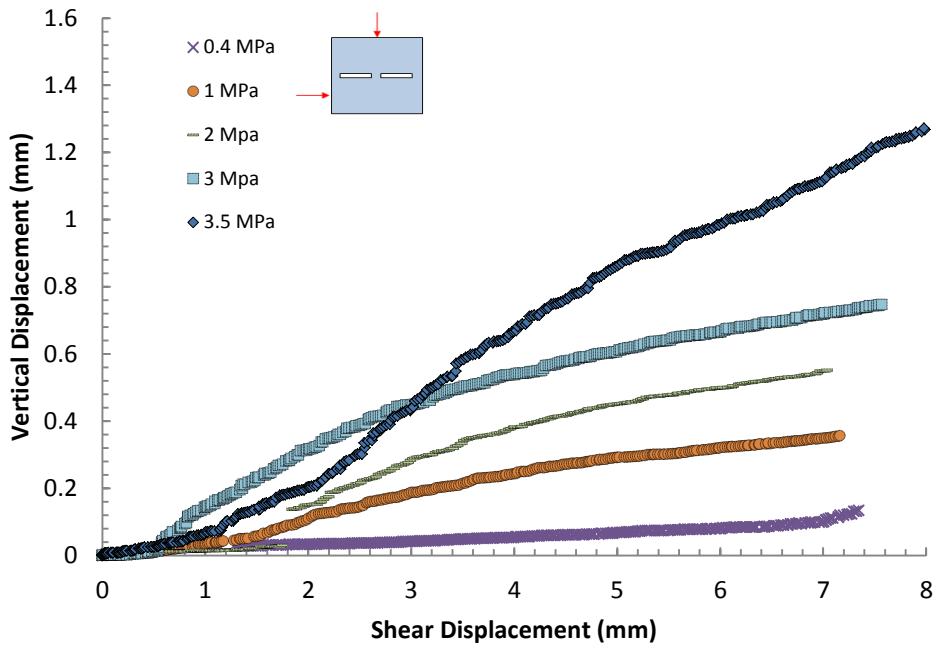
Figure 4.20. Dilation behaviors along the shear displacement of Sample B under different normal stresses.

4.4.3 Crack development during shearing

The section pictures taken after the test are shown in Figure 4.21 below, the rest are shown from Figure A. 12 to Figure A. 14 in Appendix A.
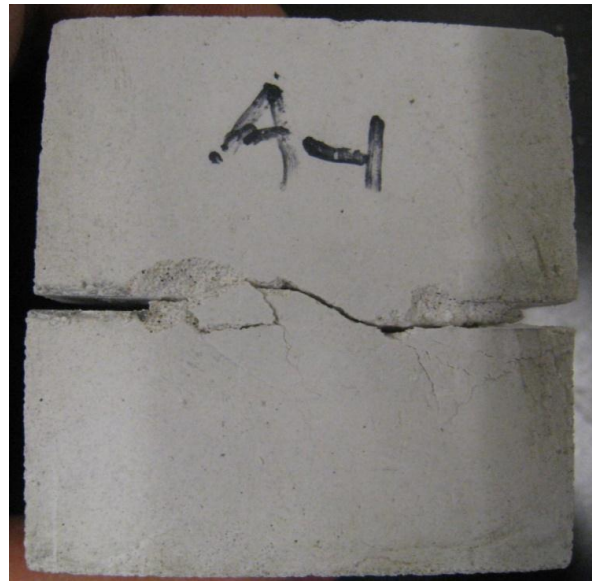
(a)
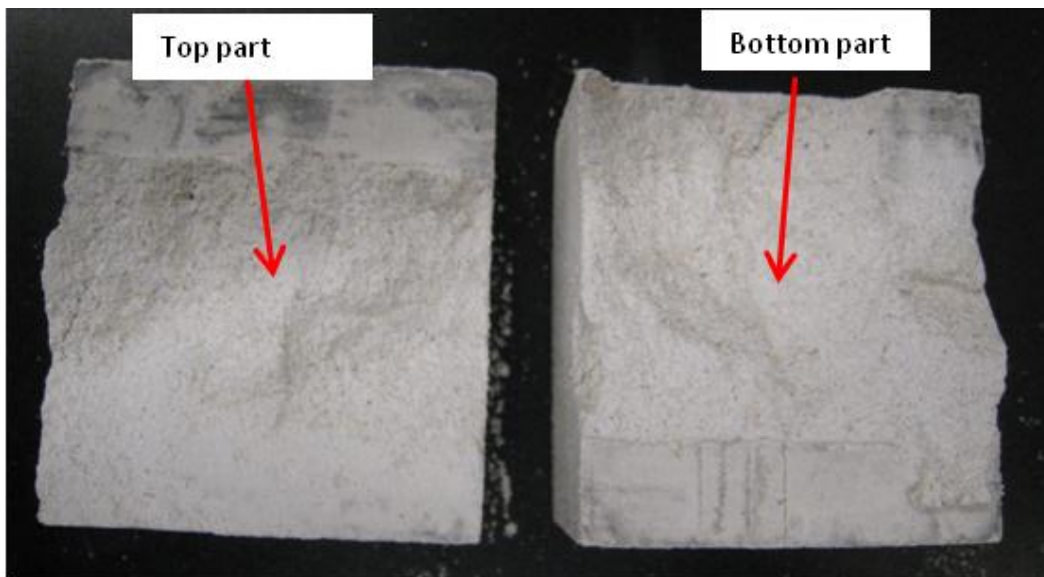
(b)

Figure 4.21. Failure shape of sample A after a direct shear test under 1 MPa normal stress. (a) Cross-sectional view, (b) Planar view.

Form the comparison of sample A under different normal stresses shown in Figure A. 12, it was found that the shear plane at a lower normal stress of 0.4 MPa has an low angle of less than 30 degrees to the primary horizontal predicted shear surface, while the shear plane nearly approaches to the primary horizontal surface with an angle equal to 0 degrees when under a high normal stress of 2 MPa. This is because when a horizontal shear force shears the sample, a large moment will be created clockwise at the tip of the left open crack. However, a high normal stress will create another moment counter clockwise to overcome the initial moment created by the shape of the open crack at the pre-peak stage.

Sample B is more sensitive to tension failure. Figure A. 13 (a) shows the development of a secondary shear fracture followed by the main shear fracture. Figure A. 13 (b) and Figure A. 13 (c) show oblique tension gashes at the middle and tip of the original open crack. The tension crack then propagates to the base of the sample. The secondary tension crack developed after the primary tension crack was observed in Figure A. 13 (d).

Figure A. 14 (a) shows the shear fracture connecting the two open cracks. Lajtai[1] got the same results and concluded that the sub-horizontal shear fracture is the result of a secondary state of stress set up after the first fractures. Figure A. 14 (b) also shows the primary oblique tension gash in the middle of the solid bridges connected to joint ends by a secondary shear fracture. Combination of shear and tension failure were observed in Sample C in Figure A. 14 (c). A notch shape fracture was observed in Figure A. 14 (d) because of too much tension was applied at the end of the open crack. Figure A. 14 (d) shows the destruction of both top ends after testing under high normal stress. A dilation in fractures by shear and tension processes at the lower part of the sample was also found. The results of sample C coincide with Xia's [5] microcosmic explanation. With the increase of shear stress, the initial crack grew on the tip of the joints with the direction of growth not parallel to the shear plane. The tensile crack then appeared on the tip of the fissure in the direction of horizontal shear stress under higher shear stress. The dilation process makes the shear stress highly concentrated on the solid bridge. A shear crack then propagated until the failure of whole rock sample.

4.5   Discussion of laboratory results

4.5.1   Peak Shear Stress

The peak shear stress for the discontinuous joints as a function of normal stress is shown in Figure 4.22. All the results tend to form a nonlinear function that increases sharply at low normal stress, and then approaches a lower bound residual strength envelope at high normal stress. These results at low normal stress are in general agreement with Lajtai's [3-4] findings. However, many of the results at the normal stresses greater than 2 MPa show a peak strength that is far greater than the residual, which is not consistent with Lajtai's findings. The failure

envelope for all the samples shows a complex failure process. At normal stresses of less than 2 MPa, the strength is dominated by cohesion while at normal stresses greater than 2 MPa, friction appears to dominate the shear strength.

At high normal stress the joints that required the development of a rupture surface through intact material generally displayed peak strengths above the residual envelope.
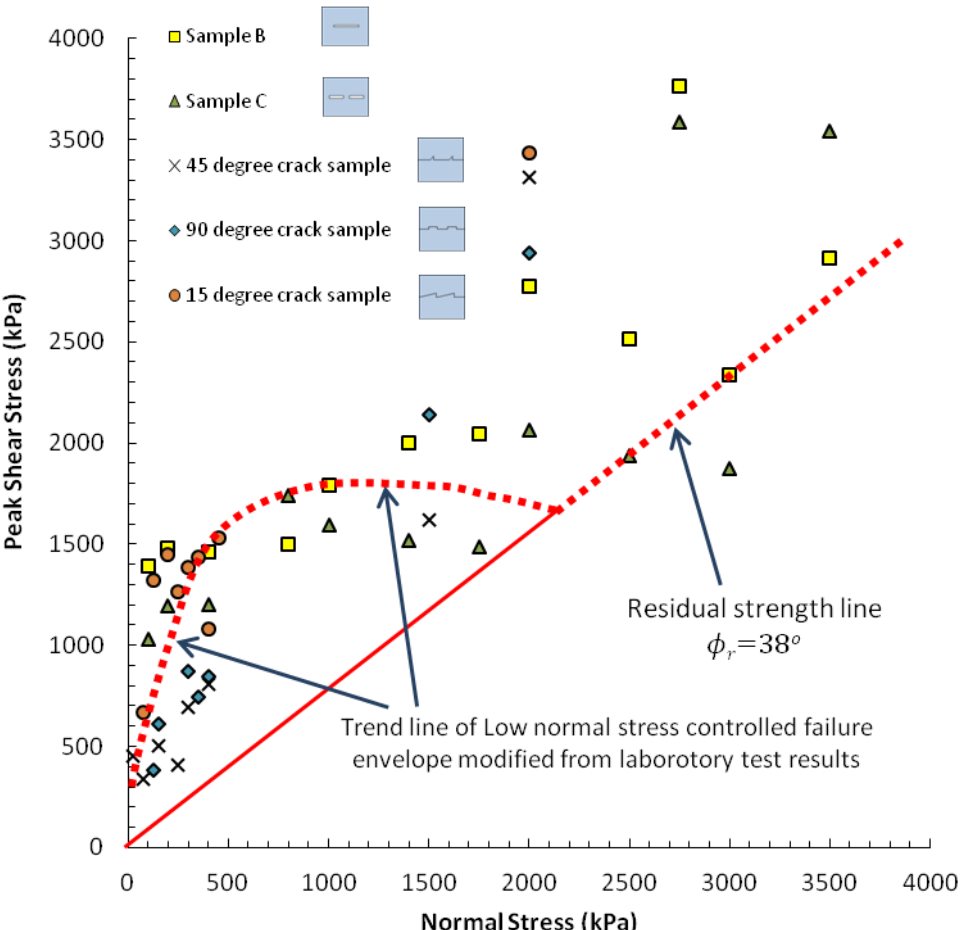
Figure 4.22. Possible strength envelopes for various discontinuous joints.

4.5.2 Deformation to peak strength

The horizontal displacements required for full mobilization of peak joint resistance are shown in Figure 4.23. As shown in Figure 4.23 the amount of displacement is a function of the characteristics of the joint geometry and normal stress. The open joint samples B and C, the full mobilization need more deformation than the completely closed joint samples. This

follows Lajtai's[3] conclusion that internal friction needs more deformation to become fully mobilized than joint friction. However, the 90 degree joint samples need more deformation to reach the peak stage even under low normal stress. This may be due to the geometric effect. The tooth-shaped joint under the horizontal shear force will lead a large bending moment perpendicular to the direction of shearing, which will cause overturning of the sample during the peak stage.
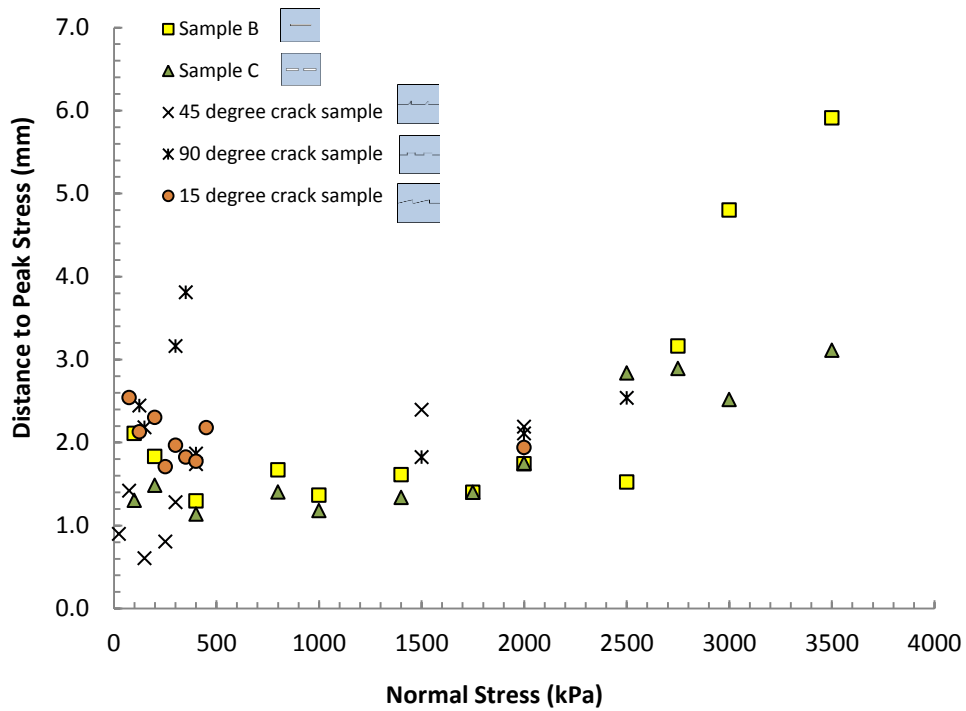
Figure 4.23 Deformation to peak strength with the increase of normal stress

4.5.3   Brittleness Index Behaviour with Normal Stress

The brittleness index of rock samples defined by Bishop's [5] state the percentage reduction in strength passing from the peak to the residual. The brittleness index I_b is calculated as below:

$$I_b = \frac{\tau_f - \tau_r}{\tau_f}\% \ ,$$ (4.4)

where τ_f is the peak shear stress and τ_r is the residual shear stress obtained from each test.

The samples under high normal stress (larger than 2 MPa) will not drop to residual strength under 8 mm shear distance; the residual strength is calculated by assuming the residual strength had reached the residual strength line with a residual angle of $\phi_r = 38^o$. From the resulting plot shown in Figure 4.24, it is clearly shown that increasing the normal stress reduces the

62

brittleness index of rock samples from nearly one hundred percent to zero. The negative brittleness index indicates that the sample had a strain hardening behavior under high normal stress. It is assumed that this arises from the crashing of small particles on the shear surface during shearing. However, no clear evidence was found.
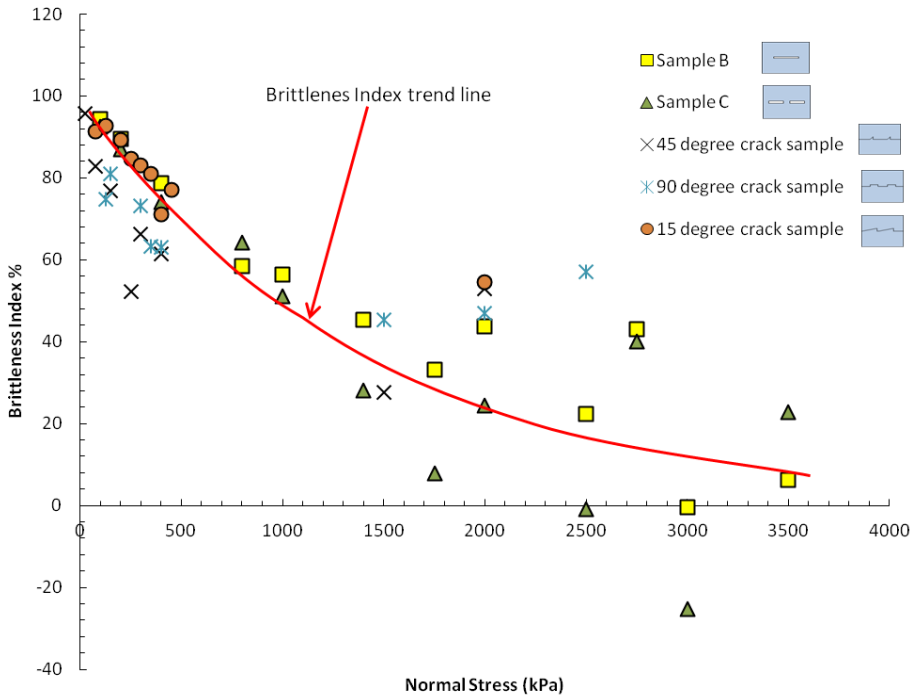
Figure 4.24. Brittleness index for various samples, using the calculated τ_r in Equation 4.4 based on a residual friction angle of 38 degrees.

4.5.4   Shear Stiffness with Normal Stress

The shear stiffness values of the samples were established using the slope of a shear stress-displacement curve in the pre-peak stage. Figure 4.25 shows the shear stiffness for the open joints as a function of normal stress. For the open joints, the shear stiffness is independent of the normal stress. Figure 4.26 illustrates the shear stiffness values for the closed joints. An inspection of Figure 4.26 shows that there is a clear increase in shear stiffness as the normal stress increases for the closed joints. This increase is particularly evident below a normal stress of 1 MPa. Note that the increase in shear stiffness is also observed for the smooth planar joint as well as for the stepped joint. Bandis et al. [6] concluded from studies on weathered and fresh joints that the shear stiffness always increased as the normal stress increased. Their findings appear to apply to the closed joint when the normal stress is less than 1 MPa, but does not apply when the joints are open or for the closed joints when the normal stress is greater than 1 MPa. Rosso [7] concluded that the differences in shear stiffness could be due to joint type

63

including thickness, roughness and test parameters such as stress path, maximum normal stress, and environmental conditions.
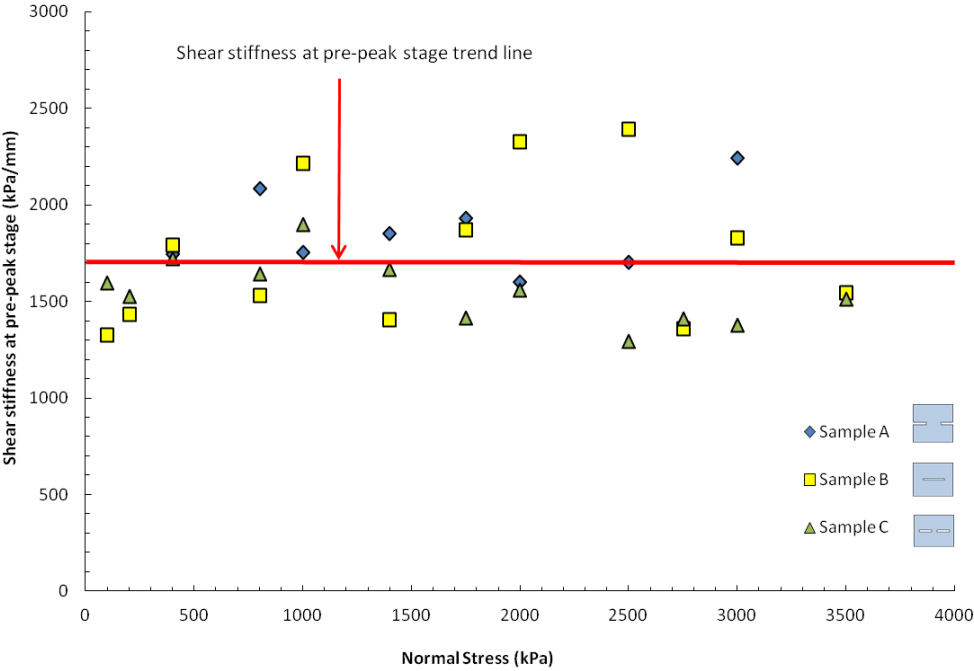
Figure 4.25. Shear stiffness behavior at the pre-peak stage of all open joints.
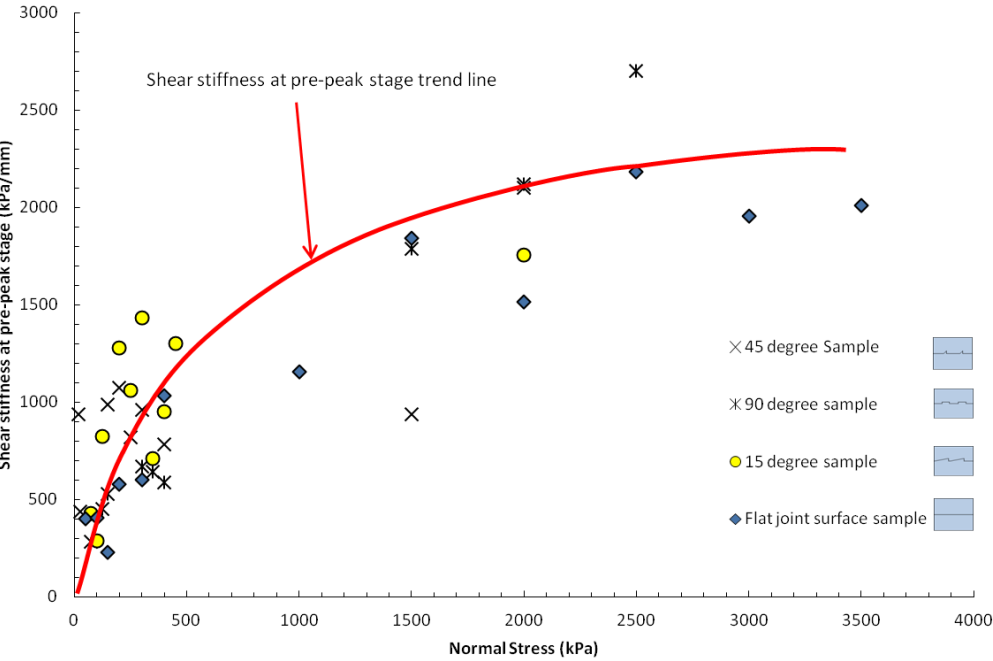
Figure 4.26. Shear stiffness behavior at the pre-peak stage of all closed joints.

4.5.5 *Shear strength at 7 mm of shear displacement*

The peak shear strength for the joints, regardless of shape, is readily determined. However, as shown in many of the test, data beyond the peak strength display two characteristic results: (1) there is no reduction in strength beyond the peak strength regardless of shear displacement and this is referred to as the residual strength, or (2) the strength continues to decrease beyond the peak strength as shear displacement occurs. For the latter case, the term "residual shear strength" is not appropriate and will be referred to as τ_r. In order to compare the strength beyond the peak strength, the τ_r at 7mm of shear displacement are evaluated (Figure 4.27). The results indicate that shear strengths of 7mm are similar to the residual strength with $\phi_r = 38^o$. It is clear from Figure 4.27 that while some samples had not reached the residual shear strength; other samples display shears strengths that are lower than the residual shear. Note that nearly all of the samples with τ_r at 7mm less than $\phi_r = 38^o$ are associated with the open joints.
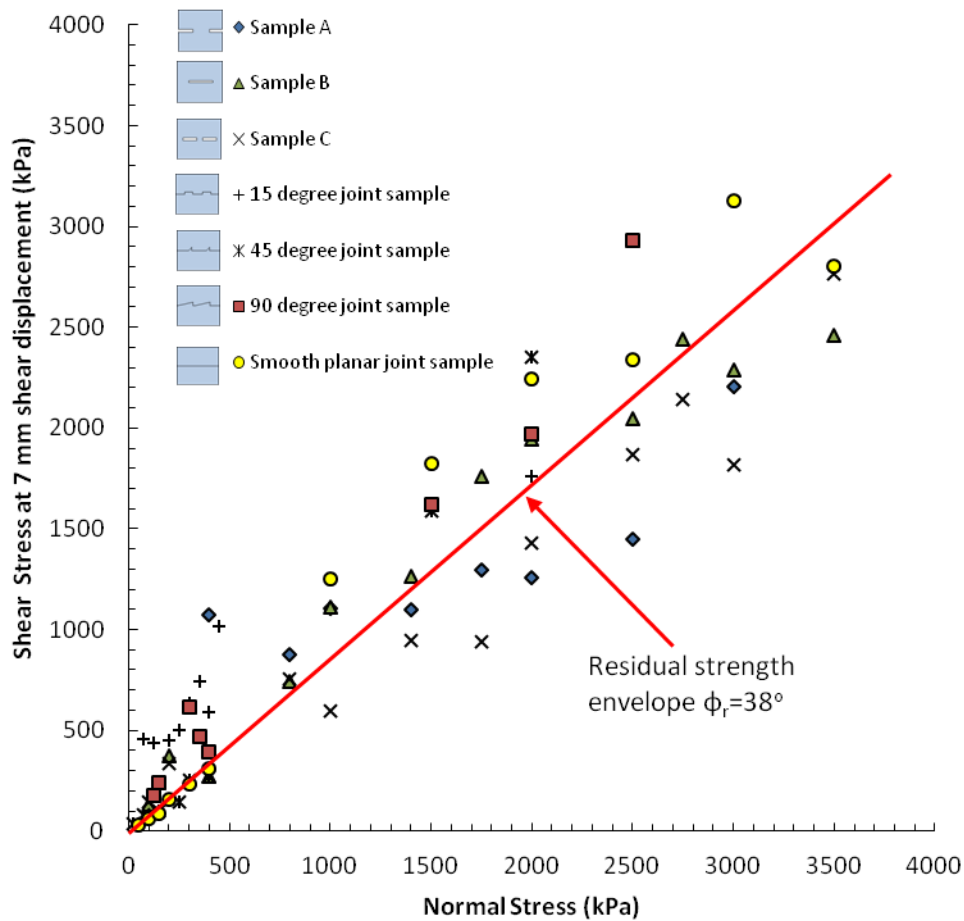
Figure 4.27 Shear strength at 7 mm shear displacement versus normal stress for different shape of samples

4.6 Summary

88 samples of a synthetic rock containing different joint shapes, both closed and open were subjected to direct shear loading. Examination of the shear stress versus shear displacement plots for these samples suggests the following:

- Many of the plots show initial nonlinear behaviour during the initial application of shear stress. This nonlinear portion is attributed to seating of the sample during the initial loading. There is no indication that this nonlinear behaviour is related to crushing of pores in the intact rock.

- *Planar closed joint*: The planar closed joint shows an elastic-perfectly plastic response for all normal stress values of less than 2.5 MPa. For these samples the peak strength

66

equals the residual strength. When the normal stress is 2.5 MPa or greater, the shear resistance is characterized by a strain weakening response. In other words, the shear strength decreases as shear displacement occurs beyond the peak strength.

- *Open Joints*: The shear stress versus shear displacement curves for the open joint show that these samples display a brittle behavior after peak shear stress is reached when the normal stress is less than 3MPa. However, for the three open joint geometries, the brittle behaviour is essentially suppressed when the normal stress is 3 MPa.

- *Stepped closed joints*: The shear behaviour of all the stepped closed joints display either a brittle or strain-weakening response for all normal stresses below 0.4 MPa. The strain weakening can be significant.

- The *residual friction angle* based on the closed planar joints was estimated as $\phi_r = 38^o$. Not all samples tested reached the residual shear strength given by the planar joints. At normal stresses greater than 2 MPa, the shear strength of the closed joints at 7 mm shear displacement had not reached the estimated residual value based on $\phi_r = 38^o$. Meanwhile the open joints, at high normal stress often displayed shear strength values lower than the estimated residual strength assuming $\phi_r = 38^o$. It is likely that the shearing of open joints at high normal stress involves apparent cohesion.

- The failure envelope for all the samples shows a complex failure process. At normal stresses of less than 2 MPa, the strength is dominated by cohesion while at normal stress of greater than 2 MPa, friction appears to dominate the shear strength.

- The *normal stiffness* of a closed planar joint was obtained by using the vertical displacement during the application of the normal stress. The elastic displacement of the top steel cap and rock mass were taken into consideration in calculating the normal stiffness. The normal stiffness showed a nonlinear increase in stiffness as the normal stress increased.

- The *shear stiffness* for the open joints is independent of the normal stress, while there is a clear increase in shear stiffness as the normal stress increases for the closed joints.

4.7   References

[1]   ISRM. 1974. Suggested Methods for Determining Shear Strength. *International Society for Rock Mechanics Commission on Standardization of Laboratory and Field Tests*. No.1: 135-137.

[2]   Hajiabdolmajid, V., Kaiser, P., Martin, C. D. 2003. Mobilised strength components in brittle failure of rock. *Geotechnique,* Vol. 53, No. 3: 327-336.

[3]   Lajtai, E. Z. 1969. Strength of discontinuous rocks in direct shear. *Geotchnique*, 19(2): 218-233.

[4]   Lajtai, E. Z. 1969. Strength of discontinuous rocks in direct shear. *Geotchnique*, Vol.19, No. 2: 218-233.

[5]   Bishop, A.W. 1971. The Influence of Progressive Failure on the Choice of the Method of Stability Analysis. *Geotechnique,* Vol. 21, No.2: 168-172.

[6]   Bandis, S. C., Lumsden, A. C., and Barton, N. R. 1983. "Fundamentals of Rock Joint Deformation." *International Journal of Rock Mechanics & Mining Science and Geomechanics Abstracts* 20 (6): 249–268.

[7]   Rosso, R. S. 1976. A comparison of Joint Stiffness Measurement in Direct Shear, Triaxial Compression, and In Situ. *Int. J. Rock Mech. Min. Sci. & Geomech. Abstr.* Vol. 13: 167-172.

5 Numerical analysis of direct shear tests

The laboratory test results described in the previous chapters provide insight into the behavior of the discontinuous joints subjected to direct shear. The results show that this behavior is a function of normal stress, the joint geometry and the continuity of the joint. As shown in Figure 4.22 the failure envelope produce by these various factors is complex and challenging to describe.

Numerical analyses are often used to aid in understanding the failure process observed in laboratory tests. The finite element numerical method can simulate material heterogeneity, non-linear material responses, and complex boundary conditions (Hammah et al. [1-2]). In this chapter, the finite element software *Phase²* (available from RocScience Inc. [3-4]) was used to analyze the laboratory test results.

5.1 Phase² Finite Element Analysis

Phase² (Version 8.0) finite element software is Windows based and provides a user-friendly environment for conducting elastic-plastic analyses.

5.1.1 *Homogeneous and Heterogeneous Approach*

The fundamental assumptions in continuum mechanics modelling used in this research were: (1) material is homogeneous and isotropic, (2) material response is continuous in the displacement field, and (3) yielding is defined by a linear Mohr-Coulomb failure envelope. The software can also incorporate joint elements and as stated by Riahi et al [5] "continuum-based methods that use joint elements are accurate provided changes in edge-to-edge contacts are insignificant throughout the solution. These continuum methods can accommodate large displacements, rotations, or strains of discrete objects, so long as these mechanisms do not change contacting node couples."

The synthetic rock for the laboratory tests was created using sand, plaster, and water. The presence of granular material sand made the synthetic rock heterogeneous. As shown by Lan et al. [6] material and geometric heterogeneity of intact rock can have a significant influence on intact rock behaviour. Voronoi joint patterns have been used by Lan et al. [6] to simulate this intact rock heterogeneity. The Voronoi tessellation option in *Phase²* was used to simulate the geometric heterogeneity of the grains and/or clumps thought to be present in the synthetic rock, similar to the approach of Lan et al [6]. This Voronoi tessellation scheme when combined with discrete joints can simulate both intact rock breakage and slip along a discrete joint.

Phase^2 has an additional feature, automatic creation of the Voronoi tessellation pattern. The user can specify the region for the Voronoi tessellation and the average length of the Voronoi joint. The Voronoi joint was set at a minimum length of 0.8 mm. This was a practical minimum for the computing capacity available. The Voronoi tessellation at this scale was experimental in *Phase^2* and several modifications were made by the developers of the software to accommodate this small-scale feature.

5.1.2 Failure envelopes for intact rock

Material models in *Phase^2* include the linear Mohr-Coulomb model and the generalized nonlinear Hoek-Brown model. Based on the laboratory test results, the linear Mohr-Coulomb model was considered the most appropriate for the intact synthetic rock. The failure envelope for an elastic-plastic material can be achieved by specifying the same cohesion and friction values for both the peak and residual envelopes (Figure 5.1). Similarly, specifying different cohesion and friction values for the peak and residual envelopes can simulate a brittle material. Specifying different values for the residual cohesion and friction can also simulate a strain weakening response (Figure 5.1).

(a) Elastic-plastic stress-strain response   Failure envelope

(b) Strain weakening and Brittle stress-strain response   Failure envelopes

70
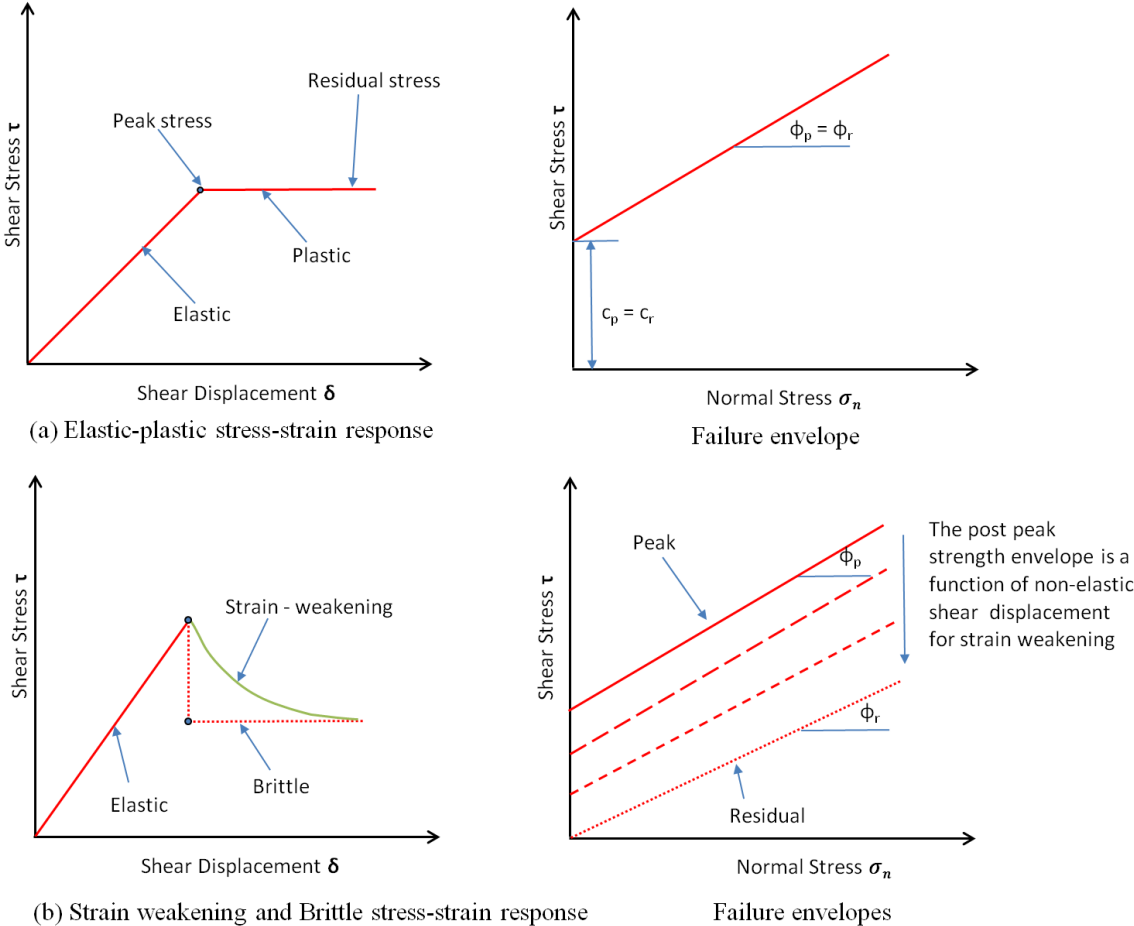
Figure 5.1 Constitutive models for various stress-strain responses

In the next section, these failure envelopes are evaluated using Brazilian and Uniaxial compression test results for the synthetic rock.

5.2 Calibration with laboratory intact properties

Before using the Phase2 to simulate the direct shear tests, calibration of the Voronoi joints properties was carried out using the Uniaxial compressive and Brazilian laboratory test results provided in Chapter 3.

5.2.1 Uniaxial Compressive Test

The *Phase^2* model had the same dimension as the cylinder specimens used in the laboratory test; 50 mm diameter by 100 mm length. A steel-loading cap with a Young's modulus of 200 GPa was put on top of the sample and separated by a horizontal joint (Figure 5.2). The joint interface provided a mechanism for assigning a friction coefficient between the steel and the sample. The base pedestal was also made of steel with the same contact property as top-loading cap. The bottom of the base pedestal was fixed to prevent movement in both X and Y directions. The load was applied vertically to the top cap and was increased in increments until the uniaxial compressive strength measured in the laboratory test was reached. The properties used for the *Phase^2* model are given in Table 5.1 and the failure envelopes are illustrated in Figure 5.3. In the laboratory test, the deformation of the sample records the deformation of the sample as well as the steel cap. Hence, it is necessary to establish the stiffness properties of the contact interface.

(a)   (b)
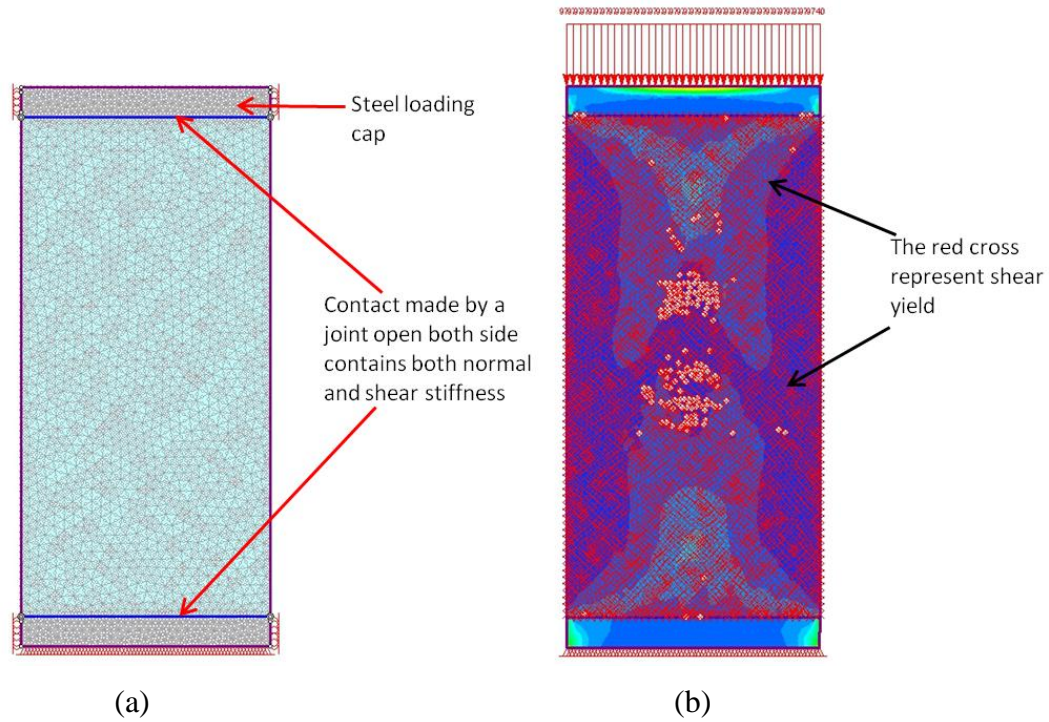
Figure 5.2: (a) Uniaxial compressive strength test in *Phase²* , (b) Yielding in *Phase²* at the peak uniaxial strength.

Table 5.1. Basic parameters used to present the synthetic rock.

Measured Laboratory Properties of Intact Synthetic Rock			
Young's Modulus (GPa)			2.134
Poisson's Ratio			0.2
Tensile Strength (MPa)			1.84
Uniaxial Compressive Strength (MPa)			9.74
Intact Mohr-Coulomb Failure Criterion		**Voronoi Mohr-Coulomb Failure Criterion**	
Cohesion Peak (MPa)	2.2	Cohesion Peak (MPa)	2.2
Friction Angle Peak (Deg)	42	Friction Angle Peak (Deg)	42
Cohesion Residual (kPa)	100	Cohesion Residual (kPa)	100
Friction Angle Residual (Deg)	38	Friction Angle Residual (Deg)	38
Tensile Strength (MPa)	1.84	Tensile Strength (MPa)	1.84
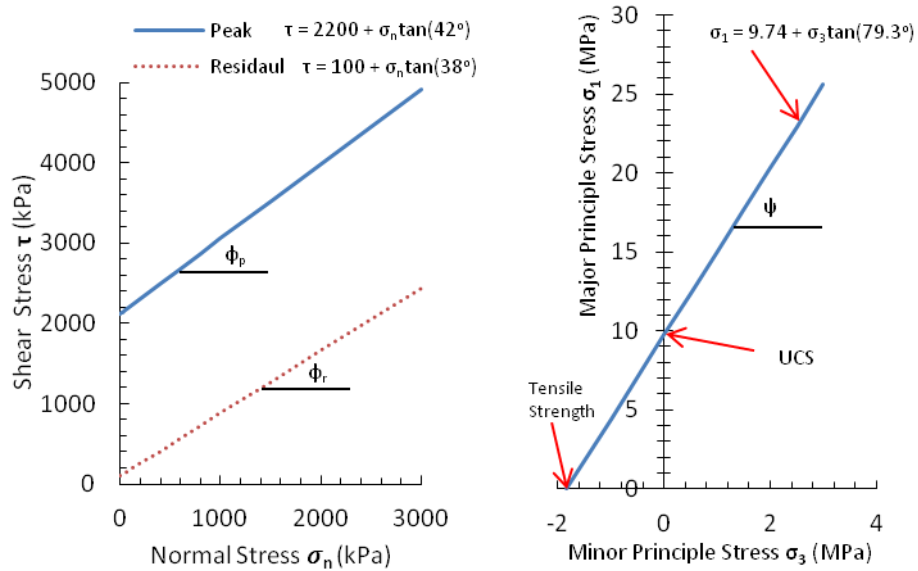
Figure 5.3 Failure envelopes of intact synthetic rock used in *Phase^2 8.0*.

In the continuum model, the normal stiffness (Kn) and shear stiffness (Ks) of the contact joint between the synthetic rock and the loading cap was adjusted until the Young's modulus of the synthetic intact rock (whole system), (E=2.1 GPa) was achieved. Those results are shown in Figure 5.4 and illustrate that in order to achieve the Young's Modulus of the intact rock, the normal stiffness must be approximately 1×10^{11} kPa/m but the ratio of normal stiffness (K_n) to shear stiffness (K_s) can range from 0.1 to 10.
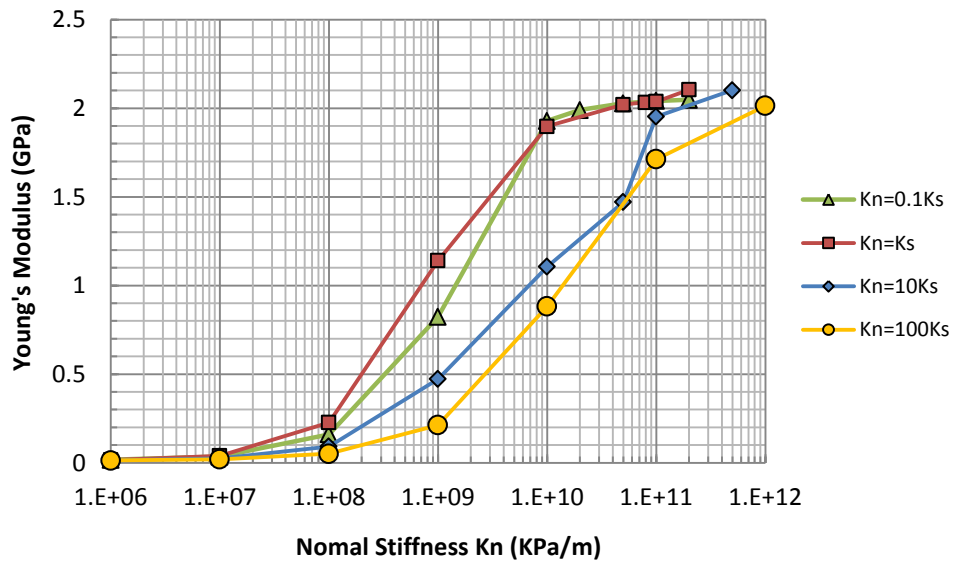
Figure 5.4. The variation in Young's Modulus of the intact synthetic rock as a function of the normal stiffness and shear stiffness of the contact joint between the intact rock sample and the "steel cap".

73

Lan et al. [4] demonstrated that the failure of intact rock involves fracturing of grain boundaries. To simulate this process, the Voronoi joint network in *Phase²*, was used to map weak grain boundaries (Voronoi joint) around elastic polygons (Figure 5.5). Using this procedure, the intact polygons display elastic behaviour and the Voronoi joints are assigned the elastic-plastic properties given in Table 5.1. The average joint length of the Voronoi polygons was set to 0.8 mm. The normal stiffness of the Voronoi polygons was varied as illustrated in Figure 5.6. As shown in Figure 5.6, normal stiffness values in *Phase²* of between 5×10^{10} and 2×10^{11} kPa/mm gave essentially the same Young's modulus value (2.15 GPa) as the laboratory uniaxial compressive test (2.13 GPa).
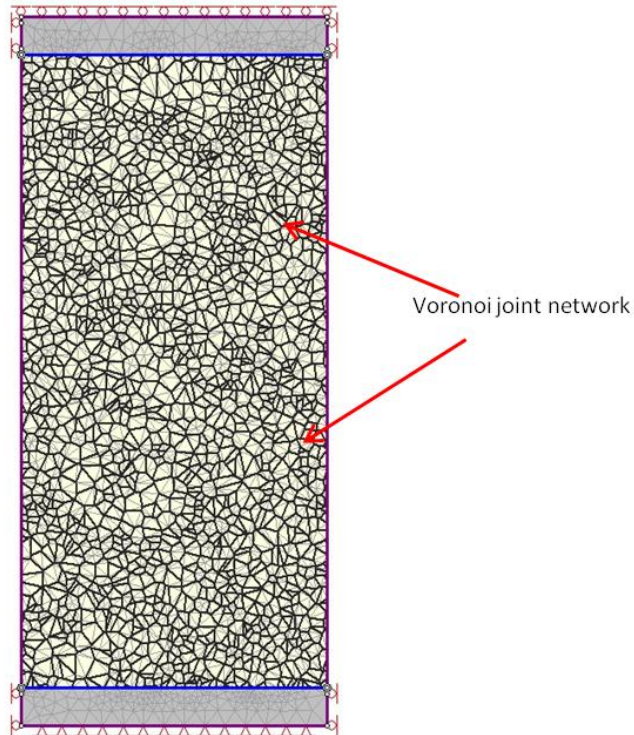
Figure 5.5: Uniaxial compressive strength test in *Phase²* using a Voronoi joint network approach.

74
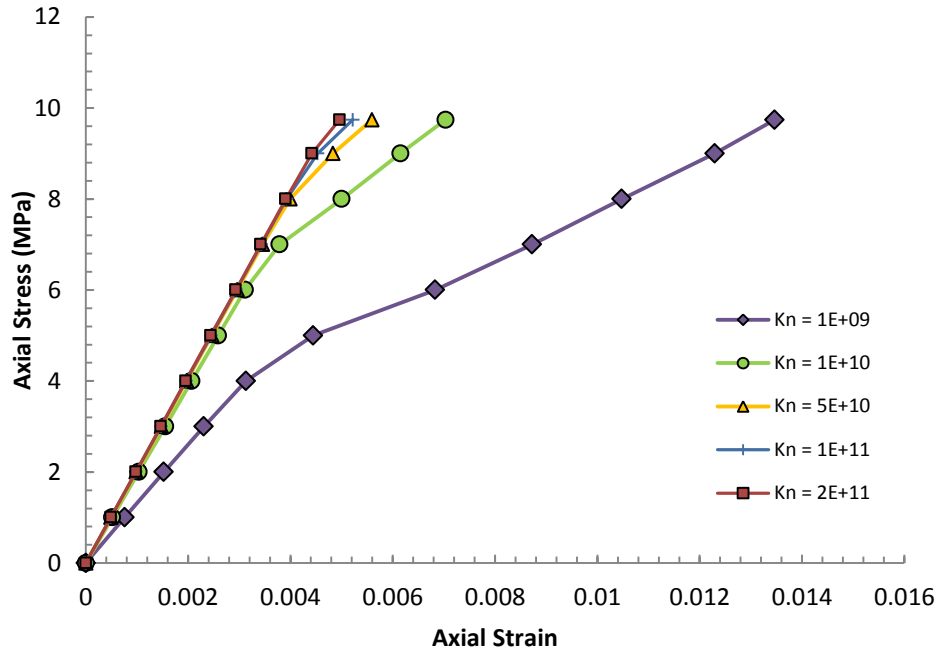
Figure 5.6. Relationship between axial stress and axial strain for various values of normal stiffness assigned to the Voronoi joints.

Once the normal stiffness of the Voronoi joint was established, the remaining unknown was the shear stiffness. It is well known that cracking in uniaxial compressive tests begins at approximately 50% of the uniaxial compressive strength (Lan et al. [4]). Cracking in the *Phase*^{2} model was tracked during the loading process by examining the failure along the Voronoi joints. Figure 5.7 shows the cracking observed in *Phase*^{2} as a function of applied stress. The initiation of cracking is caused by tensile failure of the Voronoi joint. The tensile stresses are generated by the geometric heterogeneity of the Voronoi polygons, and the ratio of normal stiffness to shear stiffness. Figure 5.8 shows the effect of this normal stiffness to shear stiffness ratio on crack initiation. Using a normal stiffness of 1×10^{11} kPa/mm and the crack initiation value of 50% of the uniaxial compressive strength, the stiffness ratio of Kn/Ks=10 provides the best approximation to the laboratory compression test properties. Figure 5.9 compares the stress strain response from the laboratory uniaxial compressive stress with the result from the *Phase*^{2} model using the Voronoi tessellation. The brittle response in *Phase*^{2} can be controlled with the residual strength parameters. In Figure 5.9 the residual parameters are chosen to illustrate this control.
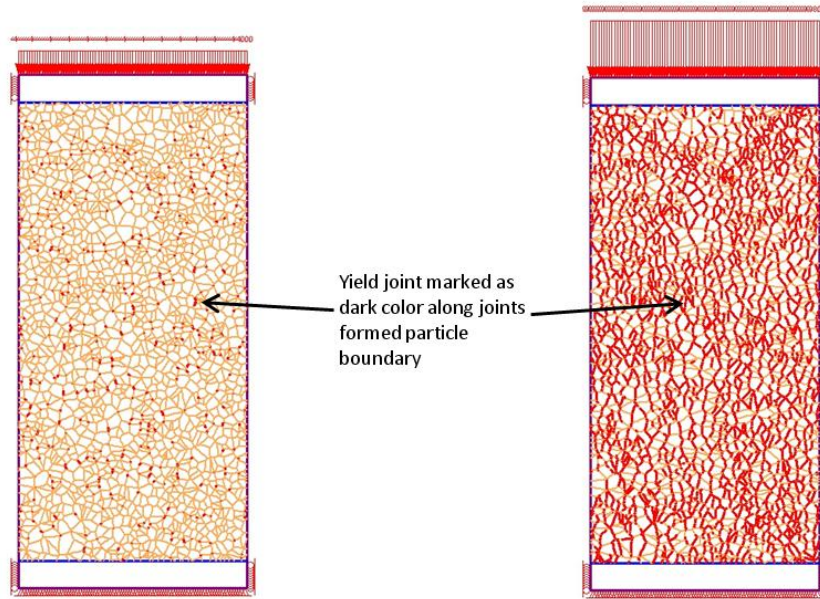
Figure 5.7: (a) Crack initiation when loading stress is equal to 4 MPa, and (b) Crack propagation vertically and reaching the failure stage when loading stress is equal to 9.8 MPa.
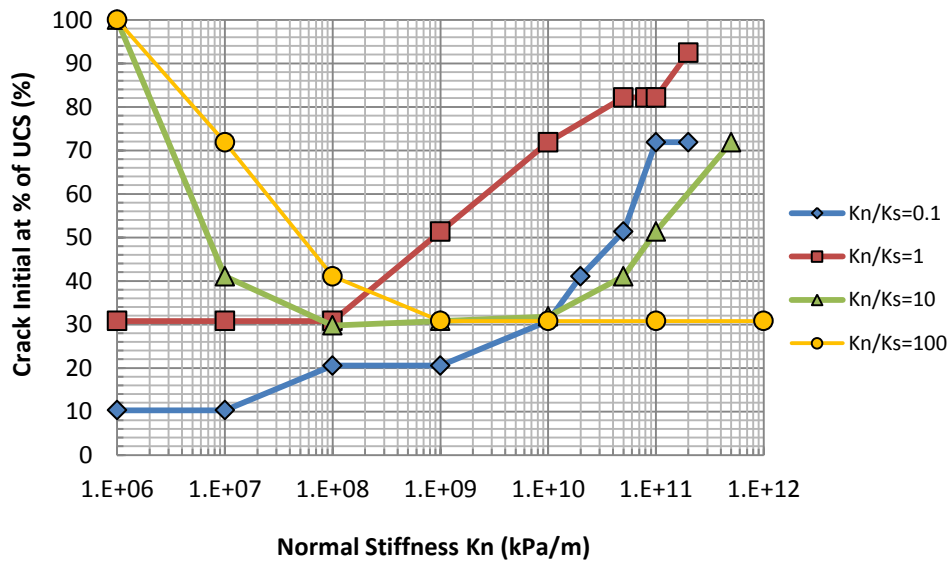
Figure 5.8. Uniaxial Compressive Test result, crack initiation at percentage of uniaxial compressive strength under different normal and shear stiffnesses.

76
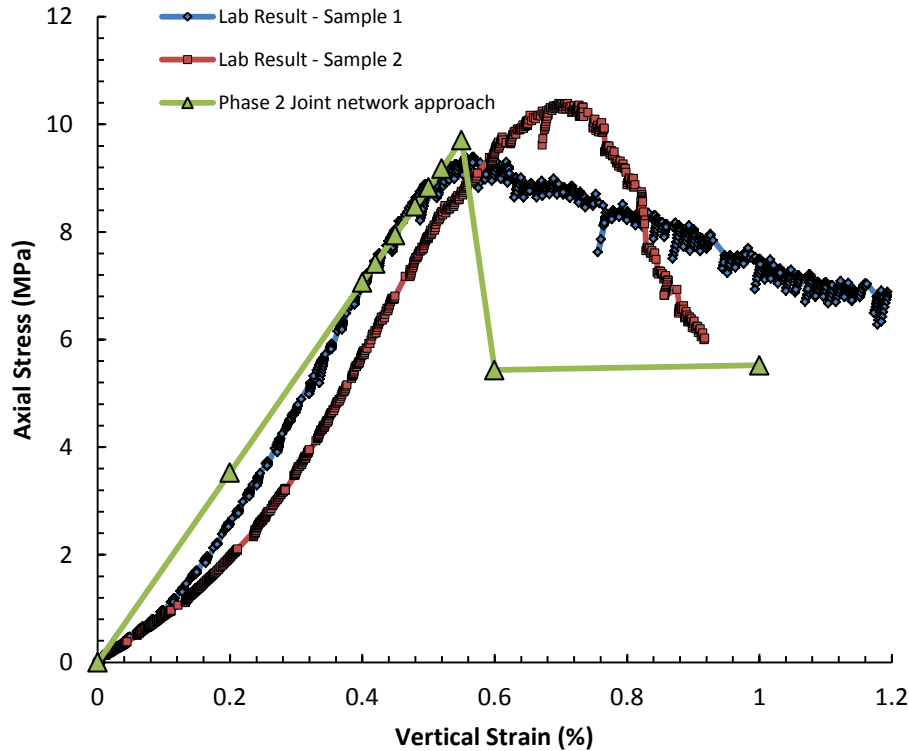
Figure 5.9. Comparison of the *Phase*^{2} response for uniaxial compression using the Voronoi joint network and the laboratory test results.

5.2.2   Brazilian Test

The *Phase*^{2} modelling of the Brazilian laboratory tests followed the same procedure used for the uniaxial compressive tests. The model diameter was 50 mm with a steel-loading cap on top of the sample, separated by an arc interface joint. The base pedestal was also made of steel with the same contact property as the top-loading cap. The bottom of base pedestal was fixed to prevent movement in both X and Y directions. The loading was applied to the loading-cap vertically downward and increased in uniform steps until uniaxial tensile strength was reached. The *Phase*^{2} model used with the traditional continuum mechanics approach is shown in Figure 5.10. Figure 5.10 also shows the failure observed in the sample. There is a clustering of tensile failure at the center of sample and shear failure near contact joint.

Calibration of normal stiffness and shear stiffness of the contact joint between synthetic rock and the loading cap was focused on the continuum mechanics approach. The normal stiffness and the shear stiffness of the contact joint was adjusted until the tensile strength reached 1.84 MPa at the last loading step by observing the tensile yielding elements at the last step marked by the white circles shown in Figure 5.10 (b).

| a) Phase 2 model | b) Yielding in the Brazilian model |
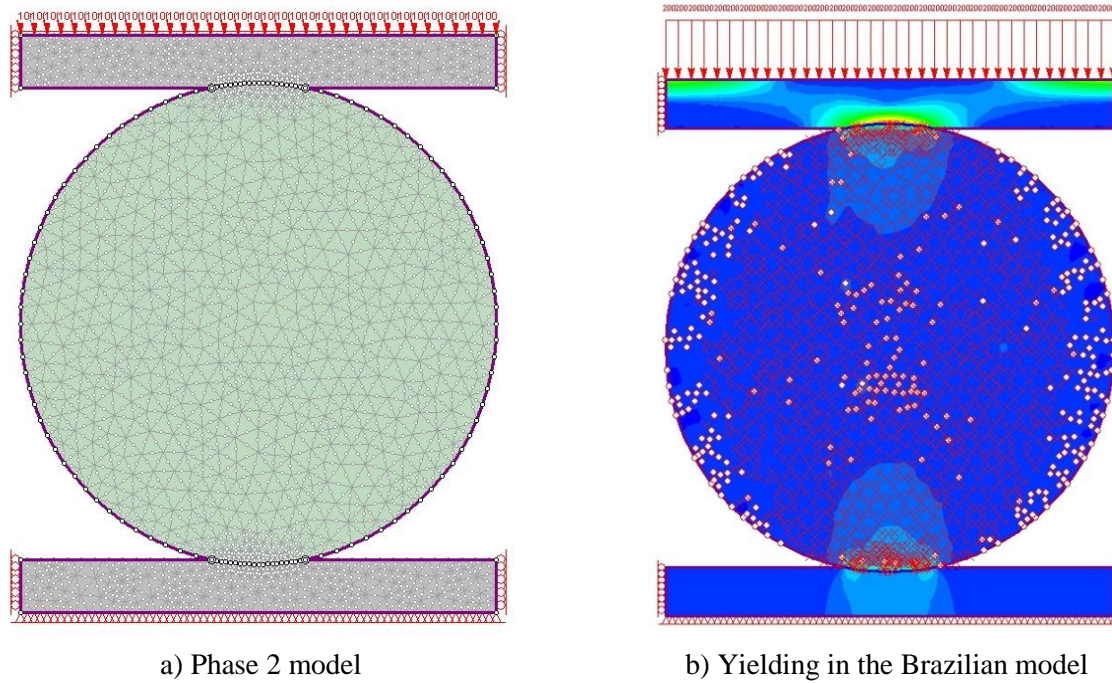
Figure 5.10. Brazilian model in Phase[2] and yielding observed in the model when the peak stress reached 2 MPa (Brazilian tensile strength); the white circles in the right figure represent tensile yield.

The adjustment of normal stiffness and shear stiffness of the Voronoi joints was evaluated in the Brazilian tests in the same way as in the uniaxial compressive test. The vertical stress – displacement curve of synthetic rock was plotted from each simulation result. Figure 5.11 shows the Voronoi Brazilian model and the location of the cracking observed as the peak load is approached. Tensile cracking initiated after reaching 80 to 90 percent of the peak tensile strength. These Voronoi results visually appear more realistic and closer to the fracturing observed in the laboratory (see Figure 3.4).
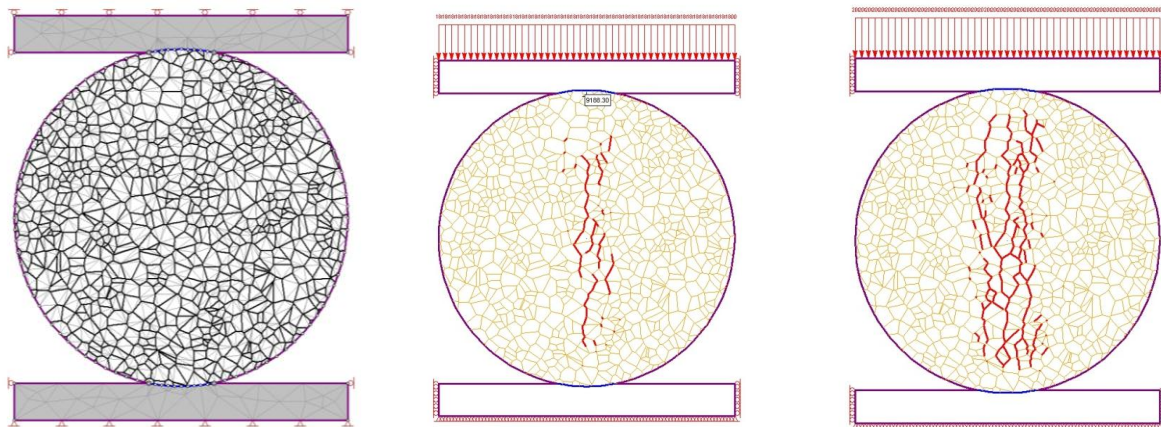
Figure 5.11. The Brazilian Voronoi model used in the *Phase^2* and the crack patterns observed at different stages of loading.

A number of simulations were carried out to establish the Young's Modulus for various joint stiffness (Figure 5.12). The normal stiffness of 5×10^{10} kPa/m with a normal stiffness to shear stiffness ratio of 0.1, which is the same as chosen in the uniaxial compressive test, provided acceptable results. The vertical stress – displacement curve of synthetic rock under the Brazilian test when the particle boundary joint Kn/Ks = 0.1 is plotted in Figure 5.13, which is close to the laboratory result shown in Figure 3.5 in Chapter 3.
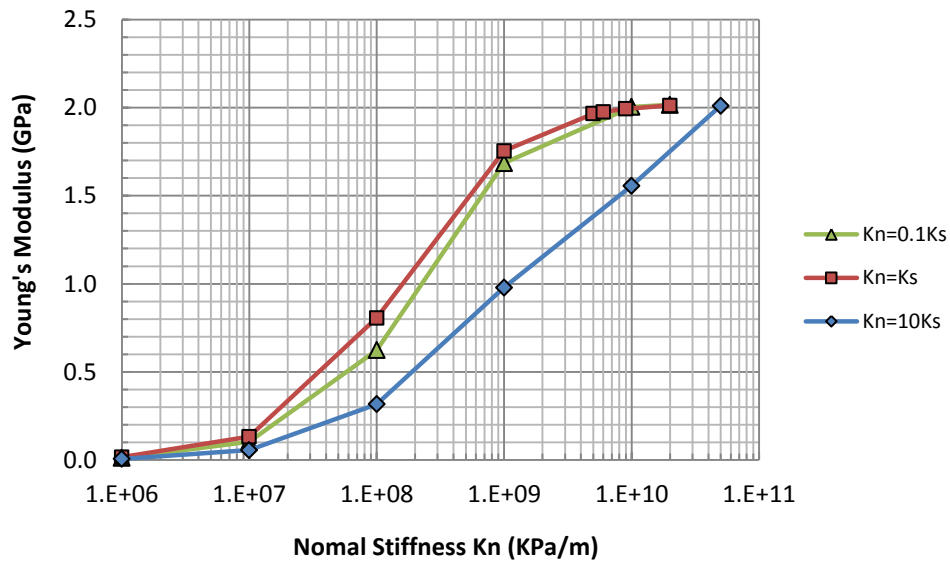
Figure 5.12. Brazilian Test results; Young's Modulus variation under different normal and shear stiffnesses.
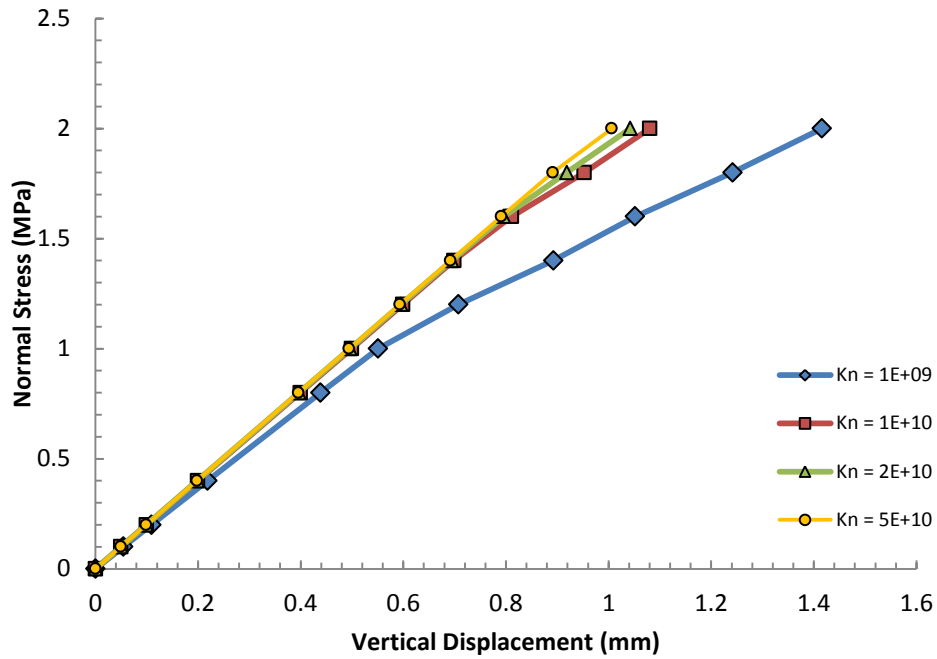
(a)
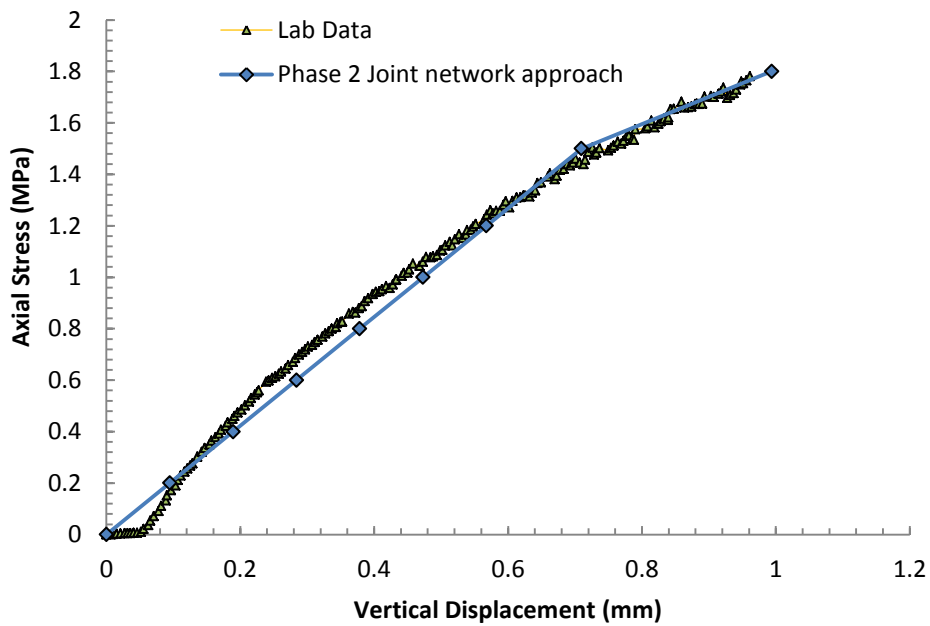
(b)

Figure 5.13: (a) Vertical Stress – Displacement behavior of synthetic rock under normal compressive stress in the Brazilian Test when the particle boundary joint Kn/Ks = 0.1, (b) Comparison between the *Phase²* joint network approach and laboratory test results

5.3 Application to direct shear tests

5.3.1 Modeling and Meshing

Finite element modelling was carried out following the procedure used in the laboratory test program. The modeling of the direct shear tests used a steel box and loading cap with a 6-mm-gap at the centre (Figure 5.14). Step 1 in the modelling was the application of the normal stress. The subsequent steps involved the application of the horizontal shear displacements in 1 mm increments to the bottom portion of the shear box. A total of 10 mm of horizontal shear displacements were applied in ten loading steps in the Phase2 model. Meshing of the direct shear tests was carried out using six-noded triangles with a uniform distribution away from the closed joint. The mesh along the closed joint was increased by doubling the density of the elements by a factor of two, which resulted in an element every 0.5 mm along the closed joint. This mesh density was used for all the joint testing in order to ensure the comparison of the results from one test to the other was not biased by differences in mesh density.

a) Application of normal stress   b) Application of shear displacement
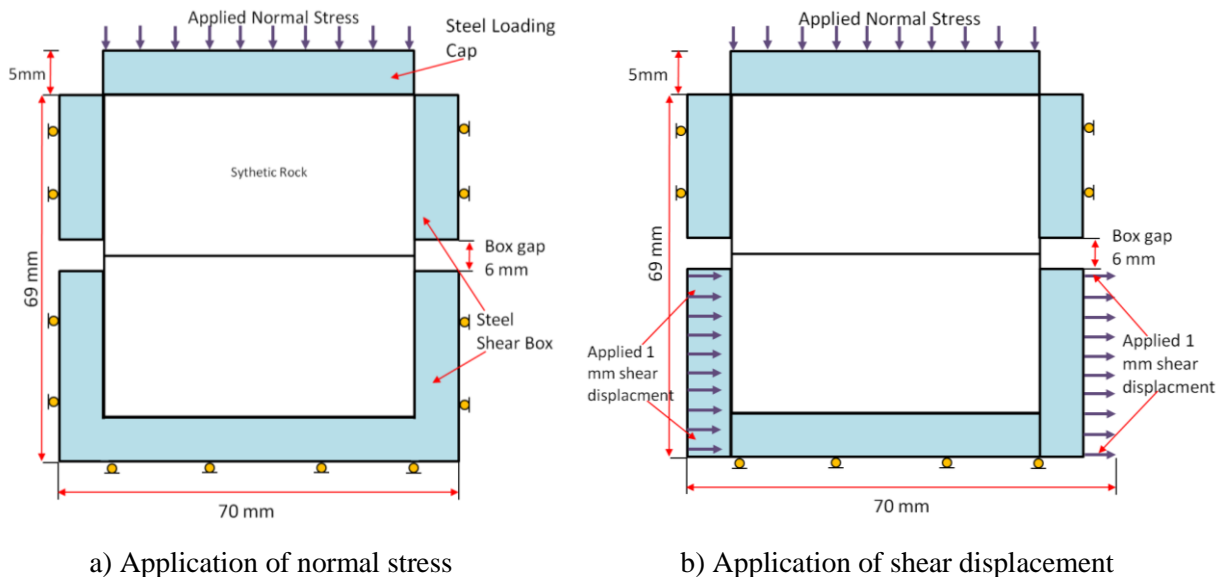
Figure 5.14. Illustration of direct shear test simulation used in *Phase²*. (a) Stage 1 - Application of normal stress, and (b) Stage 2 application of shear displacement in 1 mm increments.

5.3.2 Continuous and discontinuous joint models

The synthetic rock chosen for presenting weak rock is made of plaster and sand. The uniaxial compressive strength, stiffness and tensile strength are highly dependent on moisture content.

In order to simulate the behavior of natural brittle rock, low moisture content is required. The rock sample used here was cured for longer than one week before testing to achieve the brittle behaviour. The basic parameters tested after one week of curing were used in the numerical analysis. The basic parameters used for simulating the steel shear box and loading cap are tabulated in Table 5.2. The Rock mass and joint Mohr-Coulomb failure criterion is presented in Table 5.3.

Table 5.2. Basic parameters used for the steel shear box and loading cap.

Property of steel shear box and loading cap	
Young's Modulus (GPa)	200
Poisson's Ratio	0.28
Tensile Strength (MPa)	1000

Table 5.3. Synthetic rock and joint properties and failure criterion

Intact Synthetic Rock		
Peak Cohesion (MPa)	2.2	
Peak Fiction Angle (Deg)	42	
Residual Cohesion (MPa)	0	
Residual Fiction Angle (Deg)	38	
Young's Modulus (GPa)	2.134	
Poisson's Ratio	0.2	
Poisson's Ratio	0.2	
Tensile Strength (MPa)	1.84	
Uniaxial Compressive Strength (MPa)	9.74	
Main joint	**Low normal stress**	**High normal stress**
Normal Stiffness (kPa/m)	3.7×10^6	1.2×10^7
Shear Stiffness (kPa/m)	4×10^5	1.6×10^6
Peak Cohesion (MPa)	0.1	0.1
Peak Fiction Angle (Deg)	40	52
Residual Cohesion (MPa)	0	0
Residual Fiction Angle (Deg)	38	38

In order to fix the upper half of the shear box and to move the lower half, two boundary conditions were applied to the shear box. The left and right sides of the upper part of the shear

box were restrained from moving in the X direction and lower base was restrained from moving in the Y direction. The first stage of the loading process involved the application of the normal stress. For this stage the contacts between the shear box and the sample were assigned zero shear stiffness (Figure 5.15 (a)). Once the normal stress was achieved, shear displacements were applied to the sample by moving both the left and right lower half sides of the shear box in 1 mm increments while the upper half of the shear box was fixed to zero.

(a)   (b)
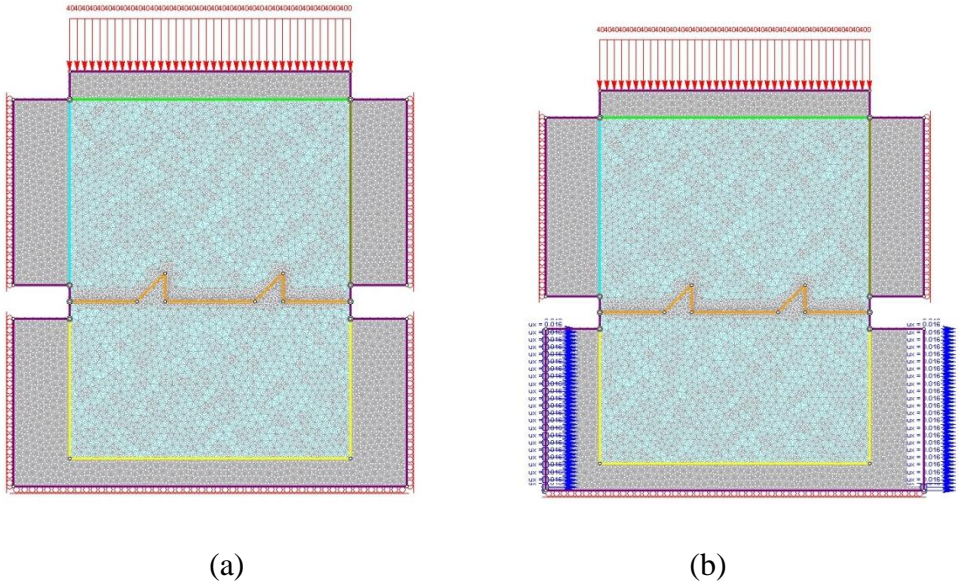
Figure 5.15. Continuum mechanics approach with a loading cap and shear box from the direct shear test on synthetic rock containing a discontinuous closed joint. (a) 45-degree joint shape with 400 kPa normal stress, Stage 1 with zero displacement applied on the lower side, and (b) 45 degree joint shape with 400 kPa normal stress, with horizontal displacement in 1 mm increments applied on both the left and right lower sides.

The open crack in the continuum mechanics approach was created in the middle of the sample as shown in Figure 5.16(a) and Figure 5.16(b). Boundary conditions and load sequencing were applied to the sample in the same manner as applied to the completely closed joint sample. The constant normal load was applied at the top and vertically downward and remains constant for all stages. The shear displacements were applied in 1-mm increments to the lower portion of the shear box.
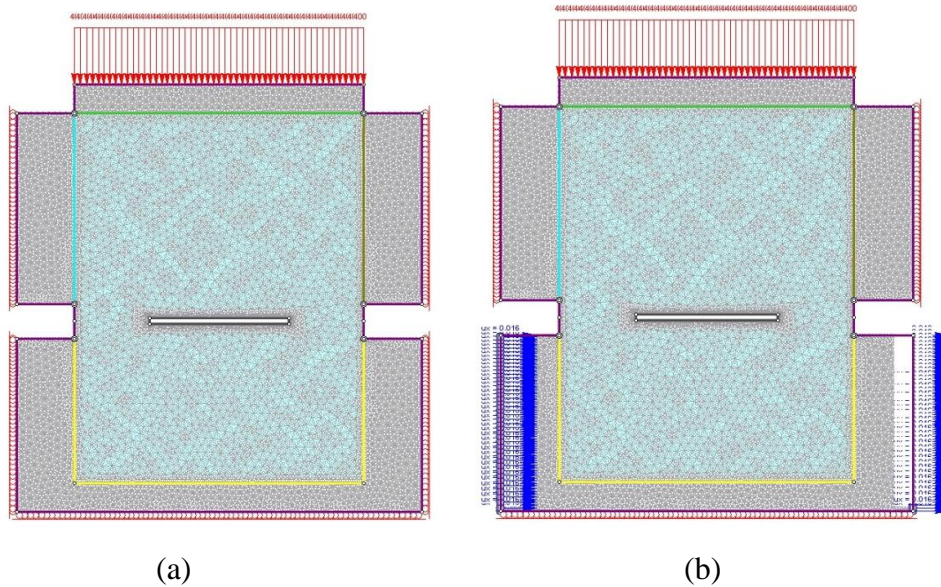
Figure 5.16. Continuum mechanics approach of the direct shear test on synthetic rock containing an open joint. (a) Sample B, Stage 1 with zero displacement applied on the lower side. (b) Application of shear displacement in 1-mm increments on the lower portion of the shear box.

5.3.3   Establishing the shear stress

In the laboratory tests the shear force is determined by monitoring the load the top right-hand side of the shear box applies as the bottom portion of the shear box moves. This load is recorded by a load cell or proving ring and converted to a shear stress by averaging the shear force over the horizontal area of the joint being tested. In *Phase^2* 8.0, the shear stress created by moving the lower portion of the shear box is recorded by monitoring the horizontal shear stress in the steel portion of the shear box in Figure 5.16.
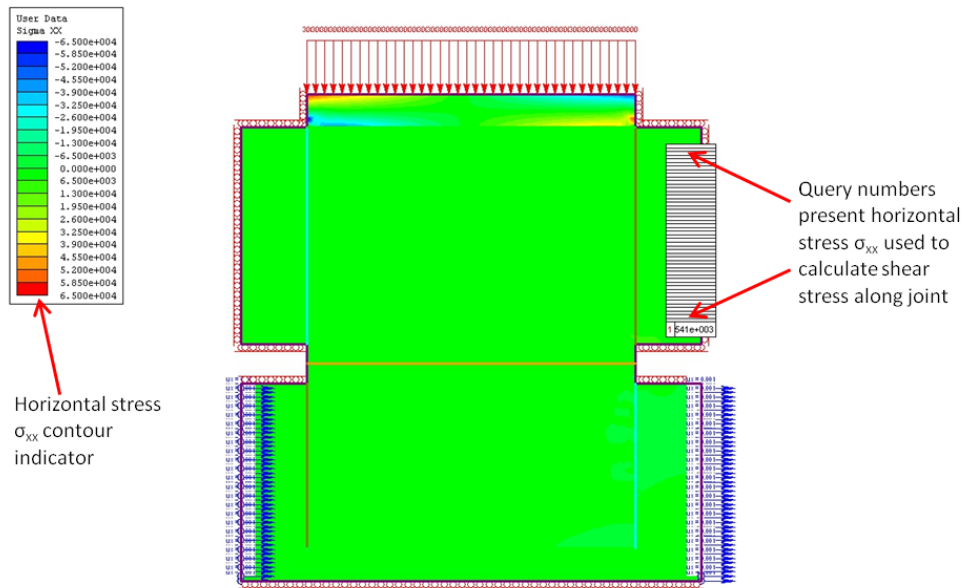
Figure 5.17. Horizontal stress averaged from the upper right shear box from query numbers.

5.4   Interpretation of Results

5.4.1   Continuous planar-joint

As shown in Figure 4.5 and Figure 4.6 in Chapter 4, the normal and shear stiffness of the main joint varies as a function of under normal stresses. Figure 5.18 shows the average values of the measured the normal and shear stiffness from the laboratory program. Phase2 cannot handle the stiffness values as a function of normal stress and therefore these stiffness values had to be applied for each test. Because of this normal stress dependency it was not possible to apply constant stiffness properties to the main joint.

Table 5.4 shows the contact joint properties that were used for the simulations. These properties were divided into two groups, based on normal stress. The boundary for the grouping was a normal stress of 400 kPa.

As noted previously, the shear displacements were applied in 1 mm increments. A total of 16 mm of horizontal displacements was applied to the models.
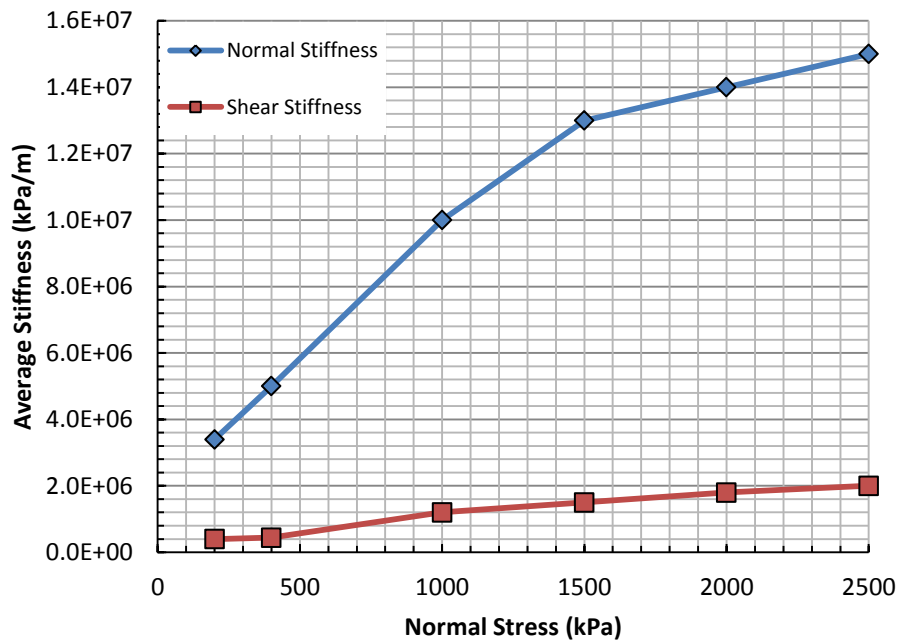
Figure 5.18 Laboratory average stiffness of the closed joint measured at different normal stress.

Table 5.5. Contact joint properties for samples with different normal stress

Contact Joint Property normal stress of 0.4 MPa or less				
Upper right side / Lower left side			Top Side / Bottom Side	
Kn (kPa/m)	Ks (kPa/m)	Peak Fiction Angle (degree)	Kn (kPa/m)	Ks(kPa/m)
6.8×10^9	6.8×10^8	10	6.8×10^9	0
Upper left side joint / Lower Right Side				
	Kn (kPa/m)	Ks (kPa/m)	Peak Fiction Angle (degree)	
Loading Stage 1	6.8×10^9	6.8×10^8	10	
Following Loading Stage	0	6.8×10^8	10	
Contact Joint Property of 3 MPa normal stress or less				
Upper right side / Lower left side			Top Side / Bottom Side	
Kn (kPa/m)	Ks (kPa/m)	Peak Fiction Angle (degree)	Kn (kPa/m)	Ks (kPa/m)
1.7×10^8	1.7×10^7	10	1.7×10^8	0
Upper left side joint / Lower Right Side				
	Kn (kPa/m)	Ks (kPa/m)	Peak Fiction Angle (degree)	
Loading Stage 1	1.7×10^8	1.7×10^7	10	
Following Loading Stage	0	1.7×10^7	10	

Figure 5.19 shows the comparison of the shear stress and shear displacement response from the *Phase²* 8.0 simulation to the measured laboratory response for the smooth planar joint for normal stresses of 400 kPa, 2 MPa and 3 MPa. For the normal stress range tested the Phase2 simulations are in reasonable agreement with the laboratory peak strengths. The laboratory tests were limited to a shear displacement of 8 mm and at high normal stress residual strength was not achieved with this amount of shear. The Phase2 simulations were sheared to 16 mm and the laboratory results extrapolated for comparison with the numerical results. The stress-displacement behaviour under high normal stress (2 MPa and 3 MPa) from Figure 5.19 shows, assuming the laboratory extrapolations are valid; there is also reasonable agreement between the numerical simulations and the laboratory results.
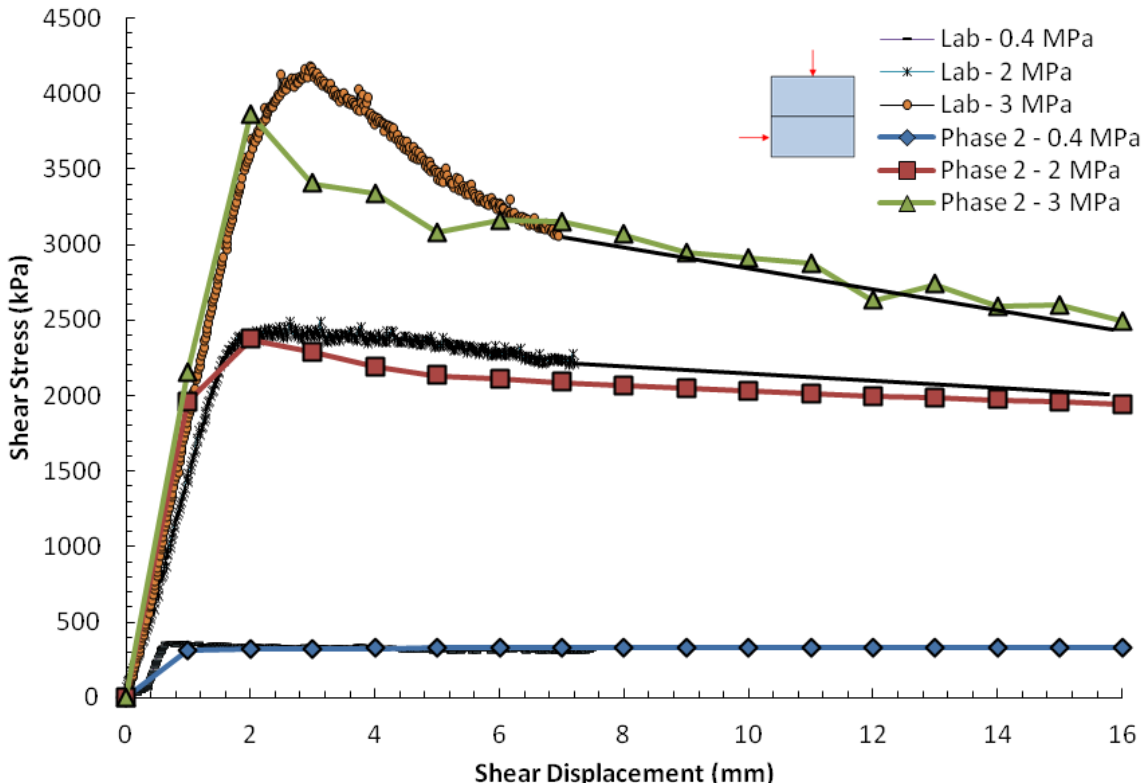
Figure 5.19. Comparison of shear stress and shear displacement responses from the *Phase²* 8.0 simulations to the measured laboratory response of synthetic planar rock samples under different normal stress: 0.4 MPa, 2 MPa, and 3 MPa.

The results in Figure 5.19 illustrate that the planar continuous joint shows increasing strain weakening behaviour and a more pronounced peak strength as the normal stress increases in

the laboratory results. Despite the planar geometry of the joint surface, it is also clear that as the normal stress increases, more shear displacement is required to reach the residual shear strength. This is somewhat surprising as it is usually assumed that smooth joints will not display a peak strength, particularly as the normal stress increases. This behaviour may be related to the sand grains that were added to the material and may reflect dragging of these grains. Inspection of the joint surfaces did not show any unusual roughness associated with the joints surfaces subjected to high normal stress. Regardless of the reasons, the laboratory and the *Phase²* simulations can capture the observed shear strength behaviour.

Figure 5.20 shows the comparison of the residual strength behavior with normal stress simulated by *Phase²* 8.0 software and laboratory results. The result indicates that the simulation result has a residual friction angle of $\phi_p = 46^o$ when normal stress between 1 MPa and 2 MPa, and a residual friction angle of $\phi_r = 38^o$ when normal stress smaller than 1 MPa or larger than 2 MPa. The *Phase²* 8.0 simulation results showed consistency with the laboratory results.
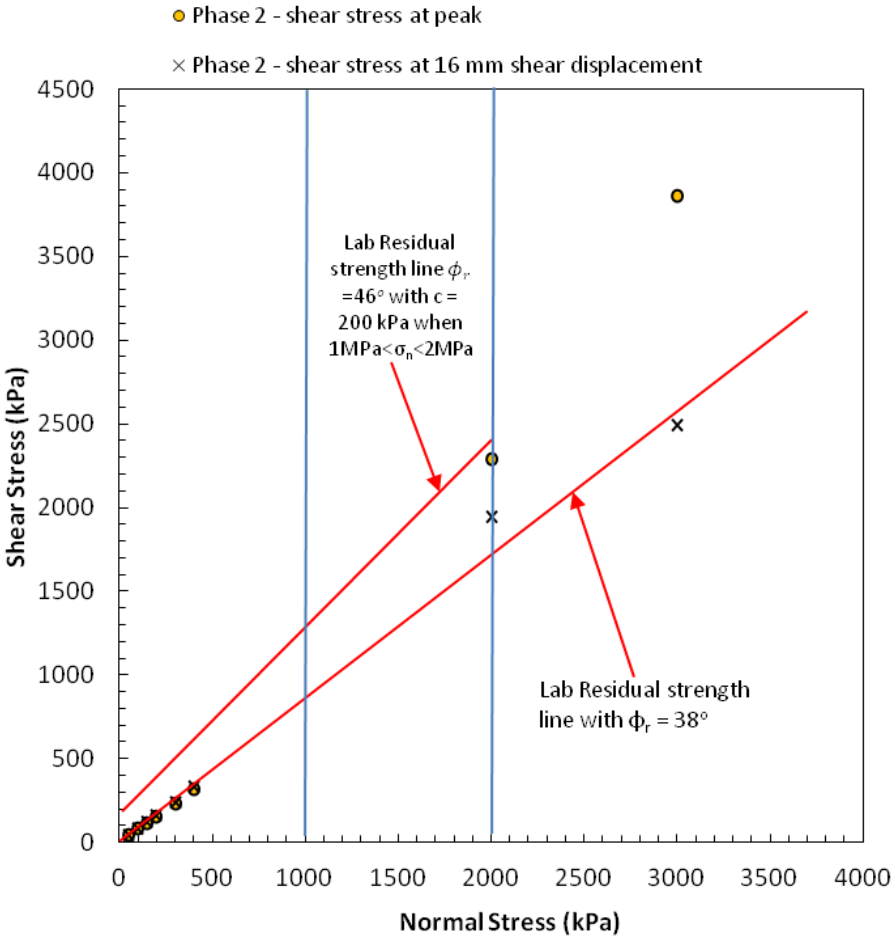
Figure 5.20. Comparison of the residual strength behavior with normal stress simulated by *Phase²* 8.0 software and laboratory results.

5.4.2 *Discontinuous stepped-joints*

The Phase2 modelling of the discontinuous joints followed the same procedure and used the same properties for as the modelling Section 5.5.1. In other words only the geometry of the main joint was changed for these simulations.

Figure to Figure 5.23 show the comparison of the shear stress versus shear displacement response from the *Phase²* 8.0 simulation to the measured laboratory. Compared to the continuous planar joint, the numerical results are not in as good agreement with the laboratory shear stiffness and peak strength of the discontinuous joints. These differences may be due to the non-uniform loading caused by the irregular geometry of the joint. For example, even at low normal stress (0.4 MPa) the laboratory discontinuous joint showed strain weakening behaviour that was not observed in the laboratory continuous planar joint. Phase2 was not able to capture this strain weakening behaviour. At high normal stress, the laboratory strain weakening behaviour is generally reduced and the Phase2 results are in better agreement with the laboratory results.
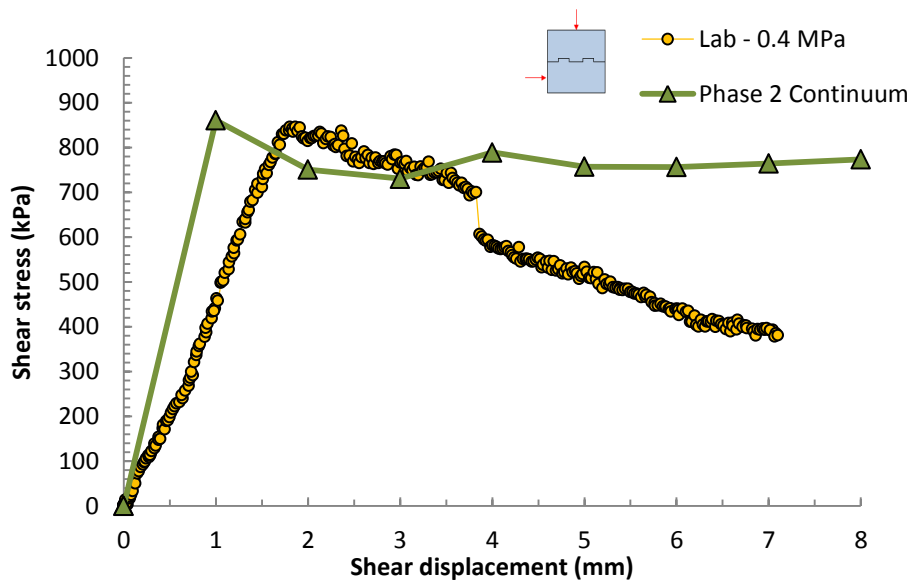
(a)
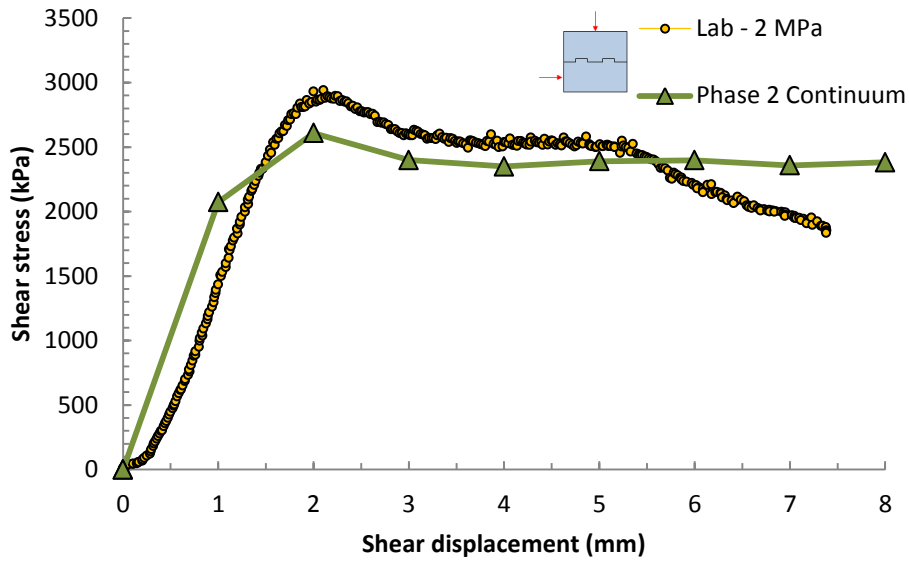
(b)

Figure 5.21. Direct shear test shear stress – displacement comparison between *Phase²* 8.0 simulation and laboratory results of the 90 degree joint shape sample: (a) 400 kPa normal stress, and (b) 2 MPa normal stress.
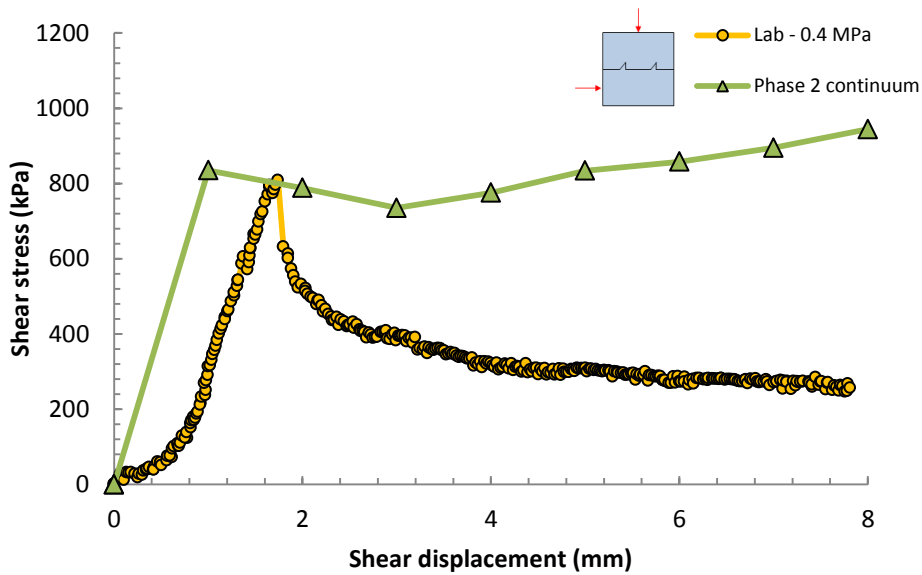
(a)
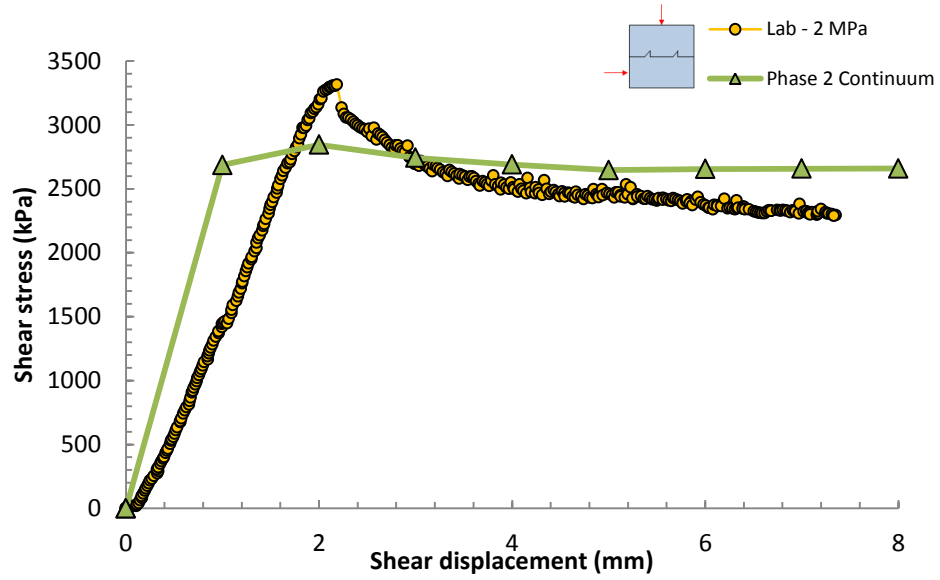
(b)

Figure 5.22. Direct shear test shear stress – displacement comparison between *Phase²* 8.0 simulation and laboratory results of the 45 degree joint shape sample, (a) 400 kPa normal stress, and (b) 2 MPa normal stress.
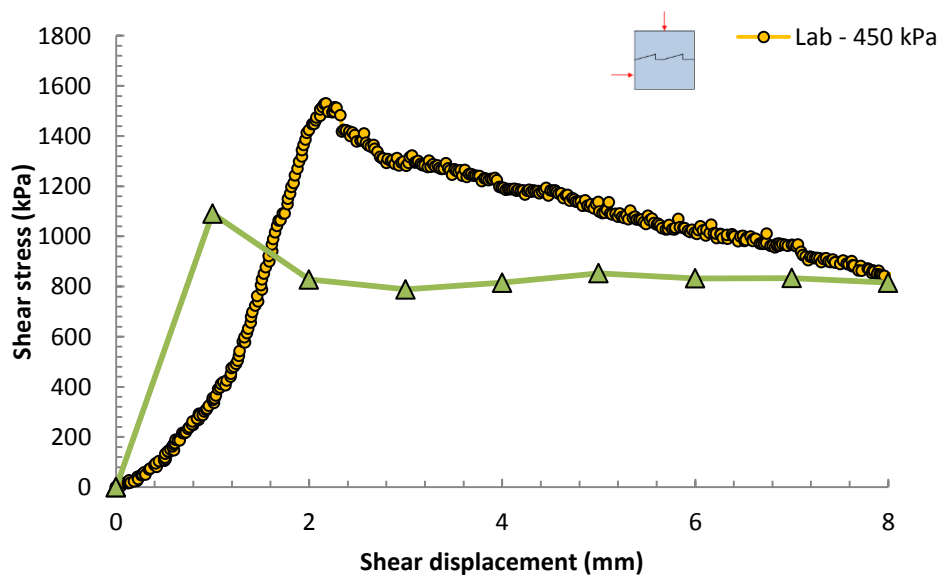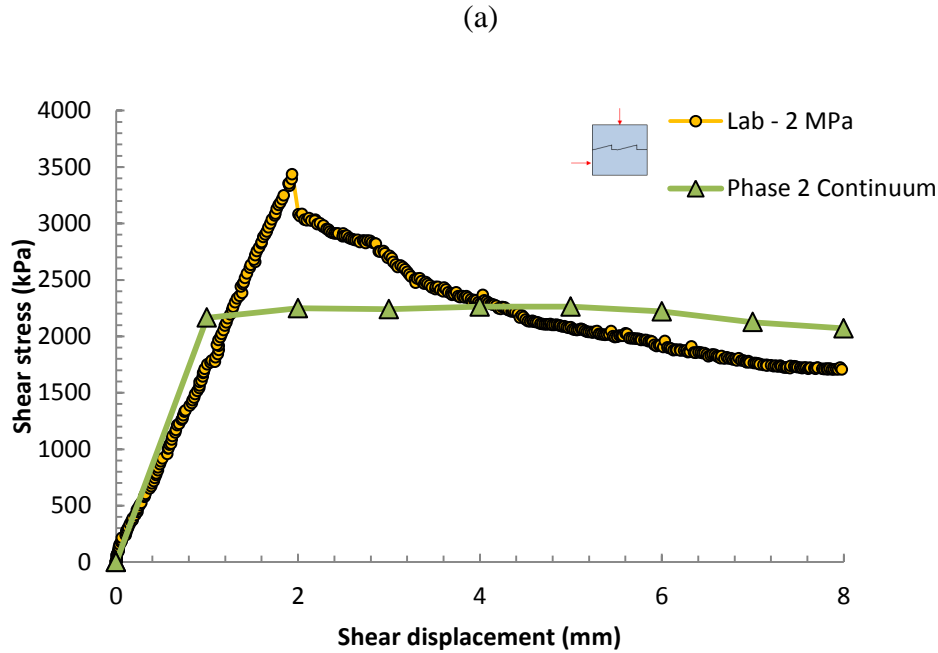
(b)

Figure 5.23. Direct shear test shear stress – displacement comparison between *Phase²* 8.0 simulation and laboratory results of the 15 degree joint shape sample, (a) 400 kPa normal stress, and (b) 2 MPa normal stress.

5.4.3 Discontinuous open-joints

Figure 5.24 to Figure 5.26 show the comparison of the shear stress versus shear displacement response from the *Phase²* 8.0 simulation to the measured laboratory results for the discontinuous open-joint samples. The numerical results are not in good agreement with the laboratory results. The properties of the intact synthetic rock were determined from the Brazilian tensile and uniaxial compressive strength and used to calibrate *Phase²*. It would appear that in order to match the shear strength of the discontinuous open-joints, the *Phase²* properties would have to be calibrated to the laboratory properties. This implies that the continuum approach can only be used if there is calibration to intact properties obtained for the stress path that will be used in the continuum model. This is in contrast to the discrete element approach used by Cho et al. [7] where their successful direct shear simulations were calibrated using properties from Brazilian tensile and uniaxial compressive strength.
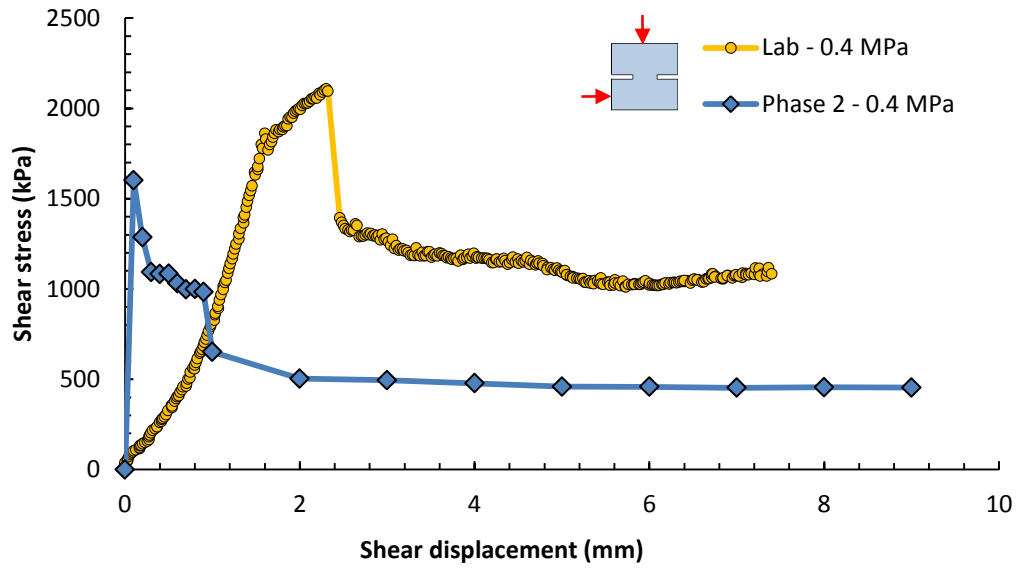
(a)
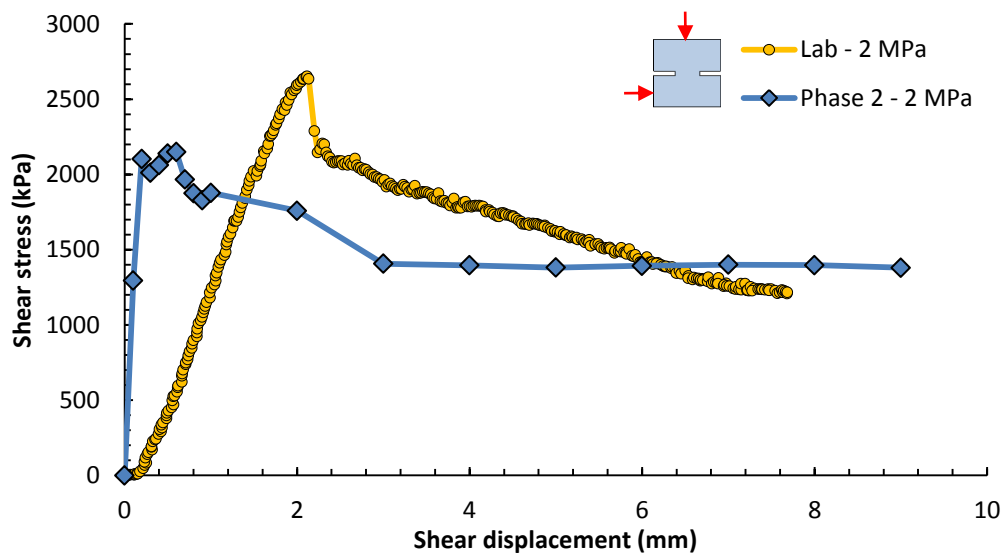
(b)

Figure 5.24. Direct shear test shear stress- displacement comparison between *Phase²* 8.0 simulation and laboratory results of Sample A open joint shape sample, (a) 400 kPa normal stress, and (b) 2 MPa normal stress.
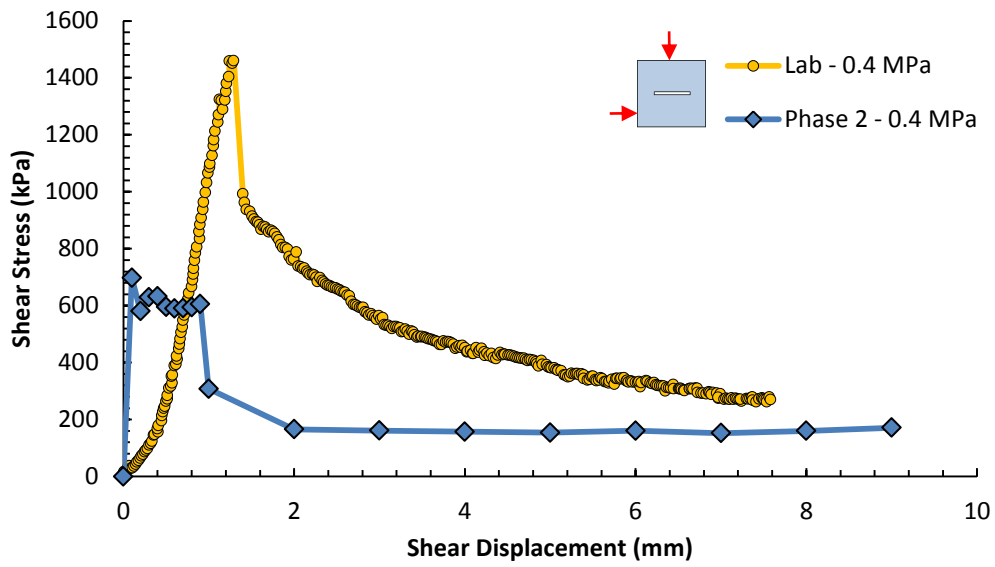
(a)
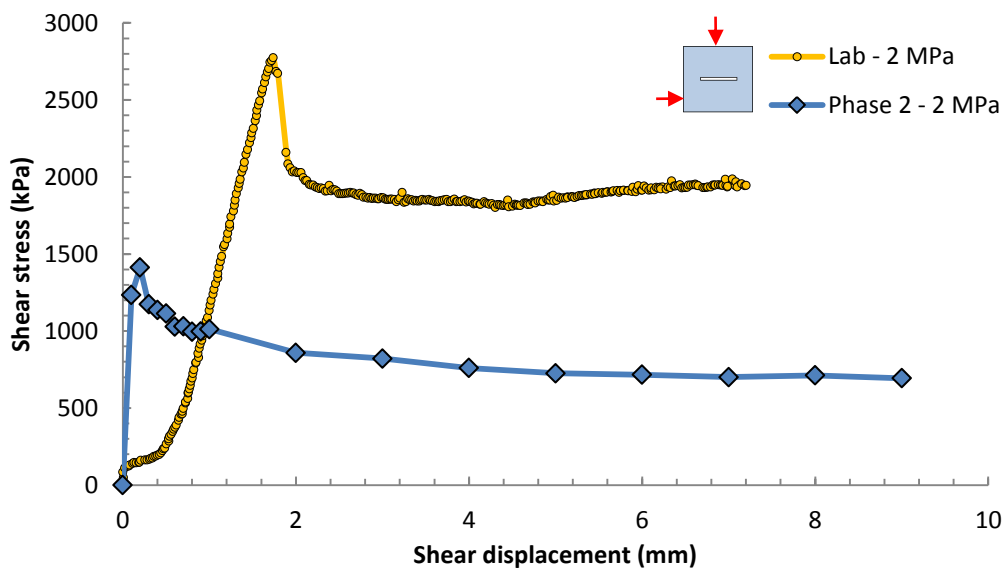
(b)

Figure 5.25. Direct shear test shear stress- displacement comparison between *Phase²* 8.0 simulation and laboratory results of Sample B open joint shape sample, (a) 400 kPa normal stress, and (b) 2 MPa normal stress.
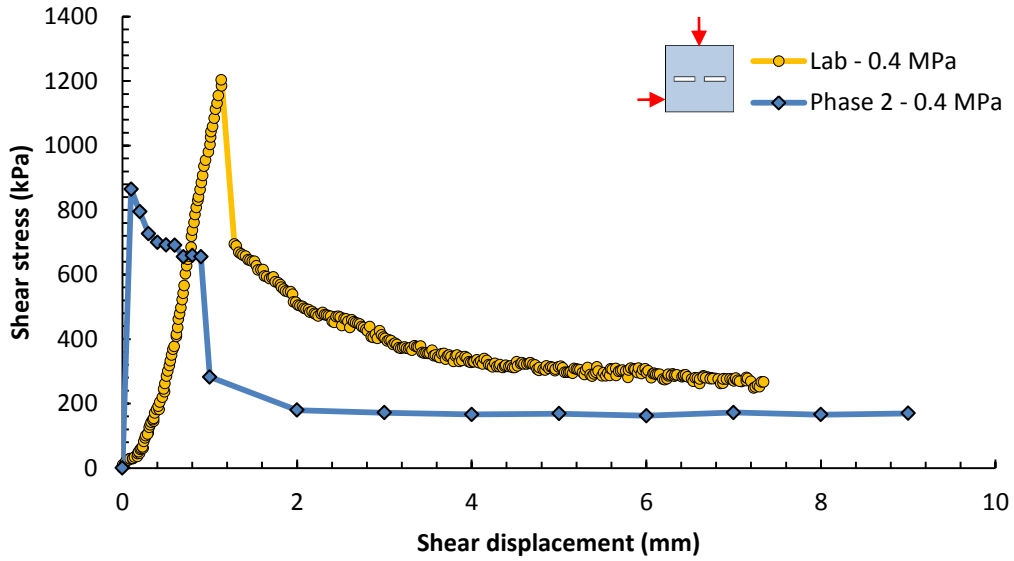
(a)
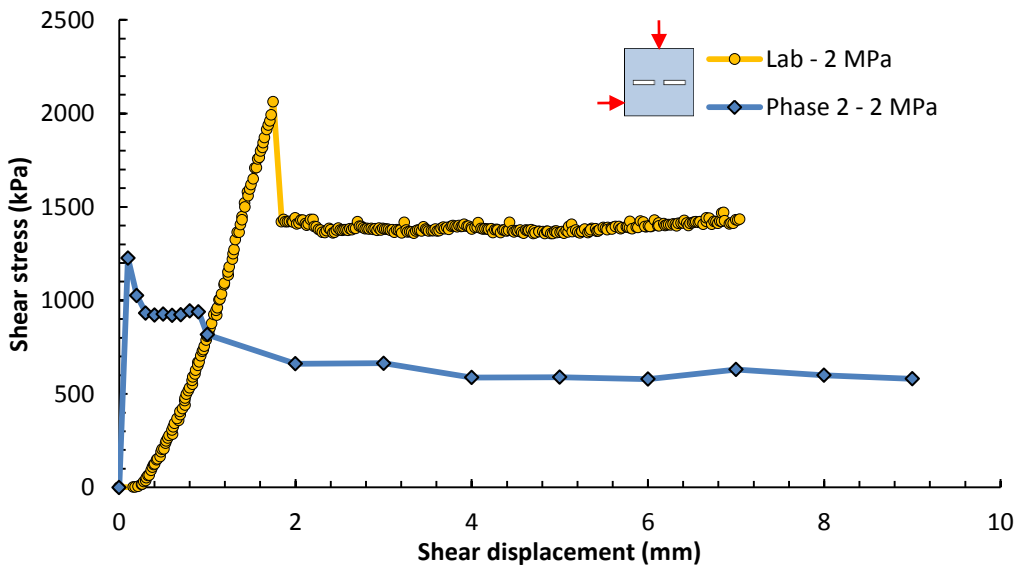
(b)

Figure 5.26. Direct shear test shear stress- displacement comparison between *Phase²* 8.0 simulation and laboratory results of Sample C open joint shape sample, (a) 400 kPa normal stress, and (b) 2 MPa normal stress.

It was observed that the shear displacement to peak in *Phase²* simulation was much smaller than in laboratory test. In the *Phase²* simulations for the open joint the stiffness variable is the contact joint of the sample with the steel shear box. A series of *Phase²* simulations were carried out to establish the effect of the contact normal stiffness on the sample shear stiffness. There is essentially no effect of the peak stress but the shear stiffness can be decreased. Hence the

modeling shear stiffness can be made to provide better agreement with the laboratory results, but the strength remains essentially unchanged. Given the limitation of the *Phase²* for simulating the discontinuous open-joint, no additional simulations were carried out.

5.5 Voronoi modelling of joints

The Voronoi modeling was used in the calibration to laboratory tests to assess its potential in *Phase²*. At this stage the Voronoi tessellation scheme in *Phase²* is experimental. For the purposes of the calibration, the behaviour of the polygons formed by the Voronoi tessellation was set as elastic. In a direct shear test this configuration would lead to large dilation as the failure can only occur along the polygon boundary. Consequently all the shear tests show strain hardening and cannot capture the observed laboratory strain weakening response. In part this is caused by the large size (>1mm) of the polygons. At this stage more information will be needed in order to complete the calibration of the Voronoi approach and a more efficient approach for handling the Voronoi geometry.

5.6 Summary

This chapter discussed the numerical analysis of continuous and discontinuous joints under direct shear conditions. The numerical analysis using the elasto-plastic finite element software *Phase² 8.0* started by calibrating the numerical properties used to describe the intact rock behaviour to those of the laboratory uniaxial compressive test and the Brazilian test. The calibration of the intact rock properties resulted in a material properties that were later used for simulating the direct shear tests.

In addition to the calibration of the intact material properties, the properties of the contact joint used as the interface between the steel shear box and the synthetic rock was also calibrated. This calibration was carried out to follow the stages in the direct shear test. The first stage in the test is the application of the normal stress. The contact joint properties were chosen so that residual shear stresses were not created by the application of the normal stress.

The results from the Phase2 numerical modelling when compared to the laboratory test results can be summarized as follows:

1. The numerical modelling of the continuous planar joint provided good agreement between the laboratory test results and the *Phase²* results.

2. The agreement between the laboratory test results and the *Phase²* results for the continuous stepped-joints were acceptable at high normal stress. At low normal

stress the *Phase^2* results could not capture the strain weakening behaviours observed in the laboratory tests results.

3. The *Phase^2* results for the discontinuous open-joints do not agree with the laboratory test results.

5.7 Reference

[1]   Hammah, R. E., Yacoub, T., Corkum, B., Wibowo, F., Curran, J. H. 2006. Analysis of Blocky Rock Slopes with Finite element Shear Strength Reduction Analysis. http://www.rocscience.com/assets/files/uploads/7690.pdf

[2]   Hammah, R. E., Yacoub, T. E., Curran, J. H. 2008. Probabilistic slope analysis with the Finite Element Method. *American Rock Mechanics Association*. 09-149.

[3]   Rocscience Inc. 2011. Convergence Criteria. Theory of *Phase^2*, http://www.rocscience.com/downloads/phase2/webhelp/theory/Theory_Overview.htm.1-4

[4]   Rocscience Inc. 2011. Joint Networks. Theory of *Phase^2*, http://www.rocscience.com/downloads/phase2/webhelp/theory/Theory_Overview.htm.1-3

[5]   Riahi, R. E., Hammah, J. H. Curran Limits of Applicability of the Finite Element Explicit Joint Model. In Proceedings of the 44th U.S. Symposium on Rock Mechanics and the 5th U.S. - Canada Rock Mechanics Symposium Salt Lake City, Utah, USA, June 2010.

[6]   Lan, Hengxing., Martin, C. D., Bo, Hu. 2010. "Effect of Heterogeneity of Brittle Rock on Micromechanical Extensile Behavior during Compression Loading." *Journal of Geophysical Research* 115 (B1) (January 26): B01202. doi:10.1029/2009JB006496.

[7]   Cho, N. 2008. Discrete Element Modeling of Rock, Ph.D. thesis. Department of Civil and Environmental Engineering, University of Alberta. 1-25.

6 Conclusions and Recommendations

6.1 Conclusions

This research had two goals: The first goal was to establish a set of laboratory direct shear results for joints in a synthetic rock that range from continuous planar features, through planar discontinuous joints with the discontinuous nature created by step features. In both of these cases there is no intact material along the joint trace length. A third set of laboratory tests was carried out to assess the behaviour of open discontinuous joints where the open character was created by thin non-contacting slits. In this third data set the joint trace a portion of intact material interrupts the joint trace length. The second goal of this research was to simulate the laboratory direct shear tests using a commercially available two-dimensional elasto-plastic finite element program, *Phase²*. The properties for the intact synthetic rock were obtained from uniaxial compressive strength and Brazilian tensile strength tests and used as input in the numerical simulations. The geometry of the direct shear tests and the loading sequence in *Phase²* followed the same sequence as used in the laboratory tests.

6.1.1 *Direct shear laboratory results*

Direct shear testing was carried out on 88 samples of a synthetic rock containing different joint shapes, both closed and open. Examination of the shear stress versus shear displacement plots for these samples suggests the following:

- Many of the plots show initial nonlinear behaviour during the initial application of shear stress. This nonlinear portion is attributed to seating of the sample during the initial loading. There is no indication that this nonlinear behaviour is related to crushing of pores in the intact rock.

- *Planar closed joint*: The planar closed joint shows an elastic-perfectly plastic response for all normal stress values of less than 2.5 MPa. For these samples the peak strength equals the residual strength. When the normal stress is 2.5 MPa or greater, the shear resistance is characterized by a strain weakening response. In other words, the shear strength decreases as shear displacement occurs beyond the peak strength.

- *Open Joints*: The shear stress versus shear displacement curves for the open joint show that these samples display a brittle behaviour after peak shear stress is reached when the normal stress is less than 3MPa. However, for the three open joint geometries, the brittle behaviour is essentially suppressed when the normal stress is 3 MPa.

- *Stepped closed joints*: The shear behaviour of all the stepped closed joints display either a brittle or strain-weakening response for all normal stresses below 0.4 MPa. The strain weakening can be significant.

- The *residual friction angle* based on the closed planar joints was estimated as $\phi_r = 38^o$. Not all samples tested reached the residual shear strength given by the planar joints. At normal stresses greater than 2 MPa, the shear strength of the closed joints at 7 mm shear displacement had not reached the estimated residual value based on $\phi_r = 38^o$. Meanwhile the open joints, at high normal stress often displayed shear strength values lower than the estimated residual strength assuming $\phi_r = 38^o$. It is likely that the shearing of open joints at high normal stress involves apparent cohesion.

- The failure envelope for all the samples shows a complex failure process. At normal stresses of less than 2 MPa, the strength is dominated by cohesion while at normal stress of greater than 2 MPa, friction appears to dominate the shear strength.

- The *normal stiffness* of a closed planar joint was obtained by using the vertical displacement during the application of the normal stress. The elastic displacement of the top steel cap and rock mass were taken into consideration in calculating the normal stiffness. The normal stiffness showed a nonlinear increase in stiffness as the normal stress increased.

- The *shear stiffness* for the open joints is independent of the normal stress, while there is a clear increase in shear stiffness as the normal stress increases for the closed joints.

6.1.2 Numerical simulations of the direct shear tests

The numerical analysis using finite element analysis software *Phase² 8.0* started from calibration of the uniaxial compressive test and the Brazilian test. The purpose of calibration from the basic test was to find out unknown properties of synthetic rock which could not gained from laboratory tests such as the normal and shear stiffnesses of particle boundaries used in the Voronoi joint network approach. The stress-strain curve plotted from calibration analysis was found to be close to the laboratory result which proves the validity of calibrated rock properties.

The Elastic Brittle model was used in *Phase² 8.0* simulations for intact rock. It presents the brittle behavior and part of strain weakening of intact rock. However, the shear stiffness from a stress-strain curve at the post peak stage is assumed as infinity because of a vertical drop in strength. Such an assumption was proven in Figure 5.11(b) from the results of a uniaxial compressive test. This obviously led to an inaccurate result compared with laboratory results at the post peak stage.

This chapter discussed the numerical analysis of continuous and discontinuous joints under direct shear conditions. The numerical analysis using the elasto-plastic finite element software *Phase² 8.0* started by calibrating the numerical properties used to describe the intact rock behaviour to those of the laboratory uniaxial compressive test and the Brazilian test. The calibration of the intact rock properties resulted in a material properties that were later used for simulating the direct shear tests.

In addition to the calibration of the intact material properties, the properties of the contact joint used as the interface between the steel shear box and the synthetic rock was also calibrated. This calibration was carried out to follow the stages in the direct shear test. The first stage in the test is the application of the normal stress. The contact joint properties were chosen so that residual shear stresses were not created by the application of the normal stress.

The results from the Phase2 numerical modelling when compared to the laboratory test results can be summarized as follows:

1. The numerical modelling of the continuous planar joint provided good agreement between the laboratory test results and the Phase2 results.

2. The agreement between the laboratory test results and the *Phase²* results was acceptable at the high normal stress. At low normal stress the *Phase²* results are not in agreement with the laboratory tests results.

3. The *Phase²* results for the open joints do not agree with the laboratory test results.

These findings suggest that the material properties for a continuum model may have to be calibrated to the laboratory results that were determined following the stress path simulated in the continuum model.

6.2   Recommendations for Future Research

This study has produced several questions that need to be answered. More work should be conducted on these questions in future research in order to better understand jointed rock mass behaviors. The most relevant questions and recommendations are shown as below:

1. The direct shear test on synthetic rock samples in this study was based on a constant normal load condition. Such tests provide useful data on engineering problems such as slope stability when there is a block of rockslide along the discontinuous joint in rock mass. However, Oii and Carter [1] pointed out that if dilation or construction were acting on a normal direction of rock while the shear process occured, the normal load was not constant.

A direct shear test under constant normal stiffness will be introduced in order to solve the above problem. The normal load applied on the sample is continuously increased by a machine while shearing occurs in order to keep a constant normal stiffness in the sample.

2. The shear stress applied to the rock sample in this test is constant strain based continuous loading. However, in tectonic activity areas such as coastal areas in British Columbia, the loading condition is kinematic rather than continuous. Kinematic loading conditions could be applied in a direct shear test along the predicted failure plane in order to present seismic loading conditions in nature.

3. The difference between finite element analysis (FEA) and discrete element analysis (DEA) is that the discrete particle could have shear displacement along the boundary joint in DEA while shear displacement was not allowed in FEA. In further numerical modeling on synthetic rock samples, it would be warranted using discrete element analysis based software, such as UDEC. However, Cho [2] mentioned that clump particles were infinitely bounded and never broke apart in most of discrete element analysis software assumption. Modeling of considerations of the crushing effect could also be applied in future numerical research.

6.3   Reference

[1]   Ooi, L. H. and Carter, J. P., 1987. A Constant Normal Stiffness Direct Shear Device for Static and Cyclic Loading. *Geotechnical Testing Journal*. 10(1): 3-12

[2]   Cho, N. 2008. Discrete Element Modeling of Rock, Ph.D. thesis. Department of Civil and Environmental Engineering, University of Alberta. 228-233.

- **Appendix**

o **Additional Laboratory Test Figures**

Figure A. 1. Rock Mechanics Testing System.

Figure A. 2 Data acquisition system connected to the rock mechanics testing system.

Figure A. 3. Loading plate and test system of the Brazilian Test.
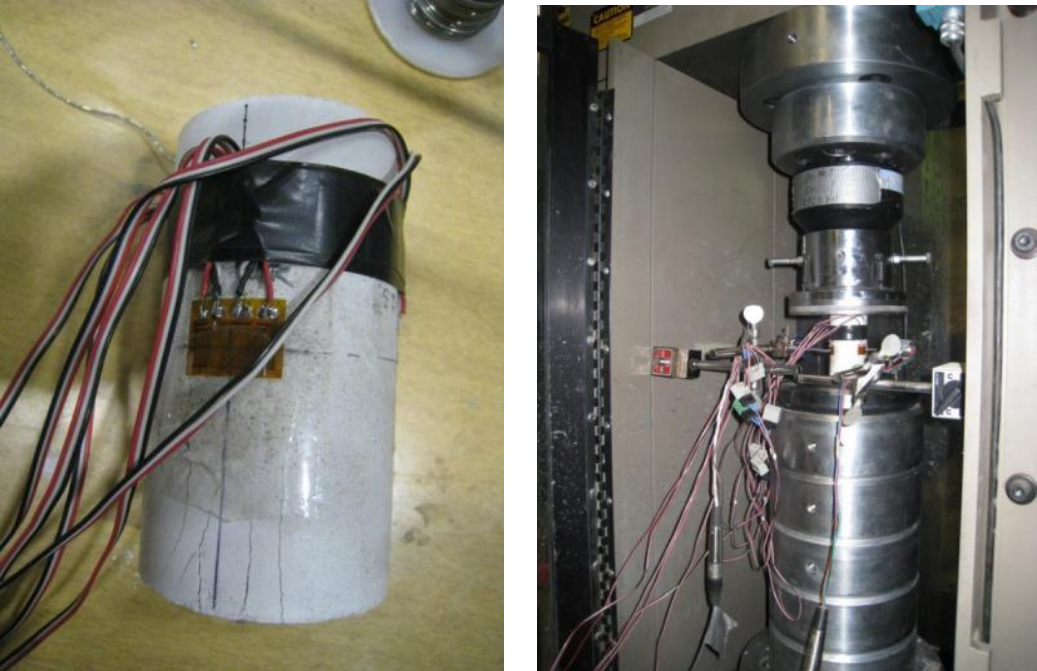
Figure A. 4. Surface strain gauge distribution and uniaxial compressive test system.

Figure A. 5. Procedure to generate a uniform mixture of plaster sand mixed sample. (a) Measure the weight of sand, (b) Measure the weight of sand plus plaster, (c) Mix the ingredients before adding water, (d) Add water and mix, (e) Uniform mix until mortar is getting thick enough like a soup, and (f) Pour the mortar into the mould.

<center>(a)</center>
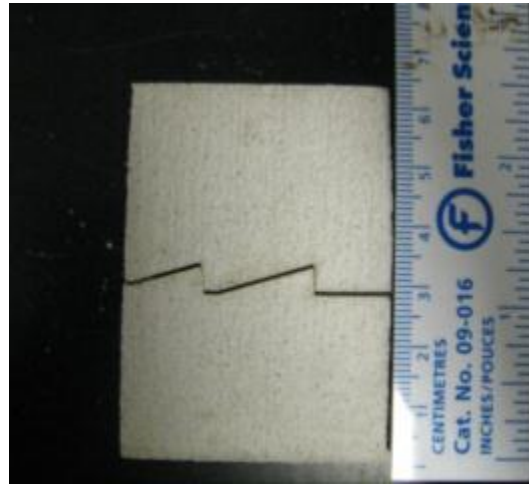
<center>(b)</center>
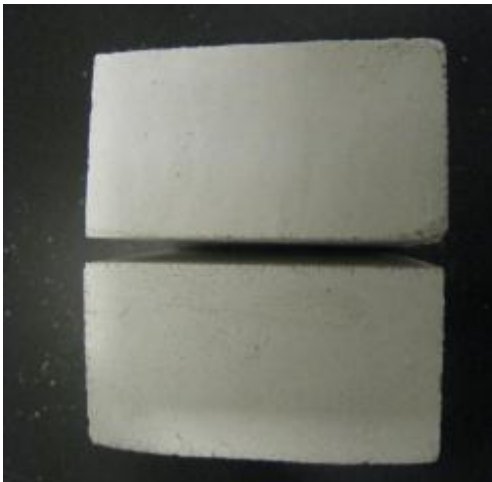
<center>(c)</center>
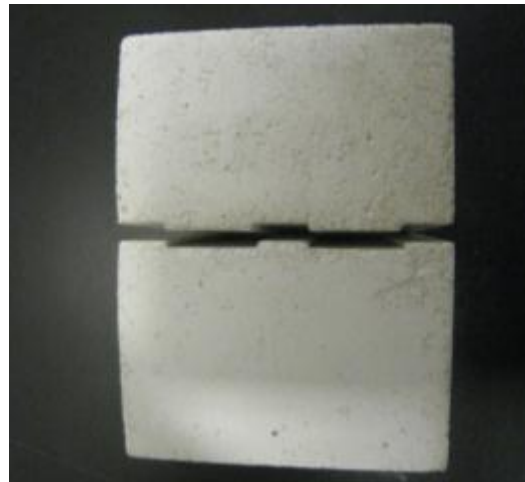
<center>(d)</center>

Figure A. 6: (a) Direct shear test synthetic rock sample with 45° crack shape, (b) Rock sample with 15° crack shape, (c) Rock sample with planar joint shape, (d) Rock sample with 90° crack shape.
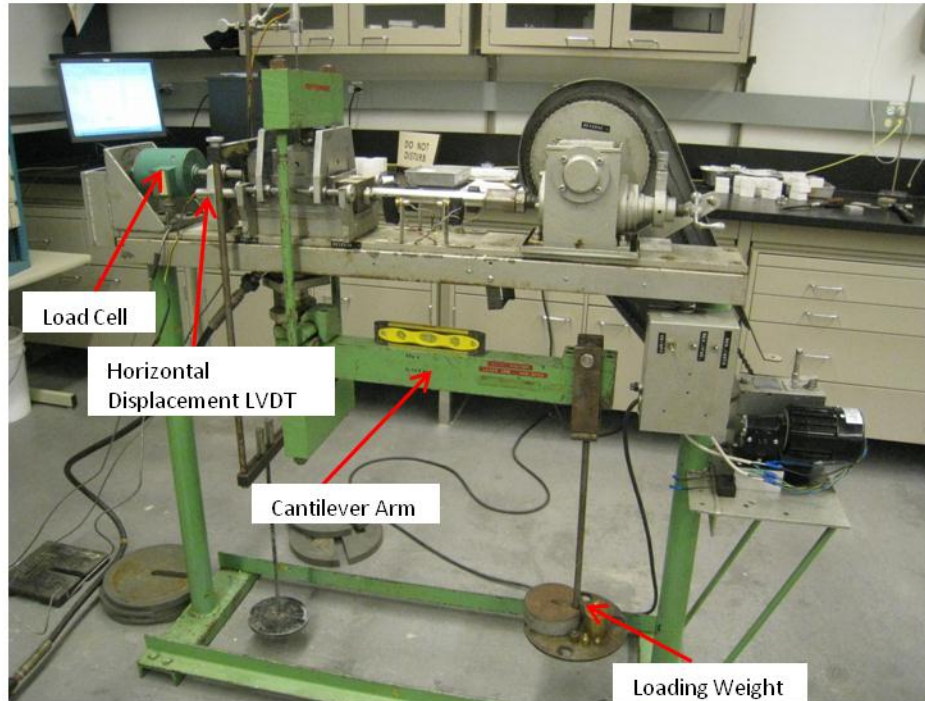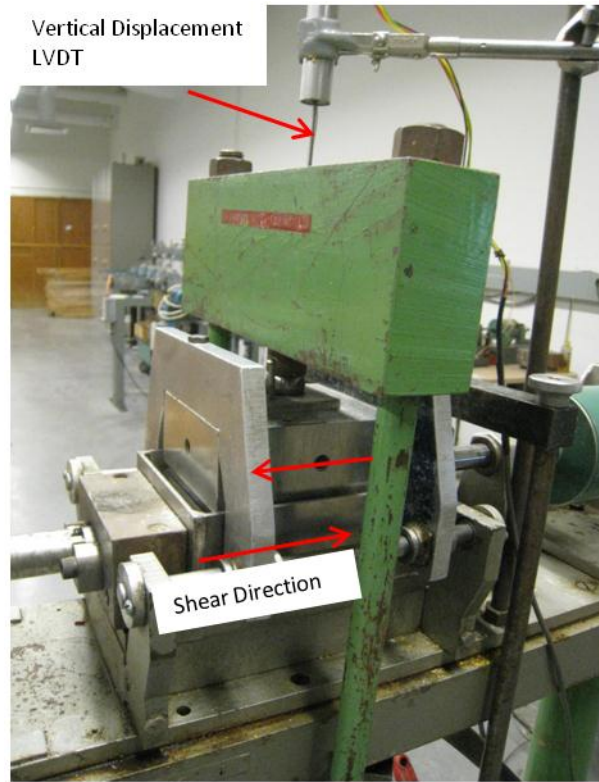
Figure A. 7. Direct Shear Test System.

Figure A. 8. Data recording system of direct shear test.
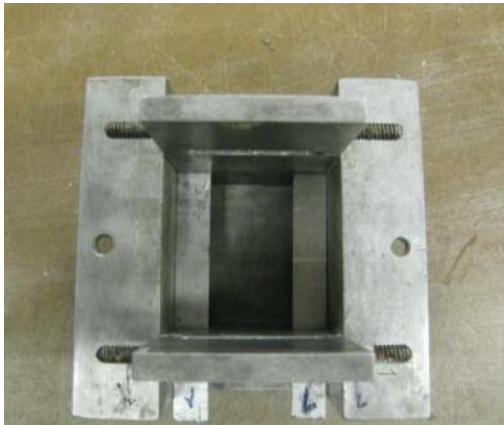
Figure A. 9. Mold used to make discontinuous synthetic rock with open crack.
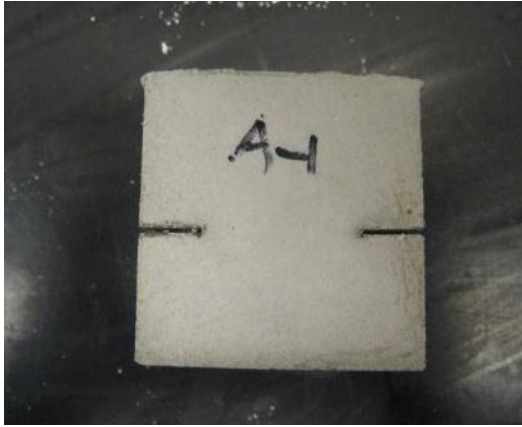
(a)

(b)
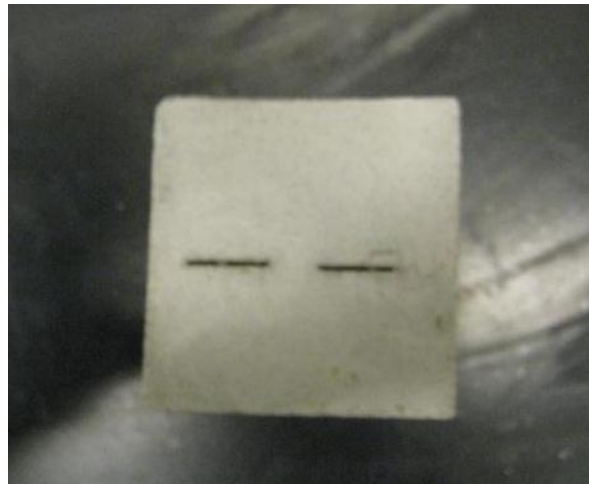
(c)

Figure A. 10: (a) Sample A with two 12 mm open flaws on the side, k = 0.48, (b) Sample B with one 24 mm open flaw in the middle, k = 0.48, (c) Sample C with two 14 mm open flaws in the middle, k = 0.56.
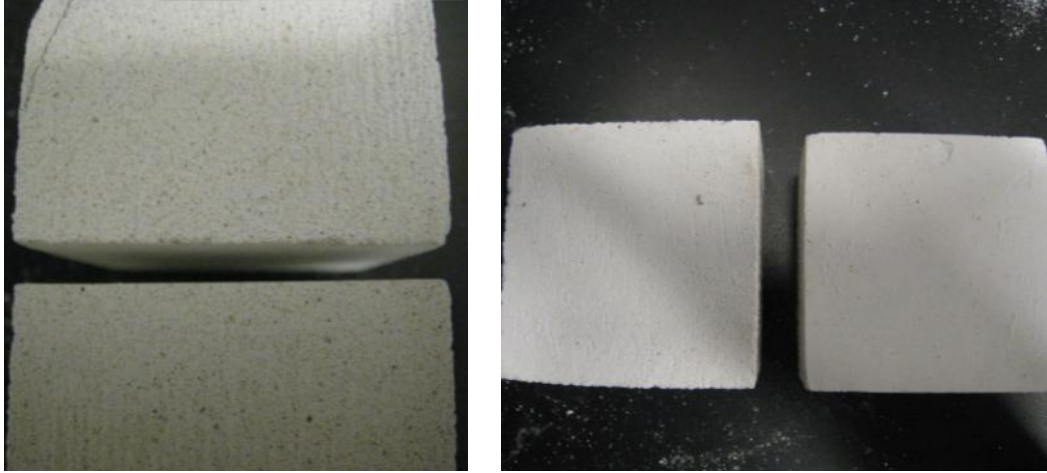
(a)
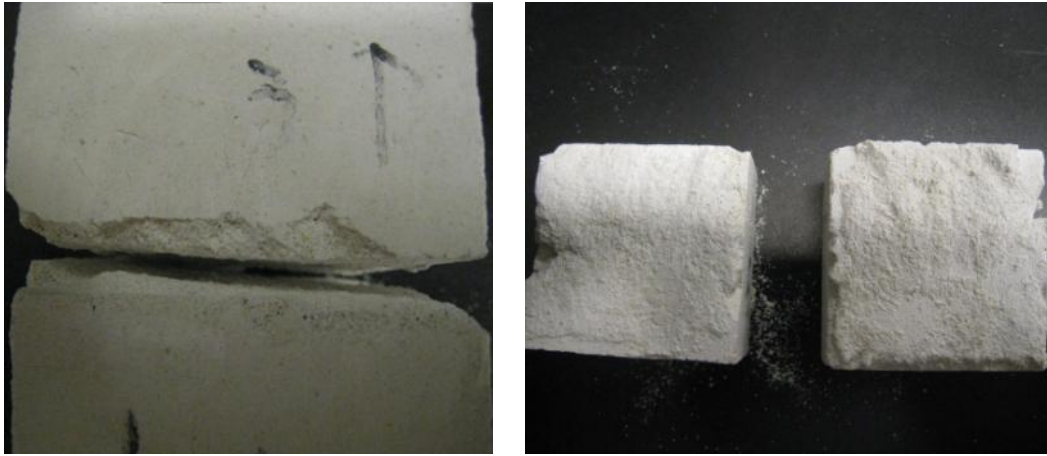
(b)

Figure A. 11: (a) Failure of planar joint sample under 200 kPa normal stress, (b) Failure of planar joint sample under 2 MPa normal stress.
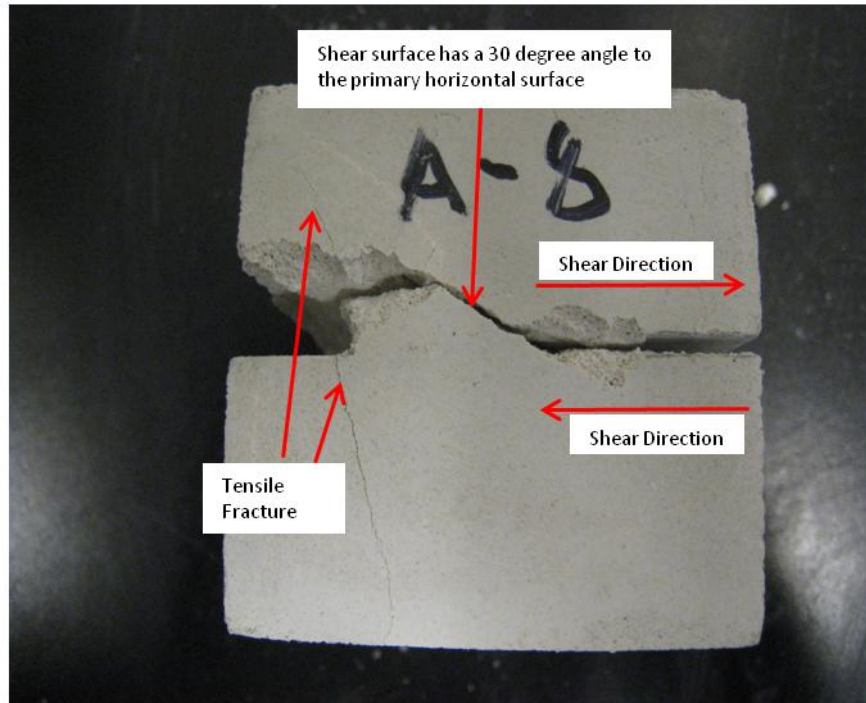
(a)
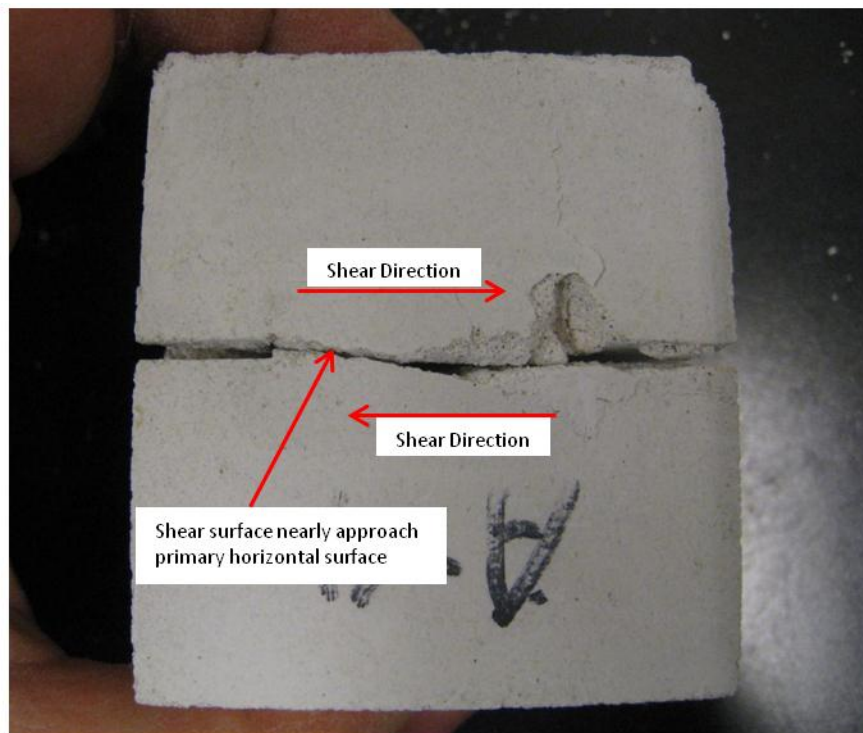
(b)

Figure A. 12: (a) Failure of Sample A under 0.4 MPa normal stress, (b) Failure of Sample A under 2 MPa normal stress.
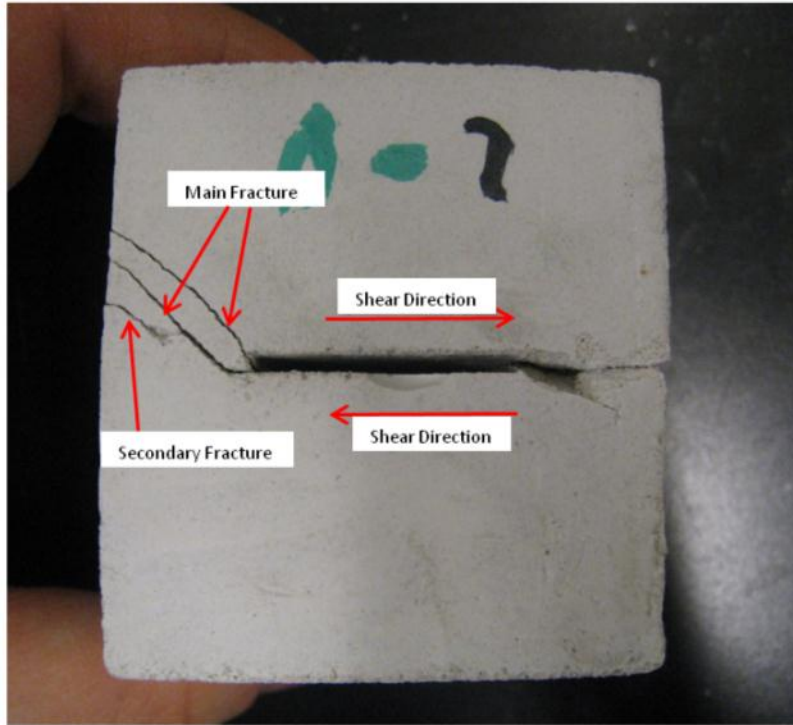
(a)
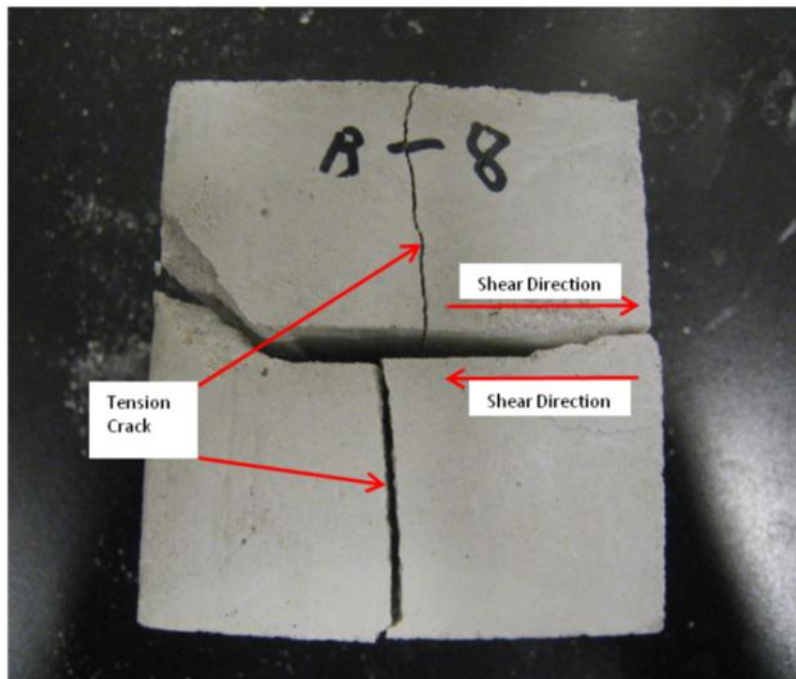
(b)
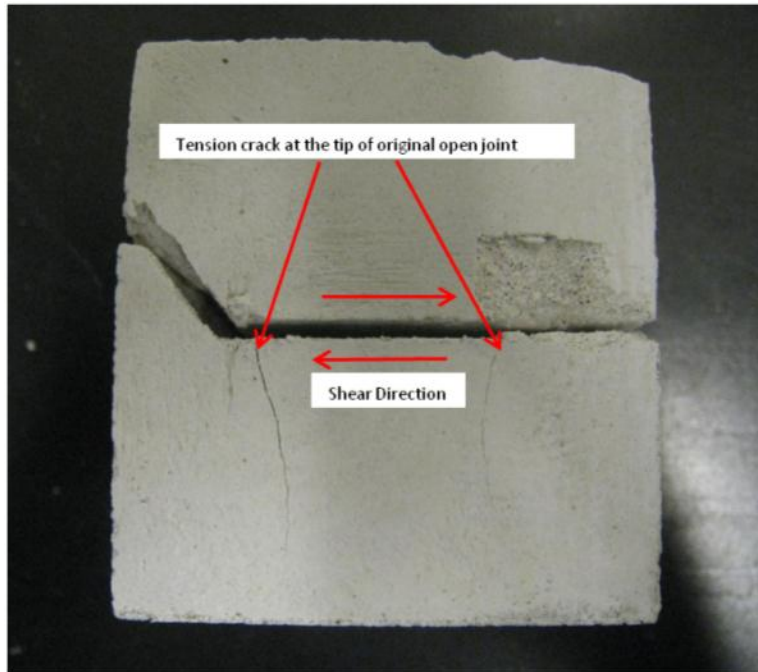
(c)
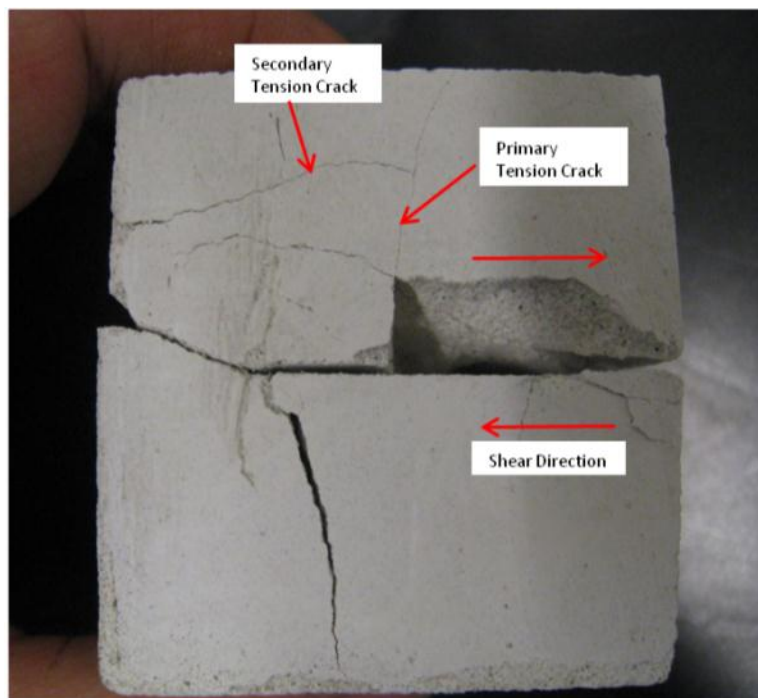
(d)

Figure A. 13: (a) Failure of Sample B under 0.4 MPa normal stress, (b) Failure of Sample B under 0.8 MPa normal stress, (c) Failure of Sample B under 1.75 MPa normal stress, (d) Failure of Sample B under 3 MPa normal stress.

(a)

(b)

(c)

(d)

Both top end sides were destroyed by main fracture under high normal stress

Dilation of fracture by shear and tension
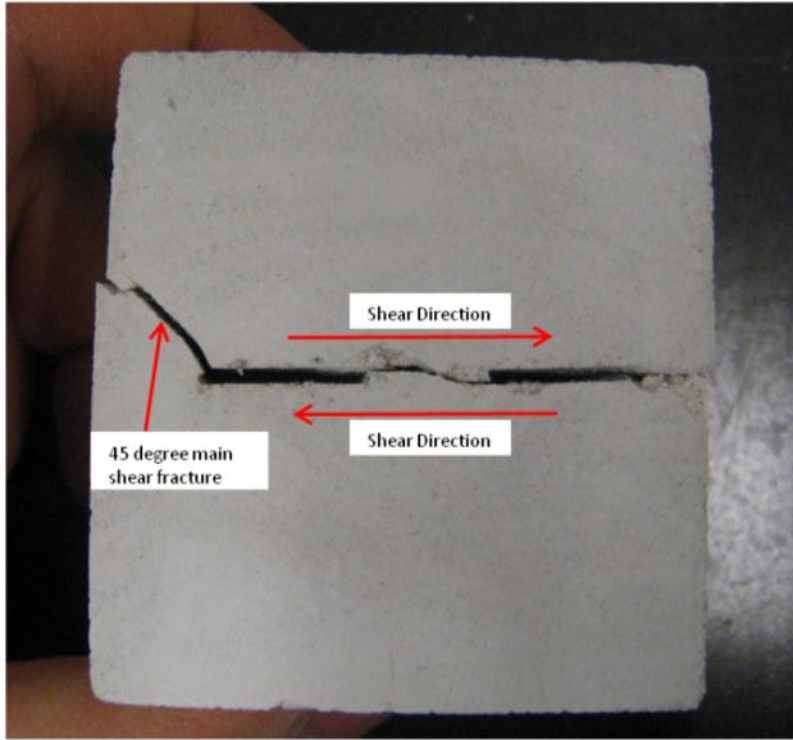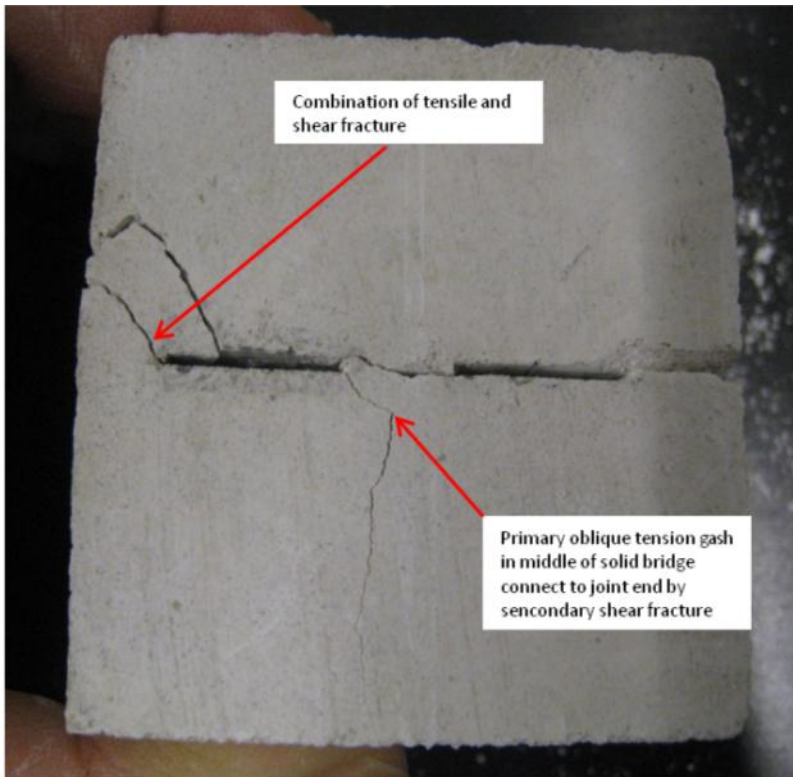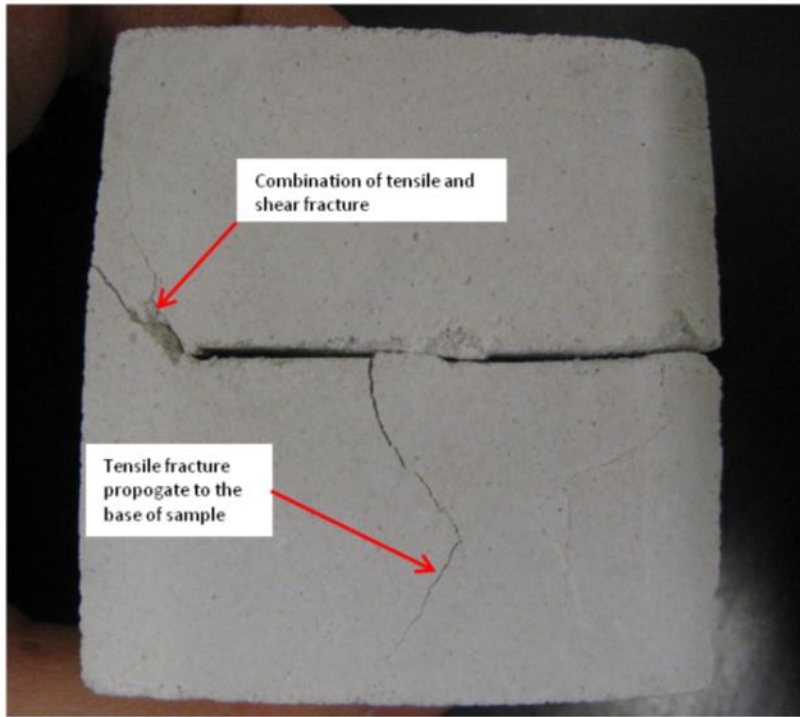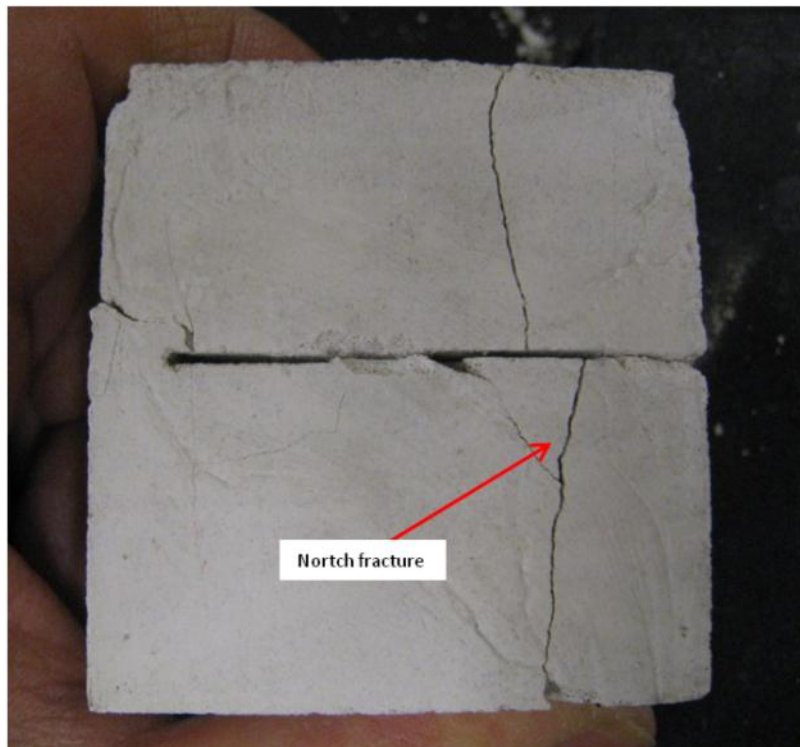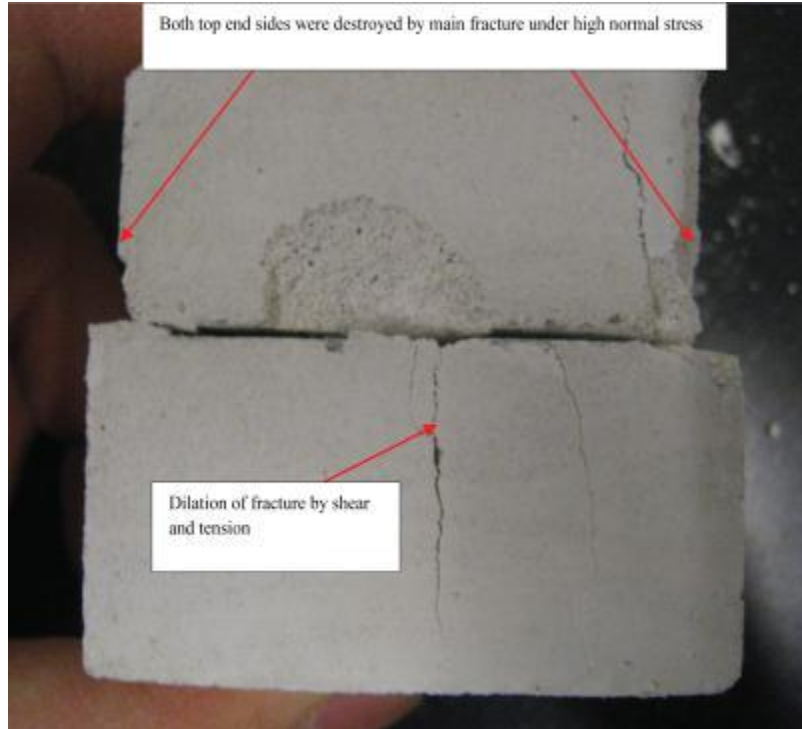
(e)

Figure A. 14: (a) Failure of Sample C under 0.4 MPa normal stress, (b) Failure of Sample C under 1.4 MPa normal stress, (c) Failure of Sample C under 2 MPa normal stress, (d) Failure of Sample C under 2.5 MPa normal stress, (d) Failure of Sample C under 3 MPa normal stress.
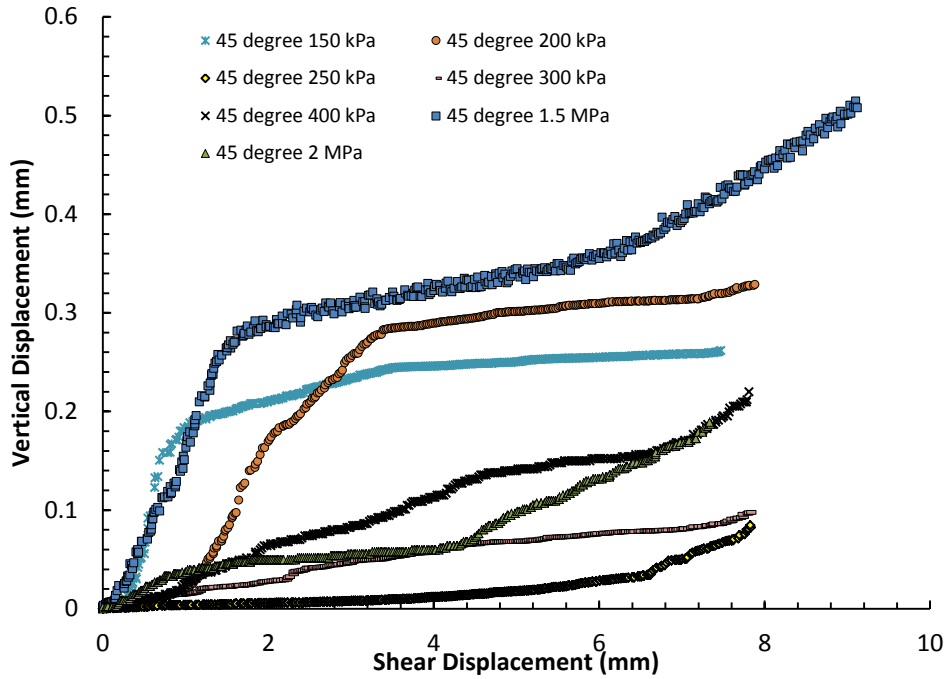
Figure A. 15: Dilation behaviors along the shear displacement of 45 degree stepped joint sample under different normal stresses.
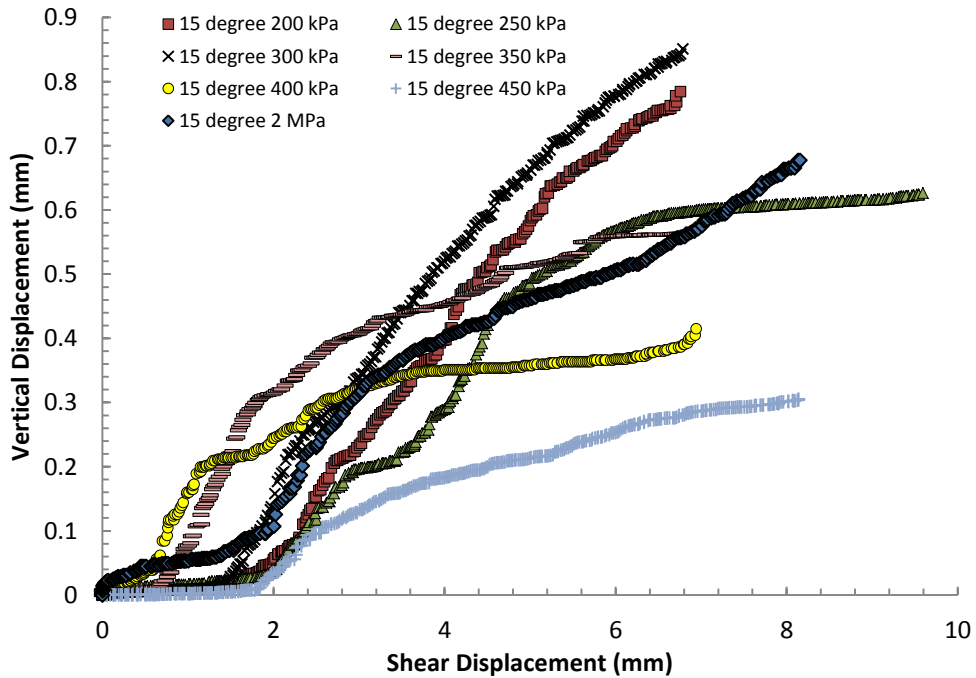
Figure A. 16: Dilation behaviors along the shear displacement of 15 degree stepped joint sample under different normal stresses.
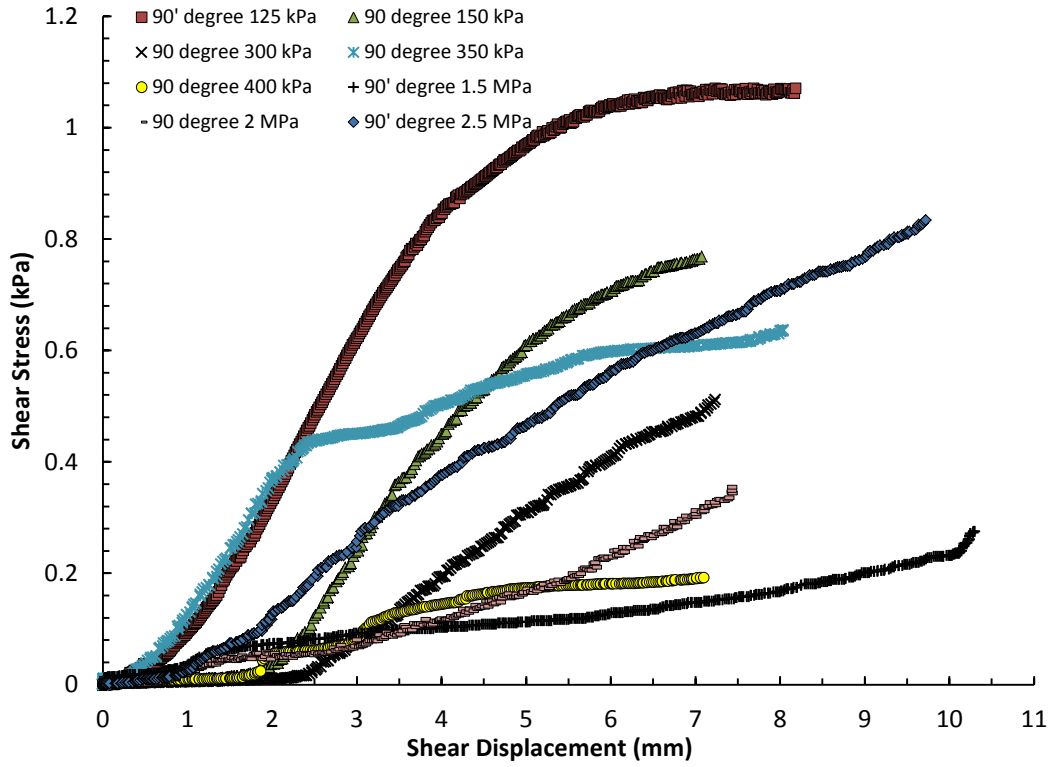
Figure A. 17: Dilation behaviors along the shear displacement of 90 degree stepped joint sample under different normal stresses.